Stony Brook University

Development of a quantitative assay for mitochondrial fusion and characterization of a lipid signaling pathway on the mitochondrial surface

A Dissertation Presented

by

Huiyan Huang

to

The Graduate School

in Partial Fulfillment of the

Requirements

for the Degree of

Doctor of Philosophy

in

Molecular and Cellular Pharmacology

Stony Brook University

August 2010

Stony Brook University

The Graduate School

Huiyan Huang

We, the dissertation committee for the above candidate for the Doctor of Philosophy degree, hereby recommend acceptance of this dissertation.

Michael A. Frohman, M.D., Ph.D. - Dissertation Advisor
Professor
Department of Pharmacological Sciences

Daniel F. Bogenhagen, MD - Chairperson of the Defense
Professor
Department of Pharmacological Sciences

Robert S. Haltiwanger, Ph.D.
Professor
Department of Biochemistry and Structural Biology

Deborah A. Brown, Ph.D.
Professor
Department of Biochemistry and Structural Biology

This dissertation is accepted by the Graduate School.

Lawrence Martin
Dean of the Graduate School

Abstract of the Dissertation

Development of a quantitative assay for mitochondrial fusion and characterization of a lipid signaling pathway on the mitochondrial surface

by

Huiyan Huang

Doctor of Philosophy

in

Molecular and Cellular Pharmacology

Stony Brook University

2010

Mitochondria continuously undergo fusion and fission, the relative rates of which define their morphology. Mitochondrial fusion is currently assayed by fusing together cells expressing GFP or RFP in their mitochondria and then scoring the frequency of cells with yellow mitochondria (representing fused green and red mitochondria). However, this assay is labor intensive and only semi-quantitative. I developed a reporter system consisting of split fragments of *Renilla* luciferase and YFP fused to mitochondrial matrix-targeting sequences and to leucine zippers to trigger dimerization. The assay enables fusion to be quantitated both visually for

individual cells and on a population level using chemiluminescence, laying the foundation for high throughput small molecule and RNAi screens for modulators of mitochondrial fusion. I used the assay to examine cytoskeletal roles in fusion progression.

The mammalian Phospholipase D superfamily member MitoPLD localizes to mitochondria and facilitates fusion by generating the signaling lipid phosphatidic acid (PA). Independently, the *Drosophila* homolog of MitoPLD, Zucchini (Zuc), was proposed to be a cytoplasmic nuclease and shown to be required for piRNA generation, a critical step in oogenesis. I show here that Zuc localizes to mitochondria. Conversely, mice lacking MitoPLD exhibit the germ cell degeneration observed in mice lacking other piRNA components. These findings identify the first mitochondrial protein required for piRNA generation. MitoPLD generates PA on the mitochondrial surface. The PA then recruits another signaling enzyme, the PA phosphatase Lipin 1, to convert the PA to diacylglycerol and promote fission, suggesting a new mechanism for mitochondrial morphology homeostasis. MitoPLD$^{-/-}$ fibroblasts exhibit shortened mitochondria and spermatocytes lack intermitochondrial cement (nuage), a structure that is implicated in piRNA generation. I propose that mitochondrial-surface PA

generated by MitoPLD/Zuc recruits nuage components critical for piRNA production.

Table of Contents

List of Abbreviations

A	adenosine
Ago3	Argonaute 3
Aub	Aubergine
C1P	ceramide 1-phosphate
CB	chromatoid body
CHX	cycloheximide
cyt c	cytochrome c
DAG	diacylglycerol
DGPP	DAG pyrophosphate
Drp1	dynamin-related protein 1
ER	endoplasmic reticulum
fld	fatty liver dystrophy
FLuc	*Firefly* luciferase
Fzo	*fuzzy onion* gene product
GAP	GTPase activating proteins
Gasz	Germ cell protein with Ankyrin repeats, Sterile alpha motif, and leucine Zipper
GEF	guanine nucleotide exchange factors

GFAP	glial fibrillary acidic protein
hGLuc	humanized *G. princeps* luciferase
IF	intermediate filament
IMC	inter-mitochondrial cement
LPA	lysophosphatidate
LPP	lipid phosphate phosphatase
MEF	mouse embryo fibroblast
Mff	Mitochondrial fission factor
Mfn	Mitofusin
miRNA	microRNAs
Miro	mitochondrial Rho GTPases
MitoEGFP	mitochondrially-targeted EGFP
MLS	mitochondrial localization sequence
mtDNA	mitochondrial DNA
mVenus	monomeric Venus fluorescent protein
NLS	nuclear localization signal
Opa1	optic atrophy type 1
PA	phosphatidic acid
PABD	PA Binding Domain

PA-GFP	photoactivatable GFP
PAP	phosphatidate phosphatase
PC	phosphatidylcholine
PE	phosphatidylethanolamine
PEG	polyethylene glycol
PGC1α	peroxisome proliferator activated receptor γ coactivator-1α
Pink1	PTEN-induced putative kinase 1
piRNA	PIWI-interacting RNA
PLD	phosphalipase D
RLuc	*Renilla* luciferase
RLU	relative light unit
S1P	sphingosine 1-phosphate
siRNA	small interfering RNAs
SNP	single nucleotide polymorphism
TAG	triacylglycerol
TMRE	tetramethylrhodamine ethyl ester
U	uridine
wt	wild-type
Zuc	Zucchini

List of Figures

Chapter 1

Chapter 2

Chapter 3

Acknowledgement

To:

Dr. Michael A. Frohman for the fantastic mentoring.

Dr. Seok-Yong Choi for laying the foundation for this dissertation work.

Drs. M. Rizzo (U. Maryland) and Lynne Regan (Yale U.) for the kind gifts of plasmids encoding mVenus and the synthetic leucine zippers, respectively, and Dr. H. McBride for critical feedback on the mitochondrial fusion assay.

Drs. S. Chuma (Kyoto U.), R. Jessberger (Dresden U. of Tech.), A. Vasileva (Mt. Sinai), S. K-Miyagawa and T. Nakano (Osaka U.), and C. Chen and T. Pawson (Samuel Lunenfeld Res. Inst.) for the kind gifts of piRNA pathway component expression plasmids, Dr. A. Newton for the DAG sensor, and B. Cyge for advice with testes analysis.

Chapter 1: Introduction

1. 1 Objective and specific aims

The overall objective of this thesis is to study the signaling functions of the lipid second messenger phosphatidic acid (PA) generated by MitoPLD on the mitochondrial surface.

Mitochondrial morphology is maintained by the balance of constant fusion and fission events (Chan 2006). Due to the unique structure of the double-membrane organelle, the machinery mediating fusion and fission is also unique from the well-known SNARE proteins for exocytosis and dynamin for endocytosis events. Nonetheless, the different sets of proteins use similar mechanisms to mediate membrane fusion and fission, although the detailed processes are still poorly understood. Recently, our lab has uncovered a lipid modifying enzyme, denoted MitoPLD, that resides at the outer membrane of mitochondria and produces the fusogenic lipid, PA, which promotes mitochondrial fusion (Choi et al. 2006). PA is a potent second messenger that

regulates a number of signaling proteins, which makes the termination of the bioactive signal important upon generation. To achieve this, some other lipid modifying enzymes function to metabolize PA. Interestingly, my preliminary data showed that MitoPLD-generated PA is able to recruit the PA phosphatase Lipin 1, which converts PA into diacylglycerol (DAG), raising questions concerning the mechanism and significance of Lipin 1 translocation. Many PA-responsive proteins have a PA-binding region, however no consensus sequence exists as a "PA-binding" domain; all that is usually found is a motif rich in positively-charged amino acids. Whether Lipin 1 was recruited to the mitochondrial surface by physically binding to PA with a PA-binding motif was unclear. Or did Lipin 1 interact with a/some mitochondrial specific protein(s) that is/are themselves PA-responsive? MitoPLD has been shown to promote mitochondrial fusion. Was the subsequent production of DAG needed for the fusion events or actually to terminate the function undertaken by PA?

During the course of my thesis research, the MitoPLD knockout mice became available. We had characterized MitoPLD as a mitochondrial-anchored PA-generating enzyme that facilitates mitochondrial fusion. However, a subsequent study with the *Drosophila* homolog, Zucchini (Zuc), reported it to be a putative cytoplasmic nuclease that was involved in piRNA generation. Did MitoPLD function differently from Zuc? Could Zucchini be a lipid enzyme as well? Conversely, could MitoPLD be involved in piRNA generation as well?

Since the discovery of the *fuzzy onions* gene product (Fzo, *Drosophila* homolog of Mitofusin 1 and 2) in mitochondrial fusion (Hales and Fuller 1997), extensive studies have been carried out to explore the fusion machinery. Mechanistic studies on mitochondrial fusion relied heavily on a classic mitochondrial fusion assay developed in 1997 (Nunnari et al. 1997). By introducing GFP and RFP into the mitochondria of two cells and then inducing cell fusion, mitochondrial fusion could be assessed by the extent of overlap of the two fluorescent proteins to produce yellow color. This assay works well when qualitatively determining the requirement of a certain protein or factor for mitochondrial fusion. However, when it comes to quantification, it becomes very labor intensive to score several hundred of fusion events under confocal microscopy. A sensitive and quantitative assay is fundamental for the advancement of any field and thus is highly desirable. Here, by using a split-luciferase complementation system, I set out to develop a less labor-intensive and more quantitative mitochondrial fusion assay that could be used for high throughput small molecule and RNAi screens for modulators of mitochondrial fusion.

Hence, the specific aims of this thesis were (1) to develop a facile and quantitative assay for mitochondrial fusion using a split-luciferase complementation system; (2) to determine the mechanism of how MitoPLD-generated PA recruits Lipin 1 to the mitochondrial surface; (3) to analyze the

cellular function of DAG produced by Lipin 1 after translocation to MitoPLD-generated PA; (4) to characterize the phenotype of MitoPLD knockout mice and solve the discrepant reports between MitoPLD and Zucchini. Ultimately, I sought to gain insight into the biological functions of the lipid signals PA and DAG on the mitochondrial surface.

1.2 An overview of mitochondrial dynamics

Mitochondria are stereotypically viewed as kidney-shaped organelles scattered throughout the cytosol, as a result of the images obtained from electron microscopy thin sections that are frequently presented in textbooks and reviews. In fact, however, most of these images are actually presenting oblique slices of long mitochondrial tubules that are part of a network-like structure that extends from the perinuclear region to the edge of the cell. Mitochondria are constantly undergoing fission and fusion, and their morphology is ultimately regulated by the fusion to fission balance, which can vary in different cell types (Chan 2006). The balance is dynamically controlled – mitochondrial tubules undergo massive

fission during cytokinesis and then rapidly fuse together again in the synthesis phase of the cell cycle (Margineantu et al. 2002; Taguchi et al. 2007). Insulin and other growth factor stimulation increase the fusion to fission balance (Wilson-Fritch et al. 2004; Pawlikowska et al. 2007), which may reflect the fact that larger mitochondria are more efficient at generating energy. In contrast, induction of apoptosis triggers mitochondrial fragmentation by increasing the rate of fission, although the fission in itself does not cause cell death (Tanaka and Youle 2008). Directed subcellular localization of mitochondria is also important to ensure that they function properly in the context of generating energy where it is needed in the cell, in particular for cells with localized high energy requirements, such as neurons, at axonal sites of synaptic transmission, which are distant from the cell body (Chada and Hollenbeck 2003; Chada and Hollenbeck 2004), and lymphocytes, at regions of myosin dynamics during chemotaxis (Campello et al. 2006). In pancreatic acinar cells, mitochondria form a belt surrounding the granule-rich region to confine Ca^{2+} signaling within the apical pole (Tinel et al. 1999). Subcellular mitochondrial trafficking is affected by mitochondrial morphology (Hollenbeck and Saxton 2005), and genetic mutations that lead to fusion and fission dysfunction not only cause mitochondrial fragmentation or tubulation in cultured cells, but cause diseases such as type 2A Charcot-Marie-Tooth, an inherited peripheral neuropathy (Zuchner et al. 2004) characterized by

blunted synaptic transmission and axonal die-back from their distal target sites, optic atrophy (Olichon et al. 2006) and neonatal lethality (Waterham et al. 2007).

Some of the proteins important for mitochondrial fusion and fission have been identified, as shown in Figure 1.1. The proteins tend to function specifically in mitochondria, but in a manner analogous to how similar types of proteins function in fusion and fission of cytosolic membrane vesicles as they bud from and fuse into subcellular membrane compartments. For example, the proteins called Mitofusins (Mfns) that mediate mitochondrial fusion perform a function similar to that undertaken by SNARE complex proteins for other types of membrane fusion (Chen et al. 2003; Koshiba et al. 2004), although there are distinct aspects to the fusion mechanism (Chan 2006; Choi et al. 2006). Similarly, fission is mediated by a dynamin-related protein, Drp1 (Smirnova et al. 1998; Taguchi et al. 2007), which functions analogously to dynamin during the process of endocytosis. Mitochondria translocate through the cell via microtubules and the actin cytoskeleton, using both unique tethering proteins and universal components of the cytoskeleton (De Vos et al. 2003; Hollenbeck and Saxton 2005), and this movement is promoted by the mitochondrial Rho GTPases (Miro 1 and Miro 2) (Guo et al. 2005; Fransson et al. 2006).

1.3 An overview of mitochondrial fusion assays

Advancement in the field of mitochondrial fusion has depended greatly on the two available major mitochondrial fusion assays, shown in Figure 1.2A and B, the development of which was both linked to progress in generating new types of fluorescent proteins.

The classic mitochondrial fusion assay (Fig. 1.2A) was first developed in 1997 to study mitochondrial fusion in yeast (Nunnari et al. 1997) and was soon adapted for mammalian cell lines. The strategy is to introduce a mitochondrial matrix targeted GFP or a mitochondria-specific red fluorescent vital dye, which later was replaced with matrix targeted DsRed shortly after its discovery, to haploid cells of opposite mating types in yeast or to two populations of cells. After mating or inducing cell fusion with polyethylene glycerol (PEG) or a hemagglutinating virus, the intermixing of the two different mitochondria is then examined under confocal microscope. This assay was invaluable in permitting investigators to observe the behavior of mitochondria dynamics and provided solid evidence for mitochondrial fusion and the subsequent rapid intermixing of contents (Nunnari et al. 1997). It also helped to confirm the role in mitochondrial fusion for several other proteins, such as Ugo1 (no mammalian homolog) (Sesaki

and Jensen 2001), and Mgm1p (mammalian homolog: optic atrophy type 1 (Opa1)) (Wong et al. 2003), identified from genetic screens in yeast. Studies in mammalian cell lines using this assay showed that mitochondrial fusion in human cells are efficient and requires an intact inner membrane potential (Legros et al. 2002) but is independent of a functional actin or tubulin cytoskeleton (Mattenberger et al. 2003). However, in studies where comparison of the fusion rate under different conditions is required, this assay became rate-limiting. For the assay to be quantitative, each experimental sample needs to be scored under confocal microscope to find and count several hundred fusion events, and this limits its potential throughput. Moreover, the requirement to incubate several hours for complete mixing of mitochondria before assessing made it impossible to examine the effect of acute changes in growth conditions.

In 2002, a variant of EGFP with a single histidine substitution at T203 that exhibits barely detectable green fluorescence was reported to be able to increase its fluorescence 100-fold after irradiation with 413-nm light, and the photostability of the photoactivated GFP was comparable to the wild-type EGFP (Patterson and Lippincott-Schwartz 2002). This photoactivatable GFP (PA-GFP) shortly thereafter became a powerful tool to study the temporal and spatial dynamics of proteins. More importantly, Karbowski et al. then developed a mitochondrial fusion assay by co-labeling the mitochondria with matrix targeted PA-GFP and DsRed2 (Fig. 1.2B). After irradiation at regions of interest, the

redistribution of photoactivated PA-GFP was monitored and the decrease in the PA-GFP fluorescence intensity, which correlates with mitochondrial fusion rate, could be quantitatively recorded (Karbowski et al. 2004). Using this newly developed assay, the authors proved that morphologically fragmented mitochondria showed inhibition in mitochondrial fusion upon activation of apoptosis. Twig et al. further adapted this assay by substituting the DsRed2 with tetramethylrhodamine ethyl ester (TMRE) to study the mitochondrial membrane potential changes during fusion and fission (Twig et al. 2006), and in a later study the authors found that mitochondrial fusion may create two potentially uneven daughter mitochondria with the depolarized unfusable one subject to autophagy after a few hours (Twig et al. 2008). The newly developed mitochondrial fusion assay provides ease of direct observation for mitochondrial fusion behaviors under physiological conditions, as it does not require artificially inducing cell fusion, and some extent of quantification. However, it only tracks limited regions of mitochondria in one cell at a time, which makes it difficult to gather information on a population level, and thus still has limits for throughput. Moreover, the requirement to incubate several hours for complete mixing of mitochondria before assessing made it impossible to examine the effect of acute changes in growth conditions.

Most fluorescent proteins can be split into an N- and a C-terminal fragment, neither of which is fluorescent on its own. However, the fragments can

reassemble and fluoresce if they are brought together by strongly interacting protein domains like antiparallel leucine zippers (Ghosh et al. 2000). This strategy has been successfully used to study protein-protein interactions by fusing each fragment to the candidate interacting proteins (Hu et al. 2002; Magliery et al. 2005). The fluorescent signal is highly sensitive and robust as only interacting proteins will bring the split fluorescent fragments together for reconstitution, which results in high signal-to-noise performance. It was conceivable to propose an alternative assay for mitochondrial fusion by introducing the two split fluorescent protein fragments fused with antiparallel leucine zippers into the mitochondrial matrices of different cells (Jakobs 2006). Upon cell fusion, the fluorescent signal would only come from mitochondrial fusion, which could be quantitatively detected with a sensitive fluorescence plate reader (Fig. 1.2C). However, this proposed version of mitochondrial fusion assay had not yet been experimentally realized.

1.4 An overview of phosphatidate phosphatase (PAP)

Phosphatidate phosphatase (PAP) enzymes catalyze the dephosphorylation of phosphatidate into DAG and inorganic phosphate (Smith et al. 1957). They are classified by the requirement of Mg^{2+} into PAP1, being Mg^{2+}-dependent, and PAP2 (or lipid phosphate phosphatase, LPP), as Mg^{2+}-independent. PAP1 activity is located primarily in the cytosol of cells and is strongly inhibited by N-ethylmaleimide. PAP2 activity is mainly associated with the plasma membrane and is insensitive to N-ethylmaleimide (Jamal et al. 1991). Traditionally, PAP1 enzymes were believed to be involved in lipid synthesis and PAP2 in lipid signaling.

During the past decade, LPP has been well studied due to the existence of its molecular information. The first LPP was cloned in 1996 (Kai et al. 1996; Kai et al. 1997) and the cloning of other isoforms of LPPs followed rapidly. There are three LPPs in mammals, namely LPP1, LPP2 and LPP3. LPPs are multi-transmembrane proteins with a conserved motif comprising three distinct sequences, termed C1 (substrate recognition site), C2 and C3 (both catalytic), located in the third and fifth extramembrane loops (Stukey and Carman 1997; Zhang et al. 2000). Modeling the topology of LPPs implies that the catalytic site faces the extracellular side of the plasma membrane and luminal side of the major membrane compartments (Fig. 1.3A) (Barila et al. 1996; Kai et al. 1996).

Biochemical studies of the enzymes demonstrated that LPPs dephosphorylate a broad variety of lipid phosphates including PA,

lysophosphatidate (LPA), sphingosine 1-phosphate (S1P), ceramide 1-phosphate (C1P) and DAG pyrophosphate (DGPP), thus are also called lipid phosphate phosphatases (Brindley et al. 2002; Pyne et al. 2004). PA, LPA, S1P and C1P are bioactive phosphate esters that regulate various signal transduction pathways. LPA, S1P and C1P are extracellular lipids and activate cells through G-protein coupled receptors. Different receptors can activate a variety of signaling pathways through different coupled heterotrimeric G-protein, (English et al. 2001; English et al. 2002; Pyne et al. 2009) and alternatively transactivate the epidermal growth factor or platelet-derived growth factor (Herrlich et al. 1998; Goppelt-Struebe et al. 2000). Some of the intracellular function of C1P and S1P has been proposed with the intracellular targets largely unknown (Brindley et al. 2002; Pyne et al. 2009). On the other hand, PA is an important intracellular regulator in membrane vesicle trafficking, receptor signaling, and cytoskeletal organization (Jenkins and Frohman 2005; Haucke and Di Paolo 2007). Therefore, an important function of LPPs is to terminate the action of LPA, PA, C1P or S1P by converting them into monoacylglycerol, DAG, ceramide or sphingosine respectively (Jasinska et al. 1999). The latter three, being bioactive themselves, can mediate further cell signaling. However, considering the topology of LPPs, it would be difficult for the extracellular catalytic site to convert the intracellular PA produced by enzymes such as phospholipase D2 (PLD2). A proposed model is that PLD2 and LPP are both present in a membrane raft, the unique lipid composition of which

might provide a possible environment for the subsequent conversion of PA by LPP (Sciorra and Morris 1999).

On the other hand, the gene encoding a PAP1 enzyme, known as *Lpin 1*, was found in 2001 as an unexpected activity from mapping the gene causing the fatty liver dystrophy (fld) mutant mouse, which exhibits the phenotype of Type-II diabetes related lipodystrophy (Peterfy et al. 2001). However, it took the field another five years to discover that Lipin 1 is a Mg^{2+}-dependent phosphatidate phosphatase (Han et al. 2006; Donkor et al. 2007). Two additional members of Lipin family, Lipin 2 and Lipin 3, were identified with 60% amino acid sequence similarity to Lipin 1 (Fig. 1.3B). Further comparing sequences from other species revealed two highly conserved regions in the N- and C-terminus known as NLIP and CLIP domains (Peterfy et al. 2001), and the latter contains a DxDxT motif critical for catalytic activity. Unlike LPPs, PAP1 enzymes have preferred substrate specificity for PA. There are two alternatively spliced isoforms for Lipin 1, Lipin 1a and Lipin 1b, in mice. Lipin 1b exhibits consistently 1.7-fold higher PAP1 activity than Lipin 1a. Notably, humans have three isoforms according to the most recent report, and the specific exon for the third isoform is also found in the mouse genome (Han and Carman 2010), suggesting the existence of another isoform for mouse Lipin 1 as well. There is only one isoform found for Lipin 2 and Lipin 3 so far. They have comparable PAP1 activity, however at about one-fourth of the relative activity for Lipin 1a (Donkor et al. 2007). All three Lipin

family members are expressed in cytosol, and as PAP1 enzymes, are believed to act at a key step in the synthesis of triacylglycerol (TAG), phosphatidylcholine (PC) and phosphatidylethanolamine (PE) by generating DAG from PA (Brindley 1984; Nanjundan and Possmayer 2003; Carman and Han 2006; Brindley et al. 2009). With growing interest in the Lipin family members, more functions have been discovered recently.

Lipin 1, Lipin 2 and Lipin 3, while widely expressed, exhibit distinct patterns of tissue expression. Lipin 1 is highly expressed in adipose tissue, skeletal muscle and testis. Lipin 1 is also detected in liver, heart, brain, kidney and other tissues. Lipin 2 is enriched in liver and is also expressed in kidney, brain and lung while Lipin 3 has a significant expression primarily in intestine and other regions of the gastrointestinal tract (Donkor et al. 2007). These results suggest that each member of the Lipin family may have independent physiological roles although they perform similar biochemical functions. Mutations in Lipin 1 are the best studied of the three. A genetic model with Lipin 1 deficiency in mice exhibits lipodystrophy, insulin resistance, peripheral neuropathy, and neonatal fatty liver (Peterfy et al. 2001). Mutations of *Lpin1* in human cause recurrent muscle pain, weakness, myoglobinauria in childhood (Zeharia et al. 2008). Interestingly, patients with *Lpin1* mutation do not appear to have lipodystrophy as has been observed in mice, probably due to the high Lipin 2 expression level in humans, but not mouse, in adipose tissue (Donkor et al.

2007), although studies in cultured mouse adipocytes showed that Lipin 2 cannot compensate for the loss of function of Lipin 1 in adipogenesis (Grimsey et al. 2008). Homozygous mutation in *Lpin2* are responsible for a rare autosomal recessive disorder called Majeed syndrome (Ferguson et al. 2005), with phenotypes including inflammation of the bone and skin, recurrent fevers, and dyserythropoietic anaemia. The pathogenic detail of Lipin 2 mutation remains unknown. For Lipin 3, very little is known due to the lack of naturally occurring mutants or maybe its natural mutations are not causing any noticeable physiological defects.

Some additional molecular mechanisms have been proposed to contribute in part to the phenotypes of Lipin 1 deficiency. Apart from its PAP1 activity to produce DAG, an immediate precursor of TAG, PC and PE, Lipin 1 has also been proposed to function as a transcriptional coactivator in liver, where it interacts with peroxisome proliferator activated receptor γ coactivator-1α (PGC1α) and the nuclear receptor PPARα in a coactivation complex through an LxxIL motif located downstream of the PAP1 active site, and is required for the expression of PPARα and several of its target genes that promote fatty acid oxidation (Finck et al. 2006). Notably, the LxxIL motif is also present in Lipin 2 and Lipin 3, suggesting a conserved function for the coactivator activity, which has indeed been shown for Lipin 2 as well (Donkor et al. 2009). The regulation of the PAP activity versus coactivator function is proposed to be achieved by SUMOylation

modification, which promotes nuclear localization of Lipin 1, however specifically in neuronal cells where Lipin 1a is enriched since no SUMOylation modification can be detected for Lipin 2 and Lipin 3 (Liu and Gerace 2009). For other cell types, the conserved polybasic region proposed to be the nuclear localization signal (NLS) downstream of NLIP domain seems to be important for the cytoplasmic/nuclear localization transition (Ren et al. 2010 *in press*). However, studies in yeast Lipin homolog Pah1p showed that all the cellular functions are dependent on PAP1 enzyme activity (Han et al. 2007). This may represent a difference between yeast and mammalian Lipin protein function.

Studies in LPPs have established their role in regulating signal transduction. Likewise, both the substrate and the product for PAP1, namely PA and DAG, are potent lipid secondary messengers. Whether the PAP1 enzymes could regulate the cytosolic PA generated by the signaling enzymes PLD1 and PLD2 from hydrolyzing PC (Jenkins and Frohman 2005) remains to be examined. Intriguingly, a study set to understand the peripheral neuropathy in Lipin 1-deficiency mice by deleting *Lpin 1* specifically in Schwann cells revealed PA as a potent activator of the MEK-Erk pathway that leads to demyelination (Nadra et al. 2008), which suggests a signaling function of Lipin 1 to terminate the bioactive signal of PA and maybe even an undiscovered function for the subsequent DAG production. Nonetheless, more studies need to be performed to explore the emerging function of Lipin 1 in signal transduction regulation.

PA and DAG have also been demonstrated to facilitate both fusion and fission of cytoplasmic membrane compartments in specific settings, for example, endocytosis from the plasma membrane (Du et al. 2004; Lee et al. 2006), budding of vesicles from the Golgi (Chen et al. 1997; Fernandez-Ulibarri et al. 2007; Yang et al. 2008), peroxisome division (Guo et al. 2007), insertion of membrane vesicles into the plasma membrane (Vitale et al. 2001; Jun et al. 2004; Huang et al. 2005), and fusion of nuclear envelope membrane precursor vesicles (Barona et al. 2005). PA generation is required for mitochondrial fusion (Choi et al. 2006), but it has not been determined whether PA directly facilitates fusion, or whether the fusion event is promoted by DAG subsequent to metabolism of the PA by a PAP such as Lipin. Even more intriguingly, a link between fusion and fission has been described. Mitochondria undergo fusion on average every 24 min, but at seemingly random times within that average time frame. Once fusion occurs, though, a fission event rapidly follows (on average, within 1.3 min) (Twig et al. 2008). Thus, some consequence of the fusion event triggers a subsequent fission event. This is an attractive finding from the perspective of a pro-homeostasis mechanism evolved to prevent excessive fusion in the cell and to target fission events onto the largest of the mitochondria. The mechanism underlying the linkage of fission to fusion is not known, but an intriguing possibility would be that early stages of the fusion reaction lead to generation of PA and the completion of fusion, following which the PA is metabolized to DAG, elevated

levels of which promote fission. Such a function would be consistent with roles for DAG in membrane fission at the trans-Golgi (Bossard et al. 2007; Fernandez-Ulibarri et al. 2007) and in peroxisome division (Guo et al. 2007). Examination of the linkage of fusion and fission in cell lines lacking MitoPLD or PAPs such as Lipin should provide insight into this possibility.

1.5 An overview on the role of piRNA in gametogenesis

As mentioned above, we reported a mitochondria-localized human PLD member, denoted MitoPLD, that is able to promote mitochondrial fusion by generating PA from cardiolipin on the mitochondrial surface (Choi et al. 2006). Interestingly, a *Drosophila* mutant, denoted *zucchini (zuc)*, was first identified in a genetic screen for female sterile mutations (Schupbach and Wieschaus 1991). Genetic mapping studies later on narrowed the region to a transcript, denoted Zucchini that encodes a member of the phospholipase D/endonuclease family with one copy of a conserved HDK motif (Pane et al. 2007), which turned out to be the *Drosophila* homolog of MitoPLD. Mutations in *zuc* induce transposon

expression due to the defect to produce PIWI-interacting RNA (piRNA). Zuc was therefore proposed to be a presumptive cytoplasmic nuclease that mediates piRNA generation, a critical step in oogenesis (Pane et al. 2007).

piRNAs are specialized small RNAs that interact with PIWI proteins. PIWI proteins, together with AGO proteins, belong to the evolutionarily conserved *piwi/argonaute* protein family. AGO proteins bind to small interfering RNAs (siRNAs) and microRNAs (miRNAs) while PIWI proteins bind to a novel class of small RNAs called PIWI-interacting RNAs, which was discovered in 2006 by cloning of small RNAs associated with PIWI proteins. In *Drosophila*, there are three PIWI proteins, Piwi, Aubergine (Aub), and Argonaute 3 (Ago3). They are expressed in both male and female germline cells with Piwi additionally in the somatic cells of ovary (Brennecke et al. 2007). There are three murine PIWI proteins as well, Miwi, Mili, and Miwi2. They are expressed specifically in male germline cells with Miwi2 additionally in Sertoli cells (Kuramochi-Miyagawa et al. 2001; Carmell et al. 2007), somatic supporting cells within seminiferous tubules.

Consistent with their expression pattern, mutations of PIWI proteins in *Drosophila* exhibit defects in both male and female germ cell development (Cox et al. 2000; Li et al. 2009; Malone et al. 2009) while all three PIWI proteins are required specifically for spermatogenesis in mouse with no obvious defects in female knockout mice (Deng and Lin 2002; Kuramochi-Miyagawa et al. 2004;

Carmell et al. 2007). Early studies in *Drosophila* showed that PIWI proteins function in the self-renewal of germline stem cells (Cox et al. 1998). Localization studies revealed that they are components of the polar granule (Megosh et al. 2006), an electron-dense structure also known as nuage found specifically in *Drosophila* germline and often associated with mitochondria (Mahowald 2001). Analogous germline structures are also seen in other organisms including P-granules in *C. elegans*, the mitochondrial cloud in *Xenopus*, and the chromatoid body (CB) free in the cytoplasm and inter-mitochondrial cement (IMC) associated with mitochondria in mammalian testes (Saffman and Lasko 1999). However, it was not until the discovery of their small RNA partners that people start to gain insights into the molecular function of PIWI proteins.

The discovery of a distinct group of small RNAs (24- to 30-nucleotide-long) associated with PIWI proteins was made by four independent groups in mammalian system around the same time (Aravin et al. 2006; Girard et al. 2006; Grivna et al. 2006a; Watanabe et al. 2006). Subsequently, piRNAs were also discovered in other model systems including *Drosophila* (Saito et al. 2006; Vagin et al. 2006) and zebrafish (Houwing et al. 2007; Houwing et al. 2008) by similar efforts. Mass sequencing projects revealed more than 52,000 piRNAs associated with Miwi and more than 1000 piRNAs with Mili. Most of them are derived from clusters of a few hundred sites in the genome (Aravin et al. 2006; Girard et al.

2006). More detailed studies on the biogenesis and function of piRNAs were carried out in *Drosophila*.

In *Drosophila*, the majority of piRNAs are derived from a limited number of pericentromeric and telomeric sites that are devoid of protein coding genes and instead are enriched in transposon sequences and other repeats (Brennecke et al. 2007). It is therefore suggested that the function of piRNAs is to repress transposon activities either by potential degradation of retrotransposon mRNAs or by epigenetic repression of transposon encoding regions via DNA methylation. However, only 17% of the piRNAs in mice were found to map to repeated elements in the mouse genome (Girard et al. 2006), suggesting other roles of piRNAs including epigenetic control (Pal-Bhadra et al. 2004; Yin and Lin 2007), translational control (Grivna et al. 2006b; Unhavaithaya et al. 2009), and other functions that need to be stringently tested.

Currently, two models for piRNA biogenesis have been suggested: the primary processing pathway and the amplification loop pathway (also known as the Ping-Pong pathway) (Fig. 1.4). The primary processing pathway generates piRNAs by sampling of long single-stranded precursors that are transcribed from piRNA clusters. Beyond this, the detailed mechanism of the primary processing pathway is largely unknown, except for the preference for a 5' uridine residue and association with Piwi. The amplification loop pathway is suggested by sequence analysis of piRNAs associated with each PIWI proteins. In *Drosophila*, Aub and

Piwi are associated mainly with antisense piRNAs that have a strong preference for a 5' uridine (U). In contrast, Ago3 is associated with sense piRNAs that predominantly contain adenosine (A) at the 10th nucleotide from the 5' end. Furthermore, piRNA sequences found in the Aub/Piwi- and Ago3-associated small RNA libraries are often complementary by precisely 10 nt at their 5' ends (Brennecke et al. 2007; Gunawardane et al. 2007). Therefore, it is speculated that an initial mixture of sense and antisense piRNAs were produced from clusters of random arrangement of transposon fragments and populates Aub and Piwi. When encountering a complementary target, a retrotransposon transcript or a piRNA cluster transcript, Piwi/Aub complexes cleave the target 10 nt away from A, which is complementary to the 5' end U of the piRNA, thus inactivating the target and also creating the new Ago3-associated piRNA with another cleavage event to generate the 3' end. Loaded Ago3 complexes can also target complementary transposon transcripts and generate Piwi/Aub-associated piRNA, forming a self-amplification loop. This amplification loop has also been implicated in zebrafish (Houwing et al. 2007) and in mammals (Aravin et al. 2007).

Recently, a number of other proteins have been found in the piRNA pathway. Most of these proteins were first identified in *Drosophila* through genetic screens for mutations that disrupt oogenesis. However, the mechanism of each protein in the piRNA pathway is still obscure. Zucchini and Squash were proposed to be nucleases (Pane et al. 2007). Armitage (Cook et al. 2004) and

Vasa (Hay et al. 1988) are germline-specific RNA helicases. Krimper (Lim and Kai 2007) and Spindle E (Kennerdell et al. 2002) are tudor-domain containing proteins, with Spindle E also a putative helicase. Maelstrom contains a High Mobility Group box, which is believed to mediate DNA binding (Clegg et al. 1997). Pimet modifies 3' end of the piRNA with 2'-O-methylation (Horwich et al. 2007; Saito et al. 2007), but the significance of this modification is unclear since mutation of Pimet in *Drosophila* results in mild or no phenotype, while mutations in all of the other proteins lead to female sterility.

Similar proteins have also been identified in the mammalian piRNA pathway. MVH, mouse homolog of Vasa, and Maelstrom are crucial for male germ cell development (Tanaka et al. 2000; Soper et al. 2008). A number of family members of the Tudor-domain containing proteins have also been implicated in the piRNA pathway to interact with discrete PIWI proteins, but only deficiencies in Tdrd1, 6, and 9 have been shown to lead to male infertility (Chuma et al. 2006; Shoji et al. 2009; Vasileva et al. 2009; Siomi et al. 2010). Additionally, Gasz (Germ cell protein with Ankyrin repeats, Sterile alpha motif, and leucine Zipper) has been shown to function to suppress retrotransposon expression with its detailed protein function unknown (Ma et al. 2009).

Notably, virtually all the proteins described above are enriched in the germinal granule/nuage, which is often associated with mitochondria. Studies in fetal piRNA pathway in mice suggest that there are two kinds of nuage with

distinct protein components. Immunostaining and immuno-electron microscopy of the piRNA-pathway proteins revealed that Mili and Tdrd1 are predominantly found between adjacent mitochondria, reminiscent of IMC while Miwi2, Tdrd9, and Maelstrom are perinuclear and appear similar to CB. MVH is detected in both structures but the significance of this observation is still unknown. Interestingly, many components of P-body, cytoplasmic complex of miRNA pathway for mRNA storage or degradation, are also found in CB. Therefore, the authors denoted IMC as being pi-body-like and CB piP-body-like (Aravin et al. 2009).

Interestingly, individual mutations in many of the piRNA pathway proteins have been shown to be able to disrupt the germinal structure. In *Drosophila*, it is found that mutants of Aubergine, Krimper, Spindle-E, and Vasa exhibited dispersed localization of Aub and Ago3 (Malone et al. 2009), while IMC is disappeared in Tdrd1 and MVH knockout mice (Chuma et al. 2006). It would be helpful to understand the mechanism if the assembly of piRNA complex is fully understood.

Unlike most piRNA-pathway proteins, *Drosophila* Piwi localizes predominantly to nuclei with some of them in the cytoplasmic nuage (Cox et al. 2000; Saito et al. 2006; Brennecke et al. 2007). These observations suggest a compartmentalized model for piRNA biogenesis and function (Lim and Kai 2007). In the cytoplasm, Aub- and Ago3-associated piRNAs inactivate transposon transcripts in nuage and generate new populations of piRNAs. Some of the mature

antisense piRNAs are loaded to Piwi and then imported to the nucleus to mediate heterochromatin assembly and transcriptional silencing.

With more knowledge gained during the past years, more open questions remain to be solved in the piRNA field. A lot of proteins identified in the pathway still require close examination of where and what the function is. Why does the absence of one particular protein lead to the disappearance of the whole complex for piRNA biogenesis? Among the rest of piRNAs in mice that are not repeat sequence associated, what are their functions?

Fig. 1.1 Model for mitochondrial dynamics. Cartoon adapted from (Huang and Frohman 2009).

A. Model for mitochondrial fusion and trafficking. During fusion, the mitochondrial outer membrane proteins Mitofusin 1 and 2 tether adjacent mitochondria through their coiled-coil domains, bringing the MitoPLD dimer into close contact with its substrate, cardiolipin, at the opposing mitochondrial membrane. This generates PA, which facilitates outer membrane fusion. Inner membrane fusion is performed by an intermembrane protein, Opa1. Mitochondrial movement along microtubules is promoted by the interaction of an outer membrane protein, Miro, with kinesin, through an adaptor protein.

B. Model for mitochondrial fission. The fission protein, Fis1, resides in the mitochondrial outer membrane and recruits Drp1 to perform mitochondrial fission. Drp1 assembles around the fission site to create membrane constriction.

Fig. 1.1

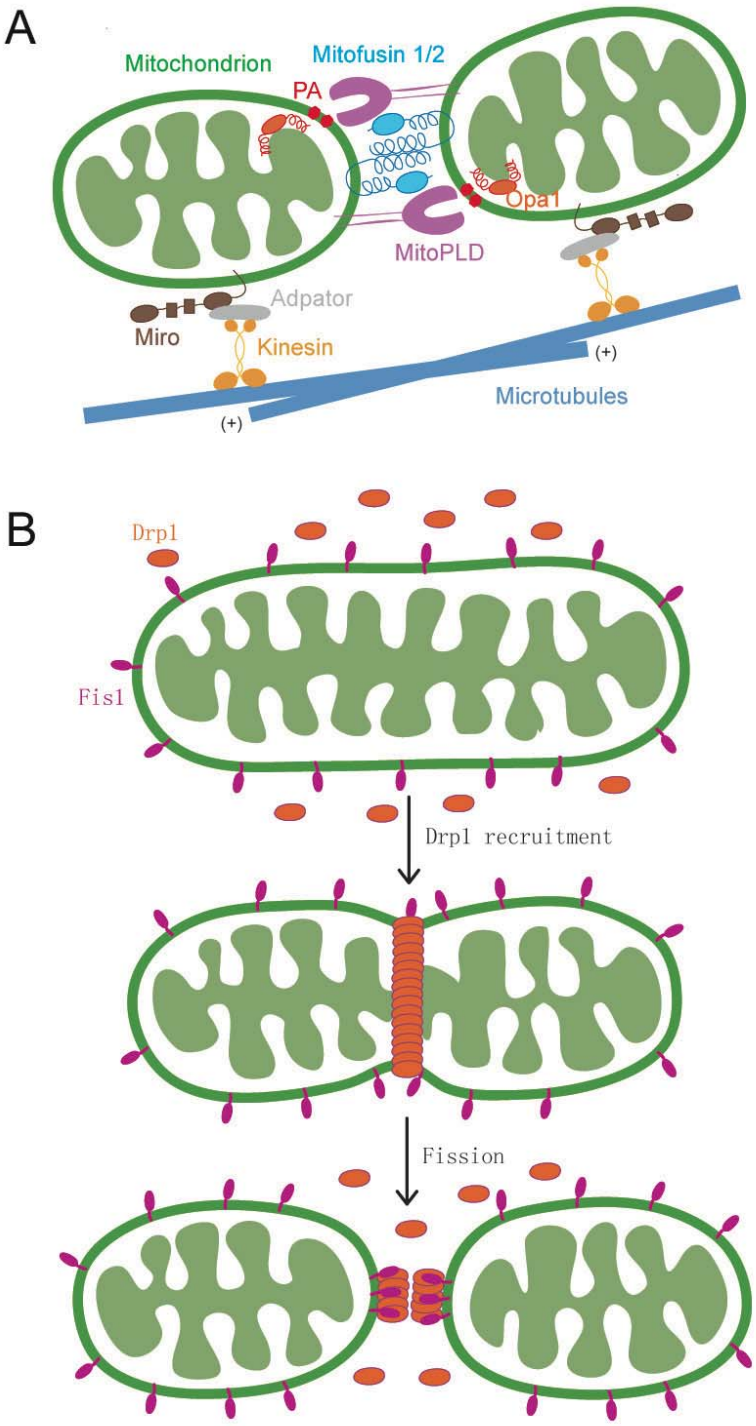
A
Mitochondrion
Mitofusin 1/2
PA
Opa1
MitoPLD
Adpator
Miro
Kinesin
(+)
(+)
Microtubules
B
Drp1
Fis1
Drp1 recruitment
Fission

Fig. 1.2 Mitochondrial fusion assays. Cartoon reproduced from (Jakobs 2006).

A. Classic fusion assay. Mitochondria from two groups of cells are labeled with matrix-targeted GFP and DsRed2 respectively. Upon cell fusion induced by PEG, the mitochondria fuse and matrix contents become intermixed. Mitochondrial fusion ability is scored by the appearance of yellow mitochondria.

B. Photoactivation. Mitochondria are co-labeled with matrix-targeted DsRed2 and photoactivatable-GFP, the latter of which fluoresces only after irradiation. A defined region is highlighted by a pulse of intense laser light at 413 nm and movement of the photoactivated PA-GFP is followed. The redistribution of GFP signal between fused mitochondria gives both green and red fluorescence.

C. Proposed split-FP fusion assay. Non-fluorescent split fragments of the fluorescent protein (example of split-YFP illustrated here) are introduced into mitochondria matrix of two cells. Upon chemical-induced cell fusion followed by mitochondrial fusion, the split fragments are brought together by two strongly interacting protein domains and reassembled to create a fluorescent protein. The intensity of the fluorescence signal is an indication of the mitochondrial fusion rate.

Fig. 1.2

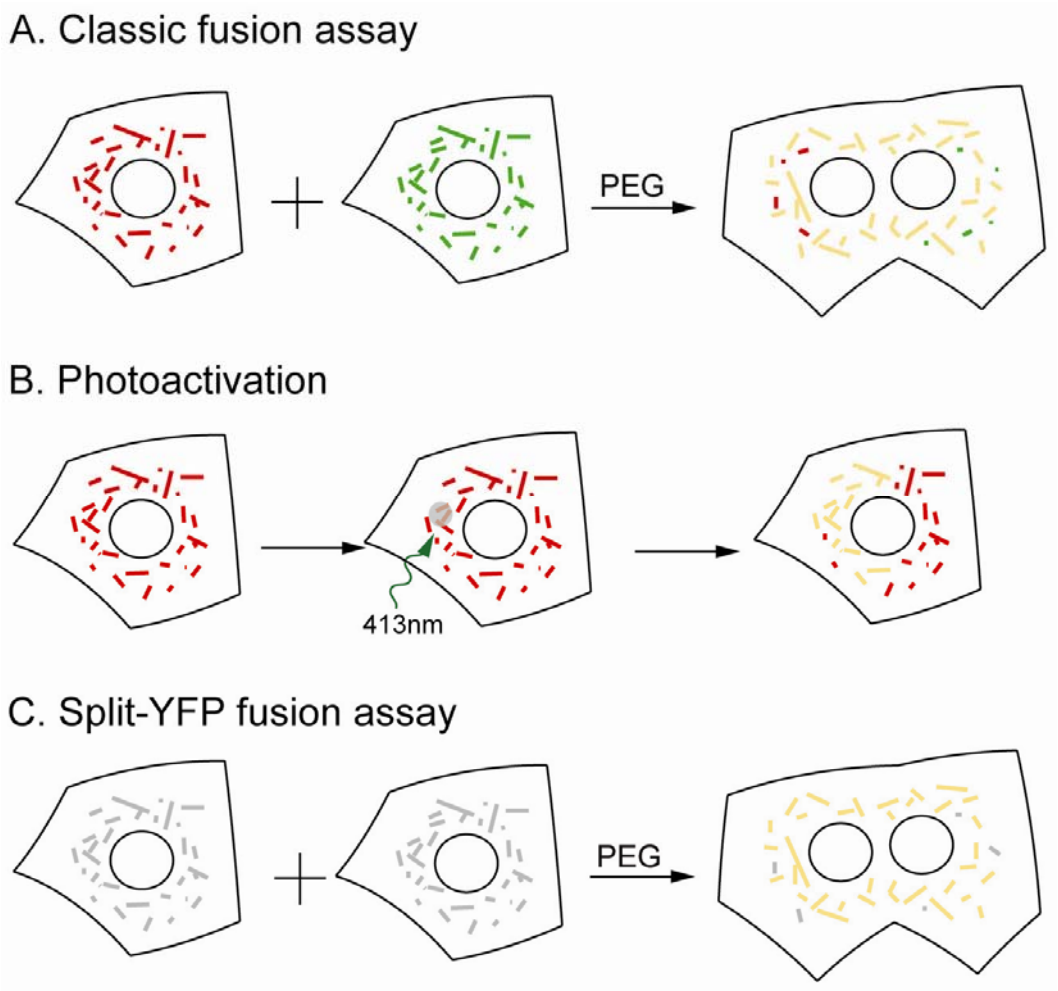
A. Classic fusion assay
PEG
B. Photoactivation
413nm
C. Split-YFP fusion assay
PEG

Fig. 1.3 Transmembrane topology of LPP and domain structure of PAP1 enzymes.

A. Transmembrane topology of LPP. Shown in green bars are transmembrane domains of LPP. The catalytic motif is located in the third and fifth extramembrane loops shown in orange. See text for details.

B. Cartoon depiction of the Lipin family in mouse. Regions of highest amino acid identity are shown as blue bars, known as the NLIP and CLIP domains. Nuclear localization signals (NLSs) are shown as red lines, which also characterize PA-binding domains. Lipin 1a and Lipin 1b are alternatively-spliced isoforms of the *Lpin1* gene product, with an additional 34 amino acids in Lipin 1b protein (from 242 to 275). The conserved catalytic domain (DxDxT) is also shown, followed closely by the coactivator motif (LxxIL).

Fig. 1.3

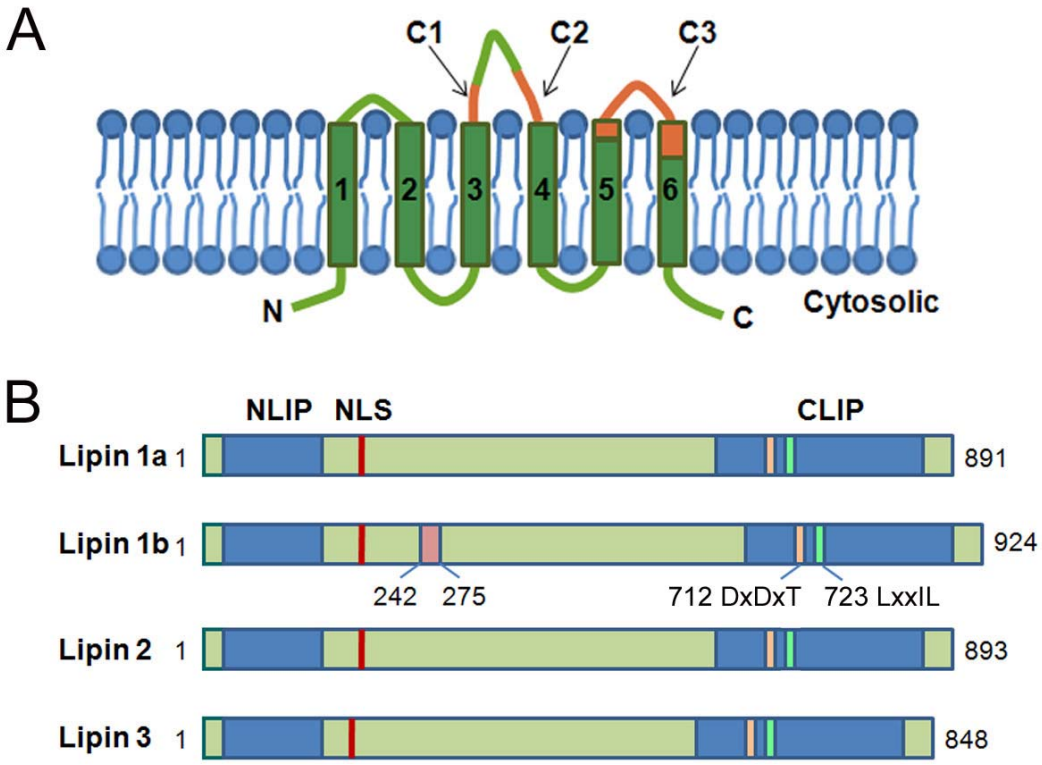
A
C1
C2
C3
1
2
3
4
5
6
N
C
Cytosolic
B
NLIP
NLS
CLIP
Lipin 1a 1
891
Lipin 1b 1
924
242
275
712 DxDxT
723 LxxIL
Lipin 2 1
893
Lipin 3 1
848

Fig. 1.4 piRNA biogenesis pathways.

A. Primary processing pathway. Long single-stranded precursors are transcribed from piRNA clusters located in pericentromeric or telomeric sites. Usually the antisense strands are processed into piRNAs, which are further loaded to Piwi.

B. Amplification loop pathway. An initial Aub/Piwi-associated piRNA recognizes its complementary target, either a retrotransposon transcript or a piRNA cluster transcript. The Piwi/Aub complex inactivates the target by a 5' cleavage and loads it to Ago3. The Ago3 complex further performs a 3' cleavage to produce a sense piRNA, which can also inactivate complementary targets and generate Piwi/Aub-associated piRNA.

Fig. 1.4

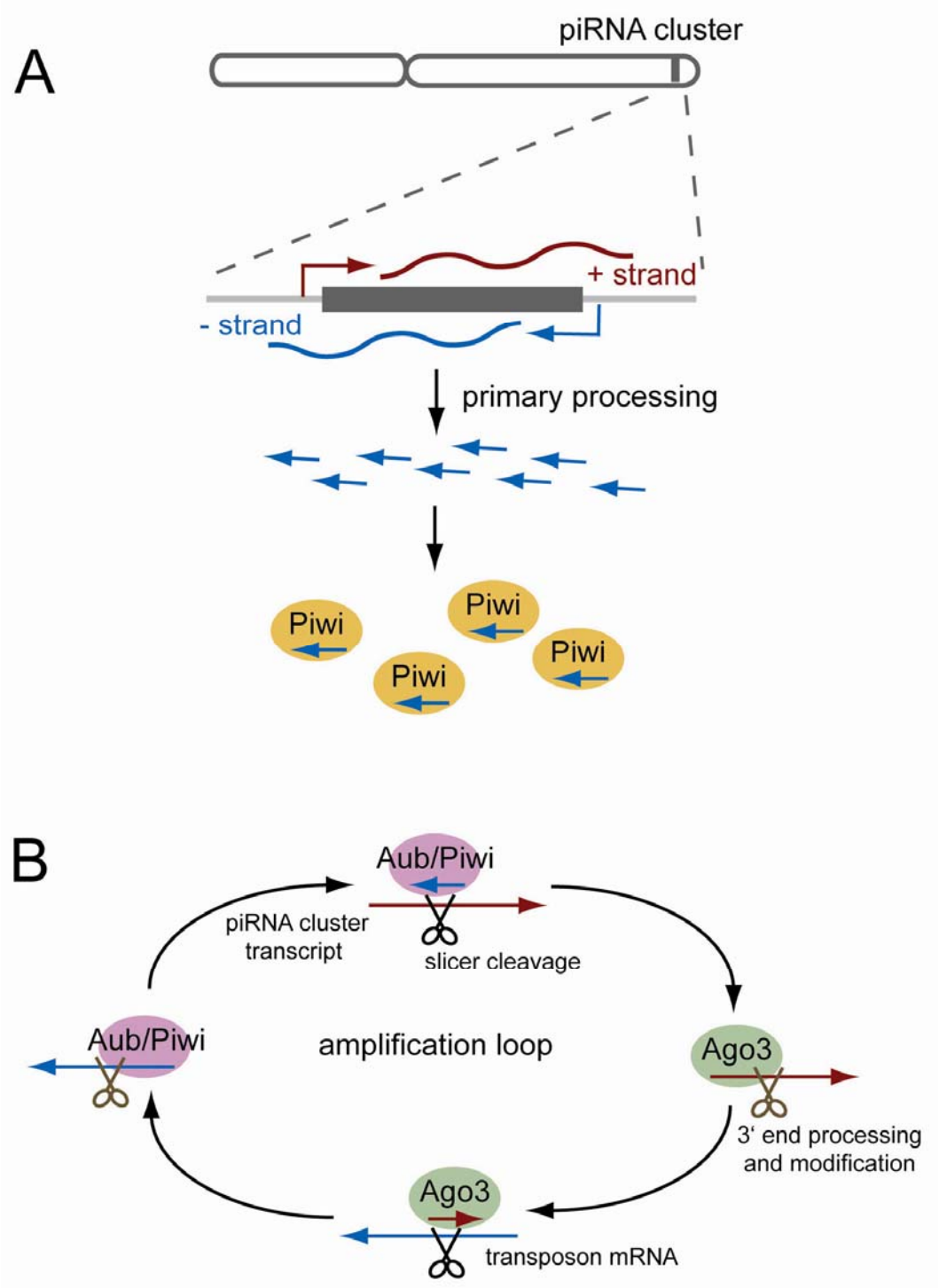
A
piRNA cluster
+ strand
- strand
primary processing
Piwi
Piwi
Piwi
Piwi
B
Aub/Piwi
piRNA cluster transcript
slicer cleavage
Aub/Piwi
amplification loop
Ago3
3' end processing and modification
Ago3
transposon mRNA

Chapter 2: A quantitative assay for mitochondrial fusion using *Renilla* luciferase complementation

This chapter has been accepted by Mitochondrion. The majority of the data were produced by Huiyan Huang. The constructs for the assay were designed and generated by Seok-Yong Choi.

2.1 Summary

Mitochondria continuously undergo fusion and fission, the relative rates of which define their morphology. Large mitochondria produce energy more efficiently, whereas small mitochondria translocate better to subcellular sites where local production of ATP is acutely required. Mitochondrial fusion is currently assayed by fusing together cells expressing GFP or RFP in their mitochondria and then scoring the frequency of cells with yellow mitochondria (representing fused green and red mitochondria). However, this assay is labor

intensive and only semi-quantitative. I describe here a reporter system consisting of split fragments of *Renilla* luciferase and YFP fused to mitochondrial matrix-targeting sequences and to leucine zippers to trigger dimerization. The assay enables fusion to be quantitated both visually for individual cells and on a population level using chemiluminescence, laying the foundation for high throughput small molecule and RNAi screens for modulators of mitochondrial fusion. I use the assay to examine cytoskeletal roles in fusion progression.

2.2 Introduction

Regulating the balance of mitochondrial fusion and fission is fundamentally important (Chan 2006), since disturbances result in mitochondrial dysfunction that causes neurodegenerative disease (Zuchner et al. 2004; Chen et al. 2007) or death of the individual (Chen et al. 2003; Waterham et al. 2007). Cells with predominant fission have small mitochondria, whereas cells with predominant fusion have large, tubulated mitochondria. The relative rates of fusion and fission are regulated by many types of signaling mechanisms (McBride

et al. 2006). Metabolic demands, such as signaled by insulin receptor activation, lead to a generalized increase in mitochondrial size and tabulation (Pawlikowska et al. 2007), potentially because larger mitochondria are more efficient producers of energy (Chen et al. 2003). On the other hand, increased needs for energy production at specific subcellular sites, for example at the rear of migrating cells where myosin activity is located (Campello et al. 2006), or at axonal sites of nerve growth factor signaling (Chada and Hollenbeck 2004), cause mitochondria to fragment and translocate to those sites. As well, mitochondria undergo fragmentation during apoptosis (Suen et al. 2008), and undergo extensive fission and then fusion during the cell cycle (Margineantu et al. 2002).

Several proteins mediating mitochondrial fusion and fission have been identified, although many aspects of how they function remain unknown. In the context of signaling-regulated changes in mitochondrial morphology, the best understood component is Drp1, which mediates fission (Chan 2006). Drp1 translocation to mitochondria and the ensuing fission is regulated by signaling-activated phosphorylation (Han et al. 2008) and/or dephosphorylation (Cereghetti et al. 2008), SUMOylation (Braschi et al. 2009), and S-nitrosylation (Cho et al. 2009). In contrast, little is known about the signaling mechanisms that regulate activity of Mfn1, Mfn2, and Opa1, the proteins that mediate mitochondrial fusion. As a consequence, although mutation of key sites in Drp1 that respond to signaling cues have suggested that controlling fission rate is an important factor in

dynamically controlling mitochondrial morphology, relatively little is known about whether rates of fusion are also controlled by signaling processes or other cues. Moreover, there is a lack of consensus about the role of the cytoskeleton in facilitating mitochondrial movement and morphology, with reports variously suggesting dominant roles for F-actin, for microtubules, or for intermediate filaments (IFs) (Anesti and Scorrano 2006).

Mechanistic studies of mitochondrial fusion have relied heavily on a mitochondrial fusion assay reported in 2002 (Legros et al. 2002). In this assay, fluorescent proteins are targeted to the mitochondrial matrix; one line of cells expresses mitochondria-targeted GFP, and another, mitochondria-targeted RFP. The cell lines are co-cultured on a coverslip until confluent, and then fused using polyethylene glycol, following which mitochondrial fusion events lead to matrix mixing and ensuing yellow mitochondria. The assay is generally allowed to proceed for 7-16 hours, and the frequency of cells with yellow mitochondria then recorded as a measure of fusion. However, this approach requires manually scanning each experimental sample using confocal microscopy to find and score several hundred fusion events, and thus is labor-intensive and not easily quantifiable or capable of gathering information about kinetics of the reaction. More recently, a quantitative mitochondrial fusion assay has been developed using photoactivatable GFP. Live cell confocal microscopy is used to monitor mitochondrial fusion via the matrix-targeted photoactivated GFP in combination

with matrix-targeted red fluorescence protein after a defined region of interest is irradiated (Karbowski et al. 2004; Twig et al. 2006). Although this method allows real time and quantitative analysis of mitochondrial fusion, it can only track limited regions of the mitochondria in one cell at a time, making it challenging to gather information on a population level, and the approach is labor-intensive for quantification.

To address these needs, I have employed a split-protein complementation system to develop a quantitative, less labor-intensive, and population-based mitochondrial fusion assay. The system consists of two inactive fragments split from a reporter protein that exhibit function only upon association. The association is promoted through fusion of the reporter protein fragments to a pair of strongly-interacting proteins (matched synthetic leucine zippers), and targeting to the mitochondrial matrix is achieved using a mitochondrial localization sequence (MLS). I validate the assay by demonstrating a loss of signal in the absence of the pro-fusion protein Mfn or mitochondrial potential or glycolytic energy sources. Finally, I examined the role of the cytoskeleton, and in particular, IFs, in mitochondrial fusion, a relatively unexplored and unsettled topic, as a proof-of-concept.

2.3 Materials and methods

Materials. Cell culture media DMEM were purchased from Invitrogen (Carlsbad, CA). Oligomycin, 2-deoxyglucose, valinomycin, CCCP, taxol, nocodazole, cytochalasin D, acrylamide and 2,5-hexanedione were purchased from Sigma (St Louis, MO). Jasplakinolide was purchased from Calbiochem (La Jolla, CA).

Plasmid construction. To construct the plasmid N-MitoVZL, DNA sequences encoding amino acid residues 1-173 of mVenus (monomeric Venus fluorescent protein) (Rizzo et al. 2006), a linker GGSGSGSS, the synthetic leucine zipper peptide (Z1) ALKKE**L**QANKKE**L**AQLKWE**L**QALKKE**L**AQ (Magliery et al. 2005), another GGSGSGSS linker (L), an HA epitope peptide, and finally residues 1-91 of hRLuc, were fused in tandem (see Fig. 2.2B). C-MitoLZV was generated by fusing DNA sequences encoding residues 92-311 of hRLuc, a FLAG epitope peptide, a linker GGSGSGSS, the complementary synthetic antiparallel leucine zipper peptide (Z2) ASEQ**L**EKKLQA**L**EKKLAQ**L**EWKNQA**L**EKKLAQ, another GGSGSGSS linker, and finally residues 155-238 of mVenus. The chimeric coding regions were cloned into a pQCXIP retroviral vector (Clontech, Mountain View, CA) containing the MLS SVLTPLLLRGLTGSARRLPVPRAKIHSL at the N-

terminus of the final protein product. Vector sequences are available upon request.

Viral infection and stable population selection. The split constructs, together with pVSVG (Clontech, Mountain View, CA), were transfected separately into GP2-293 cells using FuGene HD transfection reagent (Roche Applied Science, Basel, Switzerland). The viruses were collected 48 hours later, filtered, and used to infect cells in medium containing 6 μg/ml polybrene (Sigma, St Louis, MO). Stably-transfected cell populations were selected 2-3 days after infection using puromycin (InvivoGen, San Diego, CA) at 5 μg/ml for HeLa cells and wild-type (wt) MEF cells, 10 μg/ml for COS-7 cells, and 2 μg/ml for Mfn1/2$^{-/-}$ MEF cells for two weeks.

Cell culture and mitochondrial fusion assay. GP2-293, HeLa and COS-7 cells were maintained in DMEM supplemented with 10% calf serum (Hyclone, Logan, UT). Mfn 1/2$^{-/-}$ MEF and wt MEF cells were maintained in DMEM supplemented with 10% fetal bovine serum (Hyclone, Logan, UT).

For the mitochondrial fusion assay, a total of 4 x10^5 cells were cultured per well in 12-well plates 18 hours before cell fusion. Cycloheximide (100 μg/ml (HeLa), 50μg/ml (COS-7 and wt MEFs) or 400 μg/ml (Mfn1/2$^{-/-}$ MEFs), optimal concentrations pre-determined by fusing each cell type in increasing concentrations of cyclohexamide until baseline levels of luciferase activity were attained, as depicted in Fig. 2.3A for HeLa cells) was added 30 min before fusion

and kept in the media thereafter. The cells were incubated with 50% PEG-1500 (Roche Applied Science, Basel, Switzerland) for 60 seconds, washed four times with complete media, cultured for the indicated times, and harvested in 5 mM EDTA in PBS. Cell pellets were stored frozen until all samples were ready for the *Renilla* luciferase activity assay.

For drug treatments, the mitochondrial inhibitors were added to the media after PEG treatment to avoid impairing the cell fusion efficiency. Drugs that disrupted cytoskeleton components were added 30 minutes before PEG treatment, except for jasplakinolide and cytochalasin D, which shrank the cells promptly after treatment and thus dramatically decreased the extent of cell fusion. Instead, jasplakinolide and cytochalasin D were added to the media 1 hr after PEG treatment, by which point the cells are thought to have completed the plasma membrane fusion process.

Vimentin Stealth RNAi^{TM} siRNA and control siRNA were purchased from Invitrogen (Carlsbad, CA) and transfected into cells using Lipofectamine^{TM} RNAiMAX transfection reagent (Invitrogen, Carlsbad, CA). The cells were harvested 72 hours later, plated, and cultured overnight before being used in the fusion assay.

***Renilla* luciferase activity assay.** *Renilla* luciferase activities were measured using *Renilla* Luciferase Assay System (Promega, Madison, WI). Briefly, cells collected at the indicated time points were lysed in 1x *Renilla* luciferase assay

buffer, mixed with *Renilla* luciferase assay substrate diluted in *Renilla* luciferase assay buffer, and measured for luminescence using a 20/20 single-tube luminometer (Turner) with integration time of 5 seconds.

Western blotting. Cell lysates were subjected to 10% SDS–PAGE, transferred to nitrocellulose membranes, and probed with primary antibodies recognizing the HA epitope (3F10; Roche Applied Science, Basel, Switzerland), FLAG epitope (M2; Sigma, St Louis, MO), α-tubulin (B-5-1-2; Sigma, St Louis, MO), vimentin (clone V9; Sigma, St Louis, MO), or β-actin (Sigma, St Louis, MO), followed by secondary antibodies conjugated with Alexa 680 (Molecular Probes, Carlsbad, CA) or IRDye 800 (Rockland Immunochemicals, Gilbertsville, PA). Fluorescent signals were detected with an Odyssey infrared imaging system (LICOR Biosciences, Lincoln, NB).

Immunofluorescence microscopy. HeLa cells stably expressing the split constructs were mixed and plated onto coated coverslips. Twenty four hours later, they were stained with 500 nM MitoTracker Deep Red 633 (Molecular Probes, Carlsbad, CA) for 30 min, fixed with 4% paraformaldehyde for 15 min, permeabilized with 0.1% Triton X-100 for 10 min, and blocked with 5% normal goat serum. The cells were then immunostained using primary antibodies against the HA (Rockland Immunochemicals, Gilbertsville, PA) and FLAG (M2; Sigma, St Louis, MO) epitopes followed by fluorescent dye-conjugated secondary

antibodies. Stained cells were visualized using a Leica TCS SP2 confocal microscope. Images were processed using Adobe Photoshop.

Statistics. Experiments to determine appropriate concentrations of cyclohexamide to use were repeated three times. Kinetic experiments were repeated at least five times unless otherwise stated. Error bars on graphs display the standard deviation.

2.4 Results

A quantitative mitochondrial fusion reporter system usable for high throughput analysis

A previous lab member, Seok-Yong Choi, set out to develop a high-throughput plate-reader assay using the split-YFP system (Hu and Kerppola 2003) by adding a mitochondrial matrix-targeting sequence to the amino-termini of fragments of the Venus YFP in combination with a pair of complementary synthetic antiparallel leucine zipper peptides (Magliery et al. 2005) to trigger assembly of the fluorescent protein fragments upon mitochondrial fusion. However, the yellow fluorescent signal produced as a result of mitochondrial

fusion, which was readily visible using confocal microscopy (Fig 2.1), was not easily or sensitively detected using standard plate readers. Therefore, he further added split fragments of *Renilla* luciferase (RLuc) (Kaihara et al. 2003) to amplify the fusion signal and enable quantitative measurement via chemiluminescence (Fig. 2.2A, B). However, he failed to detect any luminescent signal when using the live cell substrate, ViviRen (Promega) for RLuc. I revisited Seok-Yong's design, and confirmed that the reporter components N-MitoVZL and C-MitoLZV exhibited stability as individually expressed proteins (Fig. 2.2C and western blot analysis, not shown, but see also Fig. 2.3C), and localized to mitochondria as designed (Fig. 2.2C). When I switched the substrate to the much more sensitive coelenterazine, though lysing the cells is required for this substrate, luciferase activity was observed when the reporter constructs were co-expressed (1,420,000 relative light unit (RLU), Fig. 2.1B), but not when they were expressed individually (< 50 RLU above negative control), and not to a substantial extent when expressed in different populations of cells that were then lysed and assayed together (< 700 RLU above negative control), indicating that < 0.1% of the non-complexed components reconstitute into active protein during the lysis and assay steps.

Validation of the *Renilla* luciferase reporter system for mitochondrial fusion

A key issue for the mitochondrial fusion assay is to ensure that protein synthesis ceases before cell fusion, since otherwise both of the reporter components would co-translocate to all mitochondria as newly-synthesized proteins and thus generate a false-positive signal. Cycloheximide (CHX) was used to block protein synthesis in co-cultures of HeLa cells stably expressing N-MitoVZL (HeLa N-MitoVZL) or C-MitoLZV (HeLa C-MitoLZV) and the cells then fused using PEG-1500 treatment (Fig. 2.3A). Measurement of luciferase activity in the cell lysates collected 7 hours after cell fusion showed that the luminescence decreased more than 90% as the concentration of CHX increased, reaching baseline at 100 μg/ml. The resulting output (138,000 RLU, n=3), which was approximately 1000-fold above the assay background (143 RLU, representing the signal obtaine from lysis of the co-cultures without PEG-1500-mediated fusion), accordingly came from reconstitution of the pre-existing split reporter components subsequent to the cell fusion event, rather than from association of co-translocated newly-synthesized reporter proteins.

I next followed the increase in luciferase activity as function of time subsequent to cellular fusion. In the classic assay, mitochondrial fusion is optimally scored at 7-16 hours post-cellular fusion. To my surprise, luciferase activity (7% of the peak activity) could be detected as early as 30 minutes after PEG-1500-induced cell fusion (in some experiments, activity could be detected within 10 minutes of the assay start point, data not shown), peaked at 3 hours at

1000-fold over background levels of activity, and then subsequently declined 2-fold (Fig. 2.3B). The decline in signal was partially due to the gradual degradation of the reporter proteins (Fig. 2.3C and D), which appeared to be less stable than α-tubulin, and death of a small fraction of the cells as triggered by the cell fusion and/or CHX treatment. This result indicated 3 hours after the cell fusion step to be an optimal assay time point, rather than 7-16 hours as in the classic assay. As expected, no increase in signal was observed over time in HeLa cells expressing each fragment alone, since the individual reporter constructs do not exhibit luciferase activity.

Mfn1 and 2 are key mediators of the mitochondrial fusion process (Chan 2006); in the absence of both isoforms, no fusion is thought to occur. To validate my fusion assay, I performed it in Mfn1/2$^{-/-}$ mouse embryo fibroblast (MEF) cells. Monitoring the luciferase signal over time revealed a small rise in chemiluminescence that peaked at 2 hour at 6% of the peak signal observed during fusion of control, wt MEF cells (Fig. 2.3E). The source of this low level of reporter reconstitution and signal in the fused Mfn1/2$^{-/-}$ cells is uncertain, but could reflect localization and reconstitution of a small fraction of the reporter proteins in the cytoplasm, release of the reporter proteins from mitochondria into the cytoplasm during apoptotic events, reconstitution during mitochondrial autophagy, or low levels of mitochondrial fusion independent of Mfn. Although visualization of the reporter constructs confirmed that they predominantly

localized to mitochondria (similar to Fig. 2.2C for HeLa cells and data not shown), low levels of mis-targeting to the cytoplasm cannot be ruled out.

Taken together, these findings show that the fusion assay is quantifiable and robust, with a 18:1 signal-to-noise ratio at 2 hours after cell fusion (in comparison to Mfn1/2$^{-/-}$ cells), and that it is capable of detecting fusion events within 30 minutes of the beginning of the assay period.

Mitochondrial fusion is selectively inhibited by mitochondrial inhibitors to different extents

The classic mitochondrial fusion assay has been used to demonstrate that glycolysis, but not ATP synthesis, is required in mitochondrial fusion (Malka et al. 2005). I thus examined effects of the glycolysis inhibitor, 2-deoxyglucose, and the ATP synthase inhibitor, oligomycin. Consistent with the prior report, oligomycin had no effect on mitochondrial fusion (Fig. 2.4A), whereas 2-deoxyglucose decreased the rate of fusion. It should be noted though that the pattern of luciferase activity over time is also informative. Although the rate of fusion was inhibited in cells cultured in 2-deoxyglucose (20% of the untreated control value at 1 hr, and 21% at 3 hrs), the luciferase signal continued to rise between 1 and 3 hours, suggesting that fusion was occurring, but 5-fold slower than in cells with normal glycolysis.

The classic mitochondrial fusion assay has also been used to show that dissipation of the mitochondrial membrane potential abolishes mitochondrial fusion (Malka et al. 2005). I further validated my assay by examining the effects of the protonophore, CCCP, and a potassium-specific ionophore, valinomycin, on the fusion reaction. Both inhibitors had a marked impact on fusion (Fig. 2.4B). An increase in luciferase signal was observed at 1 hour in the drug-treated cells, but the signal declined thereafter. In contrast, the control, untreated cells exhibited a 5-fold greater increase in RLU at 1 hour, and a 25-50 fold higher activity at 3 hours. The luciferase activity in the valinomycin and CCCP-treated cells at 3 hrs was similar in magnitude to that seen for the $Mfn^{-/-}$ cells (Fig. 2.3E), suggesting that after an initial modest round of fusion detectable at 1 hr, no further fusion occurred.

Taken together, these findings provide evidence that the split-luciferase mitochondrial fusion assay provides an accurate and quantitative method for assessing rates of fusion in mammalian cells.

Mitochondrial fusion efficiency depends on the integrity of intermediate filaments

Mitochondrial translocation proceeds primarily via microtubules in mammalian cells, and via the actin network in yeast (Boldogh and Pon 2007). Mitochondrial fragmentation occurs in yeast when cells are treated with actin-

depolymerizing drugs such as latrunculin (Drubin et al. 1993), and ablation of Kif5b, a member of the mouse Kinesin-1 family that regulates microtubule-based mitochondrial transport, results in mitochondrial clustering in the perinuclear region (Anesti and Scorrano 2006). I next examined the effect of taxol/nocodazole and jasplakinolide/cytochalasin D, which stabilize or destabilize microtubules and the actin network, respectively, without substantially affecting mitochondrial localization in HeLa cells (Fig 2.5A and B). However, no significant changes in luciferase activities were observed (Fig. 2.4C), indicating that mitochondrial fusion appears to proceed independently of microtubule and actin dynamics in HeLa cells.

It has recently been reported, however, that vimentin intermediate filaments interact with mitochondria, and that depletion of vimentin by siRNA causes mitochondrial fragmentation (Tang et al. 2008), which I confirmed for my cells as well (Fig. 2.6). It is not known, though, whether the fragmentation of mitochondria after vimentin knock-down is caused by inhibition of mitochondrial fusion, or by stimulation of mitochondrial fission. To address this question, I first treated cells with two compounds that have been shown to cause central collapse of the vimentin network, acrylamide and 2,5-hexanedione (Sager 1989), and found that they inhibited mitochondrial fusion in a dose-dependent manner (Fig. 2.4D). Integrity of the vimentin network appeared to be important, but not vital

for mitochondrial fusion, since only partial inhibition was observed (Fig. 2.4E; compare to Fig. 2.4B).

Acrylamide and 2,5-hexanedione cause degeneration of the peripheral nervous system, characteristics of patients with mutations in Mfn2, suggesting that their clinical effects might ensue from defect in mitochondrial fusion. However, these compounds presumably cross-link and impede the function of other proteins as well. Accordingly, to explore the importance of the vimentin network on mitochondrial fusion, I knocked down vimentin mRNA using two different siRNAs (Fig. 2.4F and Fig. 2.6), and found that mitochondrial fusion was decreased almost 10-fold in the absence of vimentin-based IFs in COS-7 cells (Fig. 2.4G). These results suggest that the vimentin-based intermediate network has a more profound role in promoting mitochondrial fusion in HeLa and COS-7 cells than do those of actin and tubulin.

2.5 Discussion

I have developed a quantitative and facile mitochondrial fusion assay that can be applied to the study of mechanistic and regulatory aspects of mitochondrial fusion. Microtubules are solidly established as directing long-range mitochondrial distribution in mammalian cells, with actin playing a role over short distances. However, due to the limitations of the widely-used 2-color, manually-scanned mitochondrial fusion assay, the roles of the different cytoskeletal networks in mitochondrial fusion have not been well delineated. A study using mitochondria-targeted photoactivatable GFP reported previously that microtubules function to transport mitochondria together during mitochondrial fusion (Liu et al. 2009), which differs from the finds I observed here. However, dependence on cytoskeletal components for mitochondria is known to be cell-type specific. In some cells, such as the myoblasts studied in Liu et al., the mitochondria are lined up with microtubules, while in others, such as NIH3T3 cells (Tang et al. 2008), mitochondria co-localize more with vimentin than with microtubules. In fact, microtubules are better recognized for their role in segregating mitochondria after fission: when mitochondrial fission is inhibited, novel structures consisting of thin mitochondrial extensions are formed, which can be prevented using a microtubule disrupting drug (Bowes and Gupta 2008). I show here that integrity of the vimentin IF network appears to be much more important to the progression of mitochondrial fusion than integrity of the microtubule or actin cytoskeleton networks, at least in HeLa and COS-7 cells. Vimentin interacts with microtubules,

and disruption of microtubules eventually leads to vimentin reorganization (Summerhayes et al. 1983). It is possible that some of the effects on mitochondrial morphology previously defined in the context of manipulation of microtubule networks might be indirect and ensue instead from the consequential effects on the vimentin network. It is also possible that some of the known mitochondrial dysfunctions might well be caused by primary problems in vimentin organization. Intriguingly, tau-like protein, which mediates the interaction of vimentin and tubulin (Capote and Maccioni 1998), causes neurodegenerative diseases such as Alzheimer's disease, a component of which I speculate could ensue from disrupting the tau-vimentin interaction, resulting in decreased mitochondrial fusion and hence increased sensitivity to apoptosis.

The assay described here provides a measure of complete mitochondrial fusion, that is, mixing of the matrix contents. However, the inner and outer mitochondrial membranes can fuse independently (Malka et al. 2005), and it would be possible to exploit my assay to examine each step discretely. For example, split *Firefly* luciferase (FLuc) (Paulmurugan and Gambhir 2007) could be similarly targeted to the intermembrane space or to the outer membrane. Since *Firefly* and *Renilla* luciferase use distinct substrates that luminescence in the presence of different cofactors, both could be measured sequentially in the same lysate sample. Such a dual luciferase activity assay would be more sensitive and

convenient than the three-color fluorescence method that has been used for the classic assay approach (Malka et al. 2005).

Fusion is scored in the traditional assay 7 or more hours after cell fusion, making it challenging to examine signaling events that take place in a shorter time frame. My assay robustly detects on-going fusion within 30 minutes after cell fusion, and in preliminary experiments, as quickly as 10 minutes after cellular fusion. Employing this new approach will enable many types of studies previously impractical to attempt.

A limitation to real-time measurements using the assay is that the method requires lysing cells to sample the luciferase activity. Live cell substrates exist for *Renilla* luciferase, such as ViviRen, EnduRen (Promega) and DeepBlue C (Jensen et al. 2002). However, at least in my hands, their sensitivity was modest and insufficiently robust for quantification. Intriguingly, a study on luciferase from *Gaussia princeps* showed that the signal from the humanized form of *G. princeps* luciferase (hGLuc) is 100-fold higher than the ones generated by hFLuc and hRLuc, and the substrate for hGLuc is membrane permeable (Remy and Michnick 2006), making it a very promising candidate for development of a real-time mitochondrial fusion assay in live cells.

The split *Renilla* luciferase system I described here quantitatively measures mitochondrial fusion rates in a high throughput manner, laying the

foundation for RNAi and small molecule screens for modulators of mitochondrial fusion.

Figure 2.1 Comparison of signal-to-noise ratio with split-Venus or split-*Renilla* luciferase reconstitution

(A) Visualization of reconstituted Venus fluorescence after fusion of HeLa cells stably expressing the split-*Renilla* luciferase constructs that had undergone fusion for 3 h in 100 μg/ml CHX.

(B) Luminescence of HeLa cells transiently expressing the control or indicated split-*Renilla* luciferase constructs. RLU, relative light unit.

Fig. 2.1

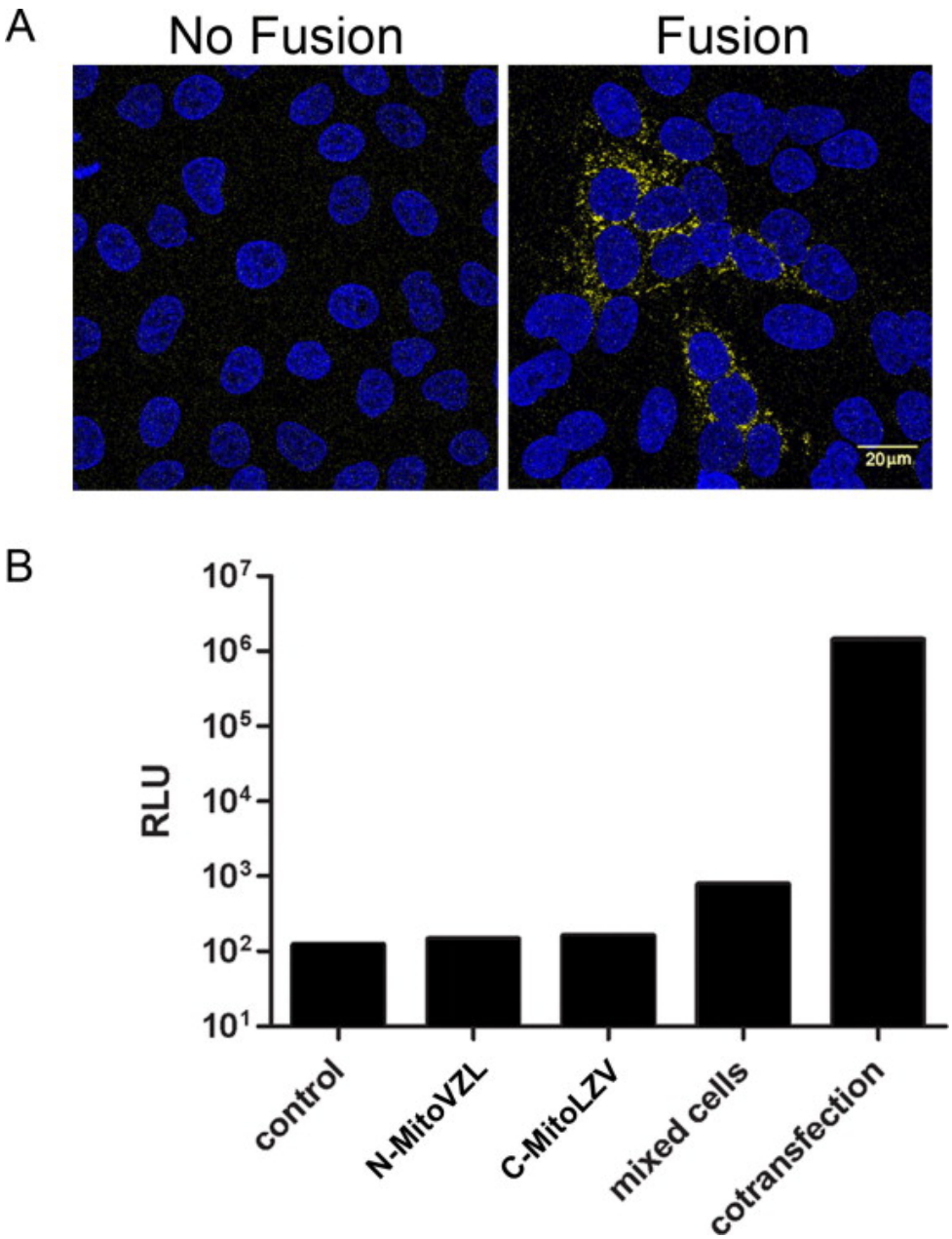
A
No Fusion
Fusion
20μm
B
RLU
10^7
10^6
10^5
10^4
10^3
10^2
10^1
control
N-MitoVZL
C-MitoLZV
mixed cells
cotransfection

Figure 2.2. Mitochondrial fusion quantification via split-*Renilla* Luciferase complementation.

(A) Principle of split-*Renilla* luciferase complementation to quantitate mitochondrial fusion. Upon fusion of two mitochondria individually expressing a hybrid protein encoding half of the split-*Renilla* Luciferase, the antiparallel leucine zipper pair (red) pulls the constructs together and the luciferase fragments reconstitute and generate luminescence in the presence of substrate. The split-Venus also reconstitutes and generates yellow fluorescence.

(B) Schematic representations of domain structures of split *Renilla* luciferase. Both constructs have a MLS in their N-termini. The N-terminal monomeric (m) Venus fragment is fused to the N-terminal hRLuc fragment with a leucine zipper peptide (Z1) in the middle flanked by two linkers (L) and an HA peptide. The C-terminal hRLuc fragment is fused with the C-terminal Venus fragment and the corresponding antiparallel leucine zipper peptide (Z2) flanked by the two same linkers (L) and a FLAG peptide.

(C) Mitochondrial localization of split *Renilla* luciferase constructs. HeLa cells expressing each construct were mixed and stained for the HA (green) and FLAG (red) epitopes built into the fusion proteins. Note that the anti-HA antibody non-specifically detects a speckled nuclear protein present in all cells. The mitochondria were stained with MitoTracker far red 633 (blue). Scale bar, 20 μm.

Fig. 2.2

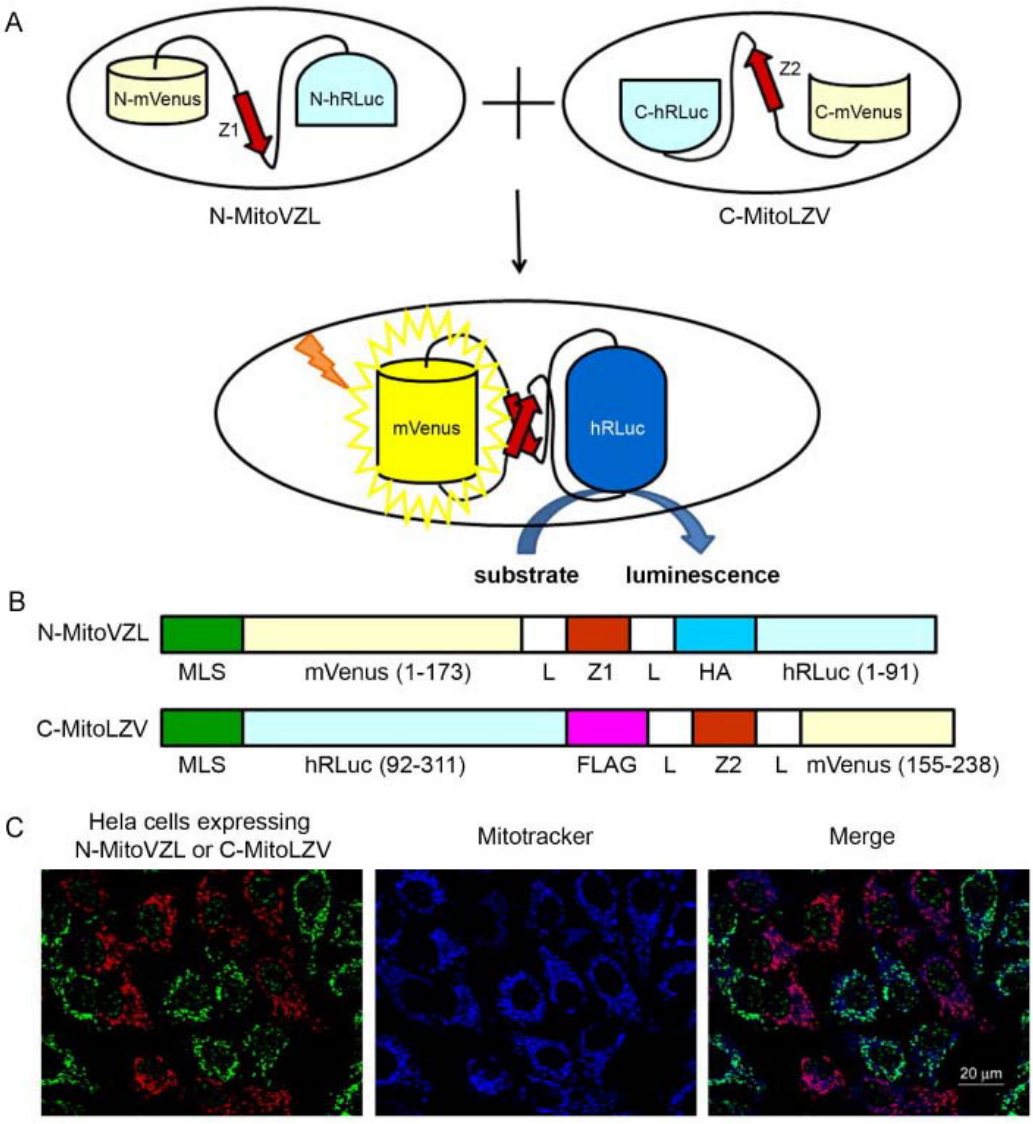
A
N-mVenus
Z1
N-hRLuc
N-MitoVZL
C-hRLuc
Z2
C-mVenus
C-MitoLZV
mVenus
hRLuc
substrate
luminescence
B
N-MitoVZL
MLS
mVenus (1-173)
L
Z1
L
HA
hRLuc (1-91)
C-MitoLZV
MLS
hRLuc (92-311)
FLAG
L
Z2
L
mVenus (155-238)
C
Hela cells expressing
N-MitoVZL or C-MitoLZV
Mitotracker
Merge
20 μm

Figure 2.3. Mitochondrial fusion kinetics measured by split-*Renilla* luciferase complementation.

(A) Luminescence of HeLa cells stably expressing the N-MitoVZL and C-MitoLZV split-*Renilla* Luciferase constructs 7 hours after PEG-1500 treatment to initiate cellular fusion, followed by mitochondrial fusion, in the indicated CHX concentrations.

(B) Luminescence of HeLa cells stably expressing N-MitoVZL and C-MitoLZV (black), N-MitoVZL only (green), and C-MitoLZV only (red) at the indicated times after PEG-1500 treatment in 100 μg/ml CHX. Time 0 represents the point of PEG-1500 addition; samples at time 0 were not treated with PEG-1500. % values indicate the RLU normalized to the signal at the 3 hr fusion time point.

(C) Western blot analysis of HeLa cell lysates harvested at indicated times after PEG-1500 treatment in 100 μg/ml CHX. N-MitoVZL was visualized using anti-HA antibody, and C-MitoLZV using anti-FLAG antibody.

(D) Quantification of protein levels in Fig. C normalized to α-tubulin.

(E) Luminescence of Mfn1/2$^{-/-}$ MEF cells stably expressing the split *Renilla* Luciferase constructs at indicated times after PEG-1500 treatment in 400 μg/ml CHX, in comparison to the levels of fusion observed for wt MEF cells. % values indicate the RLU normalized to that measured in wt MEF cells at the corresponding time-point.

Fig. 2.3

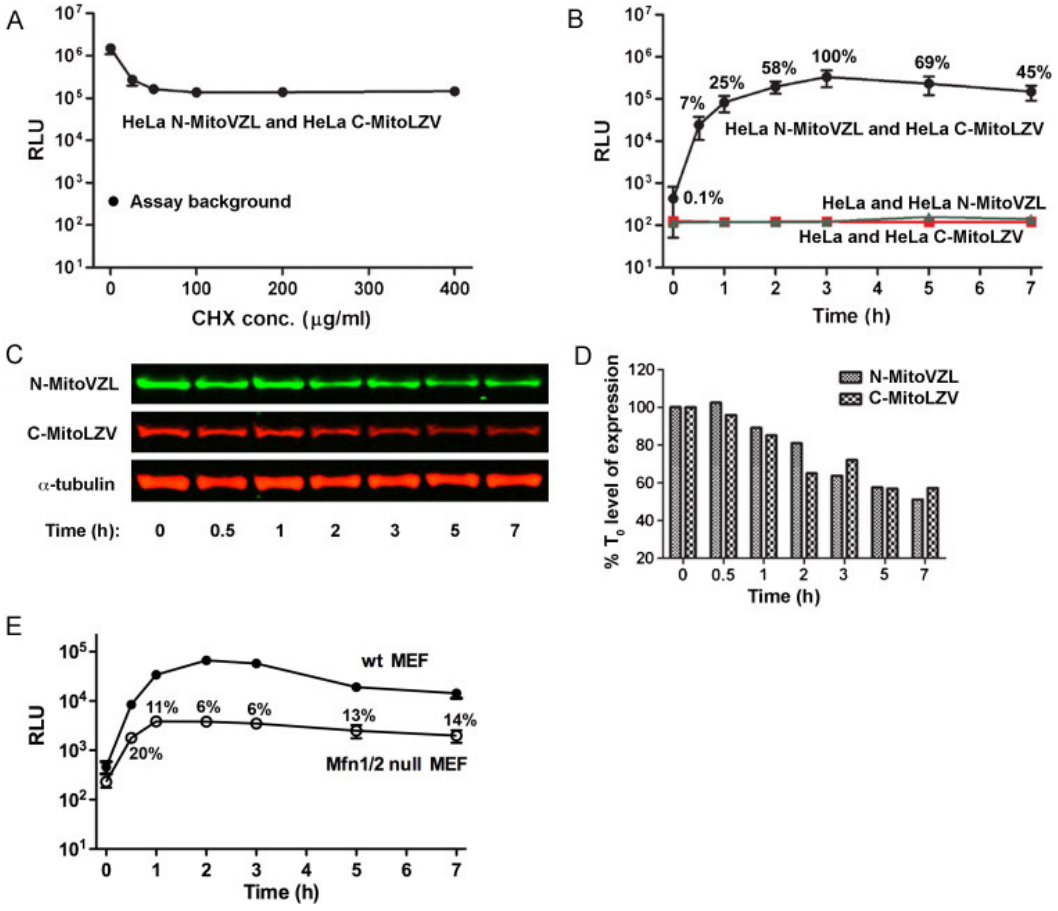
A
RLU
HeLa N-MitoVZL and HeLa C-MitoLZV
Assay background
CHX conc. (μg/ml)
B
RLU
7%
25%
58%
100%
69%
45%
HeLa N-MitoVZL and HeLa C-MitoLZV
0.1%
HeLa and HeLa N-MitoVZL
HeLa and HeLa C-MitoLZV
Time (h)
C
N-MitoVZL
C-MitoLZV
α-tubulin
Time (h): 0 0.5 1 2 3 5 7
D
% T0 level of expression
N-MitoVZL
C-MitoLZV
Time (h)
E
RLU
wt MEF
11%
6%
6%
13%
14%
20%
Mfn1/2 null MEF
Time (h)

Figure 2.4. Mitochondrial fusion rates are affected by mitochondrial function inhibitors and cytoskeleton integrity.

(A) Luminescence of HeLa cells stably expressing the split *Renilla* Luciferase constructs at the indicated times after fusion in 100 μg/ml CHX in combination with no drug, 2.5 μM oligomycin, or 40 mM 2-deoxyglucose in medium lacking glucose (glucose-lacking medium in itself did not alter rates of fusion in comparison to control medium; data not shown).

(B) Luminescence after cell fusion with no drug treatment, 10 μM valinomycin, or 10 μM CCCP.

(C) Luminescence after fusion with no drug treatment, 1 μM taxol, 5 μg/ml nocodazole, 2 μM jasplakinolide or 10 μM cytochalasin D.

(D) Luminescence 3 hours after fusion in the indicated acrylamide or 2,5-hexanedione concentrations.

(E) Luminescence after fusion with no drug treatment, 10 mM acrylamide, or 68 mM 2.5-hexanedione.

(F) Western blot analysis of vimentin 90 hours after siRNA transfection of COS-7 cells.

(G) Luminescence of COS-7 cells stably expressing the split *Renilla* Luciferase at the indicated times after cell fusion in 50 μg/ml CHX, 90 hours after control siRNA or vimentin siRNA transfection.

Fig. 2.4

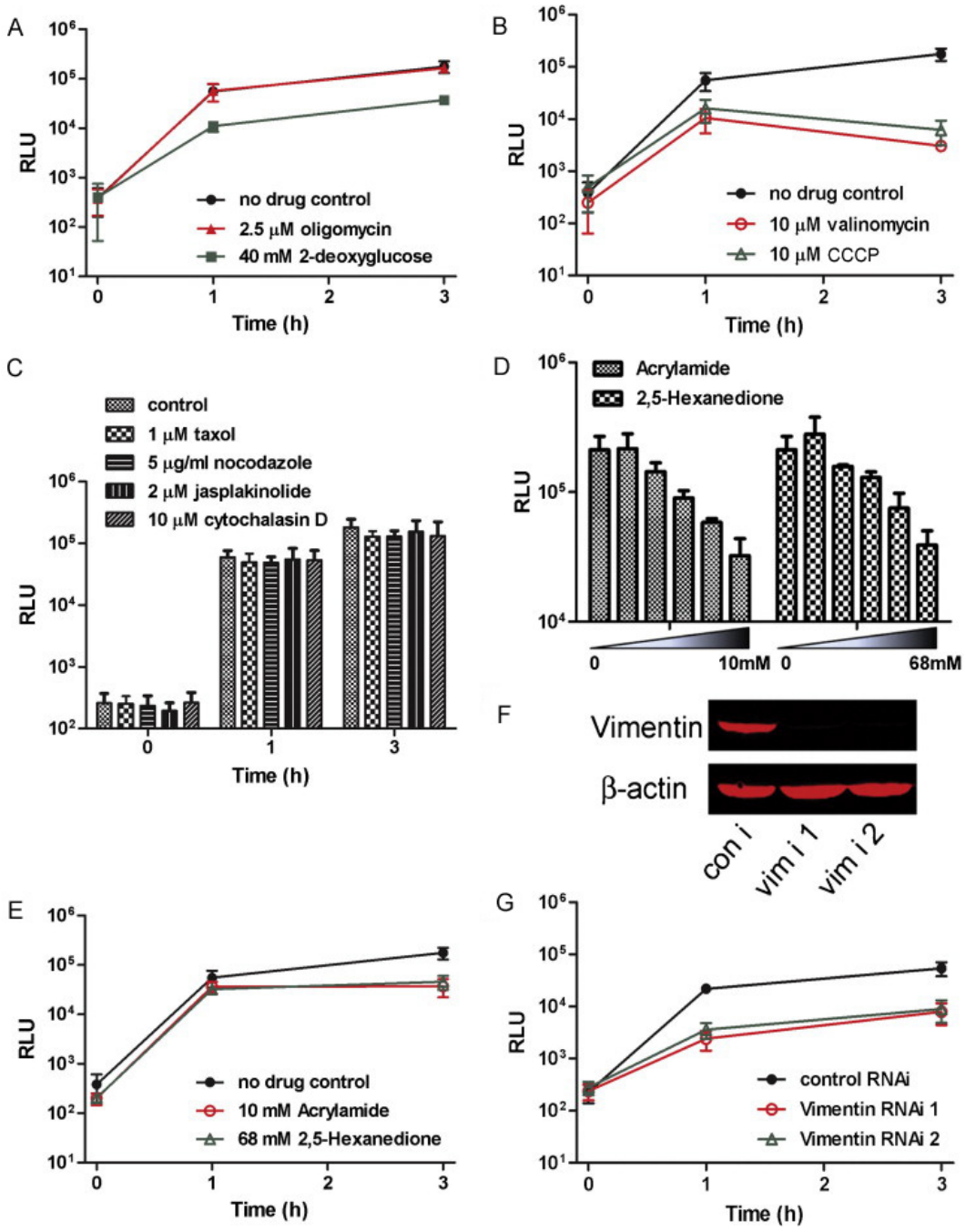
A
RLU
Time (h)
no drug control
2.5 μM oligomycin
40 mM 2-deoxyglucose
B
RLU
Time (h)
no drug control
10 μM valinomycin
10 μM CCCP
C
control
1 μM taxol
5 μg/ml nocodazole
2 μM jasplakinolide
10 μM cytochalasin D
RLU
Time (h)
D
Acrylamide
2,5-Hexanedione
RLU
0
10mM
0
68mM
F
Vimentin
β-actin
con i
vim i 1
vim i 2
E
RLU
Time (h)
no drug control
10 mM Acrylamide
68 mM 2,5-Hexanedione
G
RLU
Time (h)
control RNAi
Vimentin RNAi 1
Vimentin RNAi 2

Figure 2.5. Micrutubules and the actin network stabilizing/destabilizing reagents did not substantially affect mitochondrial localization.

(A) HeLa cells with no treatment, 1 mM taxol or 5 mg/ml nocodazole for 45 min in combination with 250 nM Mito Tracker Deep Red 633 to visualize mitochondria (red) were immunostained to detect α-tubulin (green).

(B) HeLa cells with no treatment, 2 mM jasplakinolide or 10 nM cytochalasin D for 45 min in combination with 250 nM Mito Tracker Deep Red 633 to visualize mitochondria (red) were immunostained to detect β-actin (green). Scale bar, 20 μm

Fig. 2.5

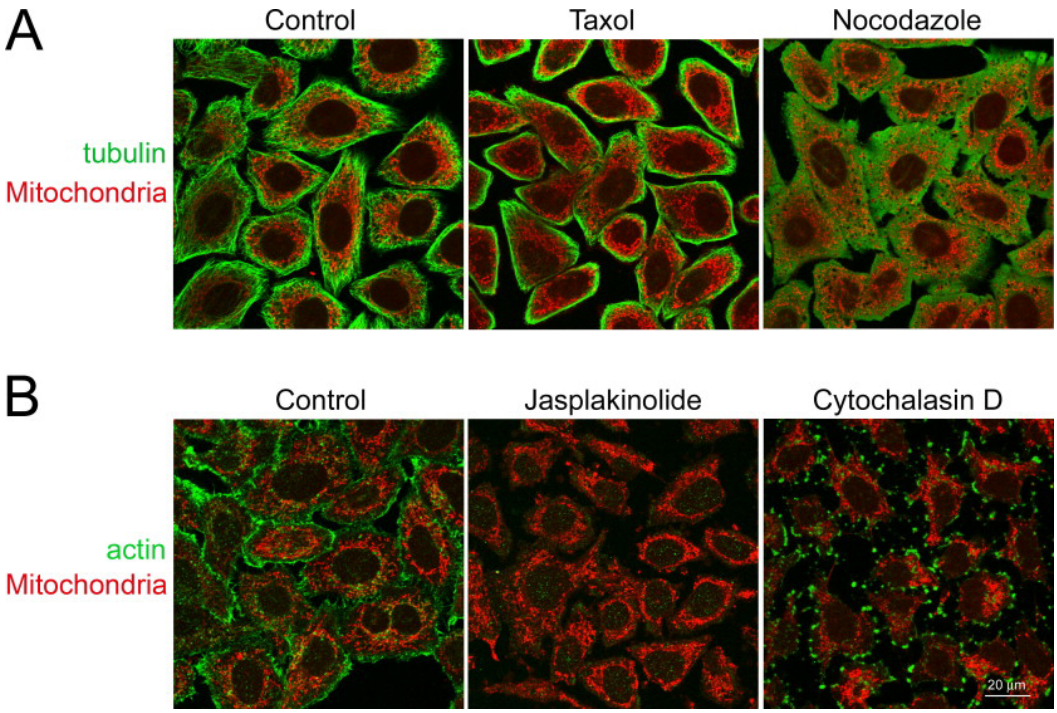
A
Control
Taxol
Nocodazole
tubulin
Mitochondria
B
Control
Jasplakinolide
Cytochalasin D
actin
Mitochondria
20 µm

Figure 2.6 Depletion of vimentin causes mitochondrial fragmentation.

COS-7 cells transfected with control siRNA or either of two vimentin siRNAs were immunostained to detect vimentin 90 h later (red). Mitochondria were visualized by transfecting mitochondrially-targeted EGFP (MitoEGFP) 24 h before immunostaining. Scale bar, 20 μm.

Fig. 2.6

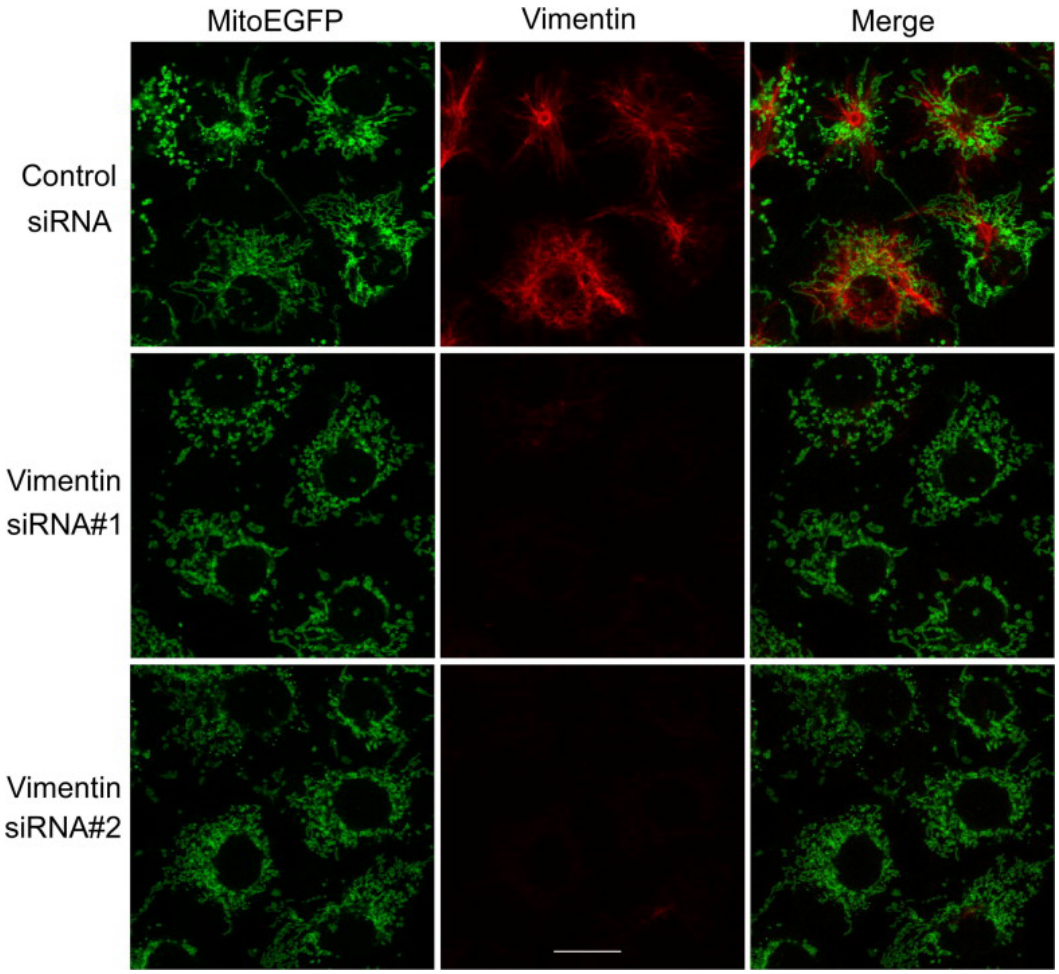
MitoEGFP
Vimentin
Merge
Control siRNA
Vimentin siRNA#1
Vimentin siRNA#2

Chapter 3: A mitochondrial-surface lipid-signaling pathway links regulation of mitochondrial morphology to the spermatogenic piRNA pathway

This chapter has been submitted to Developmental Cell. The majority of the data were produced by Huiyan Huang. The mouse histology, immunohistochemistry and EM data were produced by Qun Gao. Western blot data for the MitoPLD antibody were generated by Xiaoxue Peng.

3.1 Summary

The mammalian Phospholipase D superfamily member MitoPLD facilitates mitochondrial fusion by generating the signaling lipid PA. The *Drosophila* homolog of MitoPLD, Zucchini (Zuc), mediates piRNA generation, a critical step in oogenesis, and was proposed to be a cytoplasmic nuclease. We show here that *Drosophila* Zuc localizes to mitochondria and when overexpressed, can trigger mitochondrial aggregation as does human MitoPLD.

Conversely, mice lacking MitoPLD exhibit the meiotic arrest, transposon-mediated DNA damage, and male sterility characteristic of mice lacking piRNA pathway components. These findings identify the first mitochondrial protein required for piRNA generation. MitoPLD is shown to generate PA on the mitochondrial surface. The PA recruits the PA phosphatase Lipin 1 to convert the PA to diacylglycerol and promote fission, suggesting a new mechanism for mitochondrial morphology homeostasis. MitoPLD$^{-/-}$ fibroblasts exhibit shortened mitochondria, and spermatocytes lack intermitochondrial cement (nuage), a structure found between aggregated mitochondria that is implicated in piRNA generation. I propose that mitochondrial-surface PA generated by MitoPLD/Zuc recruits and/or activates nuage components critical for piRNA production.

3.2 Introduction

Mitochondria, in addition to their long-recognized role in energy production, are now appreciated to regulate numerous cell biological pathways including apoptosis and intracellular calcium homeostasis (Lebiedzinska et al.

2009). These regulatory processes involve communication between the mitochondria and the rest of the cell via signaling pathways on the mitochondrial surface that mediate interactions with cytoplasmic proteins. Some of these pathways involve lipids (Huang and Frohman 2009), such as cardiolipin, which serves to recruit tBid during apoptosis (Schug and Gottlieb 2009). We previously reported that human MitoPLD, a member of the PLD superfamily, generates a novel lipid signaling pathway on the mitochondrial surface that facilitates mitochondrial fusion (Choi et al. 2006). Mitochondrial fusion and fission are important for many aspects of normal cellular homeostasis, enabling mitochondria to alter their morphology to increase the efficiency of energy production, to mark unhealthy mitochondria for autophagy, and to translocate to subcellular locations at which ATP generation or calcium uptake are most needed (Chen and Chan 2009). The rates of fusion and fission are regulated by varied types of signaling events.

MitoPLD is a highly divergent PLD superfamily member more closely related to a subfamily of prokaryotic PLDs collectively called Nuc, which function as endonucleases, than to other mammalian PLDs (Choi et al. 2006). However, unlike Nuc, MitoPLD was unexpectedly found, using biochemical approaches, to cleave the mitochondria-specific lipid cardiolipin to generate the canonical PLD superfamily product PA. PA, a pleiotropic and rapidly metabolized signaling lipid, has been shown to function as a membrane anchor for

recruitment of SNARE complex proteins, small G-protein exchange factors and kinases, to activate lipid kinase enzymes and vesicle trafficking machinery, and to serve as substrate for production of the signaling lipids DAG and lysoPA (Jenkins and Frohman 2005; Cazzolli et al. 2006). Overexpression of wt MitoPLD causes mitochondria to aggregate, whereas a catalytically-inactive allele or RNAi knockdown decreases fusion resulting in mitochondrial fragmentation. This indicated that it is the production of PA that regulates mitochondrial morphology, rather than protein-protein interactions or other potential roles for MitoPLD (Choi et al. 2006). Nonetheless, the mechanism through which MitoPLD-generated PA alters mitochondrial morphology remains unknown.

The *Drosophila* homolog of MitoPLD, denoted Zucchini, was subsequently reported as a cytoplasmic presumptive nuclease with a critical role in piRNA generation during gametogenesis (Pane et al. 2007). piRNA, a germline-specific defense mechanism against transposon mobilization, is generated via a pair of multi-protein complexes with distinct subcellular localization (Aravin et al. 2009). One complex, termed the pi-body, localizes to the nuage, an electron-dense structure transiently associated with aggregated mitochondria in gametogenesis shortly before and during meiosis. The other complex, the piP-body, is physically distinct but in nearby germinal cytoplasmic granules. piRNAs are thought to be generated initially by the pi-body (primary piRNAs), following which the piP-body amplifies and expands the piRNA

population generated (Brennecke et al. 2007). Zuc is involved in the production of the primary piRNAs characteristic of the pi-body, although whether it is required (Saito et al. 2009) or has a more modest role (Malone et al. 2009) in primary piRNA generation remains unsettled. Loss of Zuc, or most any other of the identified piRNA pathway components in either complex, results in a failure to suppress transposon mobilization, ensuing DNA damage, and check point-induced meiotic arrest, leading to apoptosis and sterility (Thomson and Lin 2009), although Zuc may undertake other roles as well (Pane et al. 2007). A number of piRNA pathway components, when ablated in mice, create similar phenotypes, leading to meiotic arrest during spermatogenesis (He et al. 2009).

Taken together, these reports raised questions regarding whether the mammalian and *Drosophila* MitoPLD/Zuc homologs have evolved to undertake different enzymatic functions at different subcellular locations, or whether MitoPLD/Zuc might encode multiple types of activities and functions. I present findings in this report that largely resolve the species differences, and in doing so, link a lipid-signaling pathway on the surface of the mitochondria to production of piRNA during gametogenesis, which represents the first identification of a mitochondrial protein in this process. Moreover, I extend the lipid signaling pathway to encompass a second signaling lipid, DAG, and identify an existing human single nucleotide polymorphism (SNP) as a mutation that inactivates

MitoPLD, suggesting that loss of MitoPLD activity may underlie an unknown percentage of male infertility.

3.3 Materials and Methods

Plasmid construction. Truncation mutants of HA-tagged mouse Lipin 1b were generated by amplifying the specified region using PCR and ligating the restriction enzyme-digested PCR products into an expression vector containing a 3xHA tag. Details of construction of plasmids described in this study will be provided upon request.

Cell culture and transfection. MEF, HeLa and NIH3T3 cells were maintained in DMEM (Invitrogen, Carlsbad, CA) supplemented with 10% calf serum (Hyclone, Logan, UT). NIH3T3 cells stably transfected with mifepristone-inducible wt and H156N MitoPLD and Mitofusin1 were generated previously (Choi et al. 2006). CHO cells stably transfected with tetracycline-inducible PLD2 were generated previously (Du et al. 2004). NIH3T3, MEF and CHO cells were transfected with Lipofectamine LTX (Invitrogen, Carlsbad, CA) according to the manufacturer's

instructions. HeLa cells were transfected using FuGene HD (Roche) transfection reagent.

Immunofluorescence microscopy. 24 hours after transfection, cells were fixed with 4% paraformaldehyde for 15 min, permeabilized with 0.1% Triton X-100 for 10 min, and blocked with 5% normal goat serum for 1 hour. The cells were then immunostained using primary antibodies against cytochrome c (1:200, Pharmingen, San Diego, CA), HA epitope (1:500, Rockland Immunochemicals, Gilbertsville, PA), calreticulin (1:500, Stressgen Biotechnologies, San Diego, CA), GM130 (1:500, BD Transduction Laboratory), FLAG epitope(1:500, M2; Sigma, St Louis MO), and Drp1 (1:200, BD Transduction Laboratory) followed by fluorescent dye-conjugated secondary antibodies (1:500). Stained cells were visualized using a Leica TCS2 or Zeiss 510 confocal microscope. Images were processed using Adobe Photoshop.

Mitochondrial morphology quantification. Mitochondrial morphology was visualized by staining with anti-cytochrome c antibody. Pictures of individual cells were taken with confocal microscopy. Morphology of mitochondria for each cell was then categorized by a blinded investigator into tubular (more than 75% of mitochondria with long tubules), intermediate (25-75% mitochondria with long tubules) and fragmented (only 25% or less mitochondria with long tubules). Long tubules were defined as > 5 μm in length.

Generation of MitoPLD$^{-/-}$ mice. MitoPLD gene-targeted mice were generated using homologous recombination of C57/Bl6 stem cells as described in Fig. 3.12, by Ozgene, Australia. C57/Bl6 blastocyst embryos were used for generation of germ-line transmitted heterozygous mice, and Cre-recombinase was introduced using an egg-driven Cre gene in a C57/Bl6 background. The resulting offspring were genotyped to discard the Cre gene and maintained as heterozygotes. Genotyping was performed using PCR primers P1, 2, and 3 as shown in Fig. 3.12. P1: gttagccagccaaagccagtgtg; P2: atggcctgtgtggtccagttgag; P3: tgatacaagaggggtggatgtccac

Generation of primary and immortalized MEFs. MEFs were prepared from embryos derived from intercrossing MitoPLD$^{+/-}$ heterozygotes at embryonic day 13.5 after fertilization. Primary WT or knockout MEFs were immortalized by transfecting cells with SV40 larger T antigen expressing construct and then passaging continuously for two weeks until cells regained a fast rate of proliferation. Genotyping of MEFs was done by PCR using the primers P1-3 described above.

Electron Microscopy. Samples used for transmission electron microscopy were processed using standard techniques. Briefly, 2-5 month old mice were perfused with 4% paraformaldehyde and 2.5% EM grade glutaraldehyde in 0.1M sodium cacodylate buffer, pH7.4, and testes post-fixed overnight in the same fixative. Samples were then placed in 2% osmium tetroxide in 0.1M PBS pH 7.4,

dehydrated in a graded series of ethyl alcohol and embedded in Durcupan resin. Ultrathin sections of 80nm were cut with a Reichert-Jung UltracutE ultramicrotome and placed on formvar-coated slot copper grids. Sections were counterstained with uranyl acetate and lead citrate and viewed with a FEI Tecnai12 BioTwinG^2 electron microscope. Digital images were acquired with an AMT XR-60 CCD Digital Camera system and compiled using Adobe Photoshop.

Histology. Freshly dissected testes were fixed in 4% paraformaldehyde overnight at 4°C, processed for paraffin embedding, sectioned at a thickness of 5μm, and stained with hematoxylin and eosin.

Western Blotting. Freshly isolated adult mice testes were snap-frozen in liquid nitrogen, pulverized in dry ice using a precooled motor, and lysed in 8M urea lysis buffer. Samples were centrifuged and the supernatant used for both western analysis of protein (40 μg) on 10% SDS-PAGE, and measurement of protein concentration. After transfer to nitrocellulose membranes, the blot was probed with primary antibody, followed by secondary antibodies conjugated with IRDye 800 (Rockland Immunochemicals, Gilbertsville, PA). Fluorescent signals were detected with an Odyssey infrared imaging system (LICOR Biosciences, Lincoln, NB). Polyclonal anti-MitoPLD antibody was custom made by Covance (PA, U.S.A) using the synthetic peptide CIGLLRKAGIQVRHDQD as antigen.

Immunofluorescence on sections. 10μm cryosections of testes were fixed in 4% paraformaldehyde and immunostained with anti-TDRD1 (Abnova) or anti-

phospho-histone-H2A.X (Ser 139) (Millipore) antibody, followed by secondary antibody Alexa Fluor 568 anti-mouse IgG. Nuclei were stained with DAPI.

3.4 Results

Both human and *Drosophila* MitoPLD/Zuc localize to mitochondria and alter mitochondrial morphology in an activity-dependent manner.

As previously reported, the mechanism by which MitoPLD becomes localized to mitochondria involves a 39-amino acid N-terminal domain that functions as a trans-membrane tail to anchor MitoPLD into the outer mitochondrial membrane (Choi et al. 2006). *Drosophila* Zuc also encodes a predicted N-terminal trans-membrane mitochondrial localization sequence (Choi et al. 2006), but was reported to localize to cytoplasmic granules and to peri-nuclear cytoplasm including the nuage (Pane et al. 2007; Saito et al. 2009), potentially through complex formation with the nuage-localized piRNA-binding protein Aubergine (Pane et al. 2007). However, these studies employed *zuc* alleles N-terminally tagged with EGFP or HA. I thus examined the possibility that the

Zuc mitochondrial localization sequence had been inactivated by placing it internally in the resulting fusion protein.

Mitochondria in HeLa cells characteristically appear as an elongated and branched tubular network (Fig. 3.1A, arrow). Overexpressed wt human MitoPLD tagged C-terminally with EGFP localizes to the mitochondria and causes them to accumulate peri-nuclearly as an aggregate (Fig. 3.1A, asterisks). In contrast, catalytically-inactive MitoPLD (H156N) triggers mitochondrial fragmentation (Fig. 3.1B, arrowhead), which also frequently results in peri-nuclear accumulation. Deleting the N-terminal domain (data not shown) or placing EGFP at the N-terminus (Fig. 3.1C) causes MitoPLD to localize to the cytoplasm and prevents changes to mitochondrial morphology. Finally, in contrast to the published reports, *Drosophila* Zuc tagged C-terminally with EGFP localizes to mitochondria (Fig. 3.1D, arrow), and like WT-MitoPLD, triggers perinuclear aggregation when overexpressed sufficiently (asterisk). Conversely, an inactive allele of Zuc, H169N, causes fragmentation (Fig. 3.1E, arrowhead).

Taken together, these findings indicate that, like human MitoPLD, Zuc localizes to mitochondria and stimulates mitochondrial aggregation in an activity-dependent manner.

MitoPLD produces PA on the mitochondrial surface

We previously reported, using biochemical approaches, that MitoPLD hydrolyzes cardiolipin to generate PA (Choi et al. 2006), raising the question of where on the mitochondria the PA is generated and accumulates. A fluorescent sensor for PA, Raf1-PA Binding Domain (PABD)-EGFP (Rizzo et al. 2000), was employed to visualize changes in detectable PA as a consequence of manipulating the MitoPLD expression level. In control NIH3T3 cells, the sensor distributes throughout the cell (Fig. 3.2A). However, increasing MitoPLD expression to cause PA production induced sensor translocation to the aggregated mitochondria (Fig. 3.2B, arrow). The recruitment was specific for PA, since increasing MitoPLD expression did not elicit translocation of a mutant form of the PA sensor that lacks the ability to bind PA (Fig. 3.2E and F), nor did the wt sensor translocate in response to increased expression of the catalytically-inactive MitoPLD allele H156N (Fig. 3.2C) or Mfn1 just to induce mitochondrial aggregation (Fig. 3.2D). Detection of PA on the exofacial mitochondrial surface supports our prior model that MitoPLD is an outer membrane protein with a cytoplasmically-oriented catalytic domain that hydrolyzes cardiolipin on the mitochondrial surface (Choi et al. 2006).

MitoPLD production of PA recruits Lipin 1b which converts the PA into DAG.

In many signaling events, the PA produced by PLD is rapidly converted to DAG. In some settings, this process serves to terminate the signaling events promoted by PA; in others, DAG itself is the bioactive signaling lipid in the cell biological process (Brindley et al. 2009). I next sought to determine if MitoPLD-generated PA is converted to DAG, the enzyme involved if so, and whether accelerating the conversion of PA to DAG promoted or opposed the pro-fusion effects of PA, since DAG has been linked both to membrane organelle fusion and fission events in different settings (Riebeling et al. 2009). PA dephosphorylation to generate DAG is mediated by the Type 1 and 2 families of PAPs. PAP2s are well established as multipass transmembrane proteins with active sites on the extracellular surface or lumen of organelles, making them unlikely candidates to mediate cytosolic conversion of PA to DAG. PAP1, on the other hand, was recently identified as the Lipin family of cytosolic proteins. Lipin 1 (of three isoforms) is the best studied family member (Brindley et al. 2009). Mutations in Lipin 1 cause a Type-II diabetes-like syndrome in mice called fatty liver dystrophy that involves lipid storage dysregulation and poorly understood abnormal mitochondrial function. The localization of Lipin 1 is complex, including to the cytoplasm, endoplasmic reticulum, nuclear envelope, and nucleus in different cell types and settings, and the two alternately spliced isoforms Lipin 1a and 1b (see Fig. 3.6C) may have differences in their localization patterns.

Transfection of Lipin 1b into NIH3T3 cells revealed a punctate cytoplasmic localization (Fig. 3.3A). Surprisingly, increased expression of MitoPLD resulted in translocation of virtually all of the Lipin 1b to the aggregated mitochondria (Fig. 3.3B, arrow). The translocation was not due to protein interaction between MitoPLD and Lipin 1b, since increased expression of catalytically-inactive MitoPLD did not recruit Lipin 1b to the mitochondrial surface (Fig. 3.3C). The translocation was also not caused by mitochondrial aggregation *per se*, since forcing aggregation through overexpression of the fusion protein Mitofusin 1 (Chen et al. 2003), which does not substantially elevate mitochondrial PA levels (Choi et al. 2006), did not elicit Lipin 1b movement (Fig. 3.3D). Finally, underscoring the direct role of PA in the recruitment, Lipin 1b can alternately be recruited to the plasma membrane by overexpression of Phospholipase D2 (Fig. 3.4), a mammalian PLD that generates PA on the plasma membrane via hydrolysis of phosphatidylcholine (Colley et al. 1997).

I next employed a fluorescent sensor for DAG, PKC-C1bδ-YFP (Giorgione et al. 2006), to determine whether Lipin 1b, once brought to the mitochondrial surface, would generate DAG from the PA available there. When expressed in NIH3T3 cells, which express relatively low levels of Lipin 1b, the sensor localizes in part to the Golgi apparatus (Fig. 3.5A), a site at which DAG is abundant. Increased expression of MitoPLD alone did not cause substantial translocation of the sensor to mitochondria (Fig. 3.5B). However, increased

expression of both MitoPLD and Lipin 1b led to robust translocation of the DAG sensor to the aggregated mitochondria (Fig. 3.5C). The increase in DAG was dependent on the catalytic activity of Lipin 1b, since the catalytically-inactive allele D712A (Brindley et al. 2009) efficiently translocated to mitochondria overexpressing MitoPLD but did not trigger recruitment of the DAG sensor (Fig. 3.5D and E). Taken together, these results demonstrate that in the setting of exaggerated expression, Lipin 1b moves to the mitochondrial surface in response to MitoPLD-generated PA and converts it into DAG.

Lipin 1b is recruited to mitochondria via a PA-responsive central domain and decreases mitochondrial length.

Transient expression of Lipin 1b in HeLa cells transformed the characteristic long mitochondrial tubules (Fig. 3.6A, arrow) into moderately-sized fragments (Fig. 3.6A, asterisk). Quantitation of the shift revealed a statistically significant shift towards fragmentation, but only for the wt Lipin 1b allele, not for the catalytically-inactive one (Fig. 3.6B). This finding suggests that PA is the pro-fusogenic lipid signal, and Lipin 1b conversion of PA to DAG serves to terminate the pathway(s) activated by PA. The result also indicates that Lipin 1b can affect mitochondrial morphology at physiological levels of PA, although the fraction of Lipin 1b stably recruited to the mitochondria in this setting is below the limit of visible detection using this microscopic approach.

These findings raised the issue of the PA-directed recruitment mechanism. Lipin 1b encodes a C-terminal catalytic domain, a conserved N-terminal LIP domain of unknown function, and three basic amino acid-rich regions characteristic of the types of unstructured, positively-charged regions that mediate binding of a number of signaling proteins to PA (Fig. 3.6C). Deletion analysis revealed that none of these domains and regions mediated the recruitment, but rather, the translocation was regulated by a central domain, amino acids 430-570 (Fig. 3.6C and Fig. 3.7A, B). As before, neither catalytically-inactive MitoPLD nor Mitofusin 1 triggered mitochondrial translocation (Fig. 3.7C and D), and the Lipin 1b PA-responsive central domain could be recruited to the plasma membrane by increased expression of PLD2 (Fig. 3.8). Although there is no obvious cluster of basic amino acids in this central region, there are dispersed basic amino acids that may mediate interaction with PA. Alternately, it is possible that this region may interact with another protein that binds PA directly. However, since the region also translocates to the plasma membrane upon PLD2 expression, such a hypothetical protein partner could not be mitochondrial-specific.

The Lipin 1 catalytic domain localizes to sites of mitochondrial fission and promotes fission in a PA-independent manner.

Unexpectedly, even though elevated levels of PA on the mitochondrial surface are required to recruit a visibly detectable quantity of full-length Lipin 1b,

the isolated Lipin 1 catalytic domain (amino acids 705-924) localizes to mitochondria in cells with physiological levels of PA (Fig. 3.9A, arrow), and in fact does so even in cells expressing catalytically-inactive MitoPLD, which should lack PA on the mitochondrial surface (Fig. 3.10). Moreover, the elongated mitochondrial tubules characteristic of HeLa cells (Fig. 3.9A, asterisk) exhibit almost complete fragmentation (Fig. 3.9A, arrow), and the Lipin 1 catalytic domain localizes to the tips of the small mitochondria (Fig. 3.9B). In rare cells in which the fragmentation is incomplete, the Lipin 1 catalytic domain is observed to localize in a punctate manner on the tubules (Fig. 3.9C, D), which was reminiscent of the localization pattern for Drp1, a protein that drives mitochondrial fission (Frank et al. 2001). Co-localization of Drp1 and the Lipin 1 catalytic domain with incompletely fragmented tubules (Fig. 3.9E) revealed that both the Lipin 1 catalytic domain (Fig. 3.9I) and Drp1 (Fig. 3.9J) localize to constricted regions of the tubules (Fig. 3.9F-H, arrowheads, lines), suggesting participation in the fission process. However, there were also numerous sites of tubular constriction at which Drp1 alone was found (Fig. 3.9I, K, arrow).

These findings suggest a model in which fusion events involving MitoPLD lead to PA production on the mitochondrial surface (Fig. 3.11), which recruits Lipin 1b. I propose that the recruitment process induces a conformational change in Lipin 1b that exposes the cryptic, fission site-localizing domain, leading to focusing of Lipin 1b at future sites of fission through interaction with an

unknown protein partner, and promotion of fission through production of DAG. This hypothetical model is attractive for several reasons, including that PA has been shown in biochemical assays to dramatically stimulate Lipin 1 catalytic activity through an unknown mechanism (Han and Carman 2010). Moreover, mitochondrial fusion events have been linked temporally and spatially to future fission events, although the underlying mechanism is unknown (Twig et al. 2008; Liu et al. 2009). The model proposed here provides one such potential mechanism via a process that would promote homeostasis, i.e., mitochondria undergoing fusion would stimulate their own future fission, helping to maintain mitochondria within a relatively restricted range of sizes.

Mouse embryo fibroblasts lacking MitoPLD exhibit shortened mitochondrial tubules and fragments and are resistant to the effects of Lipin 1b but not the Lipin 1 catalytic domain.

We targeted the MitoPLD gene in embryonic stem cells to generate an allele in which the second exon, which encodes the key HKD catalytic motif, was flanked with loxP sites (Fig. 3.12). Mice harboring the targeted allele were crossed to mice expressing Cre recombinase in oocytes, and off-spring with Cre-deleted alleles identified. Mice heterozygous for the Cre-deleted allele were mated to generate homozygous mice that express only the first exon (MitoPLD$^{-/-}$), which should constitute a complete loss of gene function, since the HKD motif is

critical for enzymatic activity for all members of the PLD superfamily (Jenkins and Frohman 2005).

Mouse embryo fibroblasts were isolated from MitoPLD$^{-/-}$ and control WT E13.5 embryos. Control MEFs almost uniformly exhibited long, tubular mitochondria (Fig. 3.13A, quantitation in 3.13C), whereas MitoPLD$^{-/-}$ MEFs exhibited shortened mitochondria (Fig. 3.13B, square inset), and in almost half of the cells, mitochondrial fragments (arrow) were particularly prominent in the cellular periphery (Fig. 3.13B, enhanced in round inset). This finding confirms a role for MitoPLD in regulation of mitochondrial morphology, although the phenotype is less profound than that observed for loss of proteins that physically mediate the fusion event such as Mitofusin 1 (Chen et al. 2003).

Similar to the results shown in Fig. 3.6A and B for HeLa cells, expression of Lipin 1b in WT MEFs led to mitochondrial shortening and fragmentation (74.6% reduction in tubulation, 238% increase in fragmentation, n=336 total cells counted, $p<0.001$). However, Lipin 1b expression did not result in further shortening or fragmentation of MitoPLD$^{-/-}$ MEFs (n=346, $p>0.15$). In contrast, the Lipin 1 catalytic domain efficiently triggered fragmentation for both WT and MitoPLD$^{-/-}$ MEFs (Fig. 3.13D, E). Taken together, these results confirm that the ability of full-length Lipin 1b to promote mitochondrial fission is dependent on PA production by MitoPLD, but the isolated catalytic domain functions independently of PA production.

MitoPLD$^{-/-}$ mice exhibit meiotic arrest during spermatogenesis, loss of nuage and TDRD1, and genomic damage.

MitoPLD$^{-/-}$ offspring generated by crossing MitoPLD$^{+/-}$ mice were born in the normal Mendelian ratio and appeared grossly normal. Mating of the male and female MitoPLD$^{-/-}$ mice revealed normal fertility for females, but 100% penetrant infertility for male mice (>7 males continuously mating for 6 months). We previously reported that MitoPLD is expressed widely at low levels (Choi et al. 2006), and many ESTs in the NCBI database have been isolated from brain and lung. An anti-MitoPLD antiserum demonstrated expression of MitoPLD in the adult testes (Fig. 3.14A). Data available from published microarray studies reveal that MitoPLD is expressed at low levels in type A and B spermatogonia, increases 5-fold in spermatocytes undergoing meiosis (pachytene spermatocytes), and then decreases again in round spermatids, and that it is expressed at low levels in testes in young mice, and then increases 7-fold from day 14 to day 29 with the onset of puberty.

Gross histological examination demonstrated a substantial reduction in size for MitoPLD$^{-/-}$ testes obtained from 3-month old mice (Fig. 3.14B, C). Hematoxylin and eosin staining of fixed sections revealed a dramatic difference in morphology. Seminiferous tubules in WT testes exhibited normal architecture with an external layer of spermatogonia (Fig. 3.14D) and progressively more

differentiated spermatocytes (Fig. 3.14E, a,b) and finally spermatids (Fig. 3.14E, c) towards the lumen of the tubule. In contrast, MitoPLD$^{-/-}$ tubules were reduced in size with only a thin layer of cells around the periphery (Fig. 3.14D, E). Spermatogonia and Sertoli cells appeared normal (Fig. 3.14E, d), and spermatocytes early in meiosis (prophase) at the leptotene/zygotene/early pachytene stages were observed (Fig. 3.14E, e), but not late or post-meiotic spermatocytes nor spermatids. Instead, the tubules contained many cells with condensed, heavily staining nuclei typical of cells undergoing apoptosis (Fig. 3.14E, f, lower cell), cells with disorganized chromosomal material (Fig. 3.14D, arrowhead, inset; 3.14E, f, upper cell), vacuoles suggestive of cell drop-outs (Fig. 3.14D, asterisks), and cell debris sloughed into the lumen of the tubules (Fig. 3.14D, upper left). These findings indicate that spermatocytes in MitoPLD$^{-/-}$ mice exhibit meiotic arrest, consistent with the phenotypes for *zuc*$^{-/-}$ *Drosophila* and for a number of genes involved in piRNA production that have been shown to be required for mammalian spermatogenesis.

Electron microscopy examination of spermatocytes from wt mice at the prophase stage revealed numerous cells in which the mitochondria exhibited aggregation (Fig. 3.14F, arrowheads), separated by electron-dense nuage, also known as intermitochondrial cement (Fig. 3.14G, arrow; higher magnification in H). Nuage and aggregated mitochondria were observed in all wt samples examined. In contrast, neither aggregated mitochondria nor associated nuage were

observed in any sample of multiple MitoPLD$^{-/-}$ testes examined (Fig. 3.14I). Mitochondria could be found on occasion in close approximation (Fig. 3.14J), but they were not separated by interposed nuage (Fig. 3.14K). Loss of nuage is characteristic of some, but not all, of the previously reported knockout phenotypes for piRNA components that cause meiotic arrest (He et al. 2009).

piRNA components are known to form large multi-protein complexes, which has led to the hypothesis that loss of critical proteins physically destabilizes the entire complex (Ma et al. 2009). MitoPLD could be proposed to undertake a similar function. However, this appears unlikely, since one of the fully penetrant alleles of *Drosophila zuc* is a mutation of the key histidine in the HKD enzymatic motif (Pane et al. 2007), which should only eliminate enzymatic activity. I have shown that mutation of this residue results in a mutant protein (for both *Drosophila* Zuc and human MitoPLD) that is expressed at wt levels, localizes normally to the mitochondria, and folds sufficiently well to heterodimerize with wt protein and function as a dominant negative (Fig. 3.1, and (Choi et al. 2006)). Thus, a critical protein-protein interaction does not seem likely to underlie the requirement for MitoPLD in formation of nuage-associated mitochondria. In fact, overexpression of enzymatically-active MitoPLD in cultured cell lines aggregates mitochondria with a thin intervening layer of electron dense material (Fig. 3.14L, M, and (Choi et al. 2006)), suggesting that the formation of nuage-associated mitochondria might be driven solely by raising levels of PA sufficiently high

enough on the surface of the mitochondria, since almost all of the other piRNA-associated components are expressed only in germ cells and hence would not be present in the cultured cells.

Loss of nuage should result in mislocalization or loss of critical P-body components of the piRNA pathway. To examine this, immunofluorescent staining for TDRD1, one such component, was performed. TDRD1 expression initiates in the meiotic prophase as spermatogonia differentiate into spermatocytes, and then decreases with formation of spermatids (Hosokawa et al. 2007). TDRD1 localizes to the nuage, which appears as a collection of largely peri-nuclear punctate foci in spermatocytes in WT tubules prepared from adult male mice (Fig. 3.15A). In contrast, TDRD1 was not detected in MitoPLD$^{-/-}$ tubules (Fig. 3.15B).

Loss of critical components of the piRNA-generating pathway, such as TDRD1, leads to transposon mobilization and ensuing DNA damage, as can be visualized by imaging γH2X which localizes to double-strand DNA breaks (Soper et al. 2008). A low level of γH2X expression is observed in WT tubules as a consequence of the meiotic process and a low level transposon expression (Fig. 3.15C, F, and (Soper et al. 2008)). Markedly increased levels of γH2X were observed in MitoPLD$^{-/-}$ spermatocytes (Fig. 3.15D, E, G, H), indicative of substantial genomic damage. Taken together, the loss of nuage and TDRD1, increased genomic damage, meiotic arrest, and cell death provides compelling evidence that the role of MitoPLD in mice is similar to the role of Zuc in

Drosophila in the piRNA generation pathway that confers defense against transposon mobilization during gametogenesis.

Ablation of the PA-metabolizing enzyme Lipin 1 increases nuage and alters the localization pattern of TDRD1.

Male mice lacking Lipin 1 (*fld*, fatty liver dystrophy) are infertile, which has been proposed to ensue from their spastic neurological phenotype (Langner et al. 1991). Examination of adult *fld/fld* testes indicated that they are normal sized, appear normal histologically, and produce motile sperm (not shown). However, electron microscopy examination revealed a difference in the appearance of nuage (Fig. 3.16A, arrowheads). In contrast to the nuage observed in WT mice (Fig. 3.14F-H), which exhibited approximately the same density as the adjacent mitochondrial matrix (Figs. 3.14F, 3.16D), the nuage in *fld/fld* spermatocytes was substantially increased in density (Fig. 3.16A-D). In addition, the nuage between mitochondria in WT mice typically was short in length (15.5% $\pm$ 4.8% of the circumference of the mitochondria, range 11.6% - 21.8%, n=10), but was longer for *fld/fld* spermatocytes (52.3% + 21.3%, range = 27.9% to 67.1%). Consistent with the alteration in nuage appearance, the localization of TDRD1 was also altered subtly, in that the pattern of many small foci shifted to a less uniform collection dominated by larger foci. Taken together, these findings suggest that loss of the PA-metabolizing enzyme Lipin 1 results in elevated levels of PA on

the mitochondrial surface, leading to increased nuage formation and further supporting the role of PA in mitochondrial-nuage association.

A human polymorphism that inactivates MitoPLD.

Examination of the SNP database at NCBI revealed a number of MitoPLD polymorphisms, most of which were synonymous or in non-coding regions, or altered amino acids not conserved in cross-species comparison of MitoPLD homologs. One SNP, however, created a non-conservative change (Asp173 to Lys) at an invariant position in the catalytic site (Fig. 3.17). Expression of the mutated allele in HeLa cells revealed that it phenocopied the well-established catalytically-inactive mutant H156N, causing mitochondrial fragmentation and failing to recruit Lipin 1b to the mitochondrial surface. The allele frequency of p.N173K in the general population is unknown, but presents the possibility that loss of MitoPLD function could underlie some instances of male infertility.

3.5 Discussion

The piRNA generation pathway is an increasingly complex one involving enzymes that methylate the RNA-cleaving enzymes and piRNAs themselves, mRNAs that both serve as substrate to generate piRNAs and encode proteins that transport the piRNAs to the nucleus, and proteins of unknown function that may serve as scaffolds or recruit small G-proteins to the active complex. piRNA primary processing takes place on pi-bodies, which co-localize with intermitochondrial cement, one of six types of nuage found in germ cells (Russell and Frank 1978). A current question concerns the relationship of the primary processing in pi-bodies to the association of nuage with mitochondria. I describe here the first functional linkage of an intrinsic mitochondrial protein with the capacity to generate piRNA. Zucchini, the *Drosophila* homolog of MitoPLD, was reported as a cytoplasmic or nuage-localizing presumptive nuclease (Pane et al. 2007). As previously reported, we were unable to demonstrate nuclease activities for MitoPLD (Choi et al. 2006). Instead, we found that it generated a lipid signal using the mitochondrial lipid cardiolipin as substrate to generate PA. I show here that Zuc, when not N-terminally tagged, localizes to mitochondria and alters mitochondrial morphology, including causing mitochondrial aggregation, prompting the need for new hypotheses concerning how it regulates piRNA generation in *Drosophila*.

We showed previously that MitoPLD generates PA in the context of fusion events (Choi et al. 2006). I show here that PA is generated on the

mitochondrial surface, and that the PA recruits a second lipid-modifying enzyme, Lipin 1, to convert the PA into DAG, which then promotes fission. This proposed spatiotemporal linkage of fusion and fission is intriguing in light of two prior reports. Twig *et al*. (Twig et al. 2008) have described a temporal correlation between fusion and fission: mitochondria fuse at random points on average every 10 minutes, but many fusion events are followed rapidly (average, 70 seconds) by a fission event. This "kiss and run" type of (partial) fusion event can be discriminated from full fusion events by rapid assembly of Drp1 at the fusion site, followed by fission (Liu et al. 2009). The lipid signaling pathway I describe here suggests potential mechanisms through which such temporal-spatial targeting of fission could be achieved. Conversely, sites at which only Drp1 assembly is observed (Fig. 3.9) may represent fission events spatially and temporally unconnected to fusion events. Not explored here, the effects of MitoPLD and Lipin on mitochondrial morphology are likely to have consequences for tissues in which regulated fusion and fission are important, including in peripheral tissues such as fat and muscle. Alterations in mitochondrial fusion and fission could lead to changes in numbers of mitochondria and potentially increased capacity for fatty acid oxidation. However, the effects do not trigger lethality. This is frequently the case for lipid signaling genes for which compensatory mechanisms can moderate the loss of a single synthetic or degradative pathway. Two other Lipin genes and

another MitoPLD-related gene are present in the mammalian genome and may provide some redundancy or compensation in the long-term knockout setting.

However, the dramatic effect of loss of MitoPLD/Zuc on nuage association with mitochondria and piRNA-generation raise the question of the role played by the lipid signal PA. Examination of mice lacking Lipin 1 revealed more, not less nuage, and mature sperm were produced, indicating that PA is the bioactive lipid in this process rather than DAG, which is the key signaling lipid in other well-defined signaling pathways (Mor et al. 2007). PA is well established as a lipid anchor that recruits a variety of types of proteins with PA-binding domains and/or activates enzymes such as kinases (Jenkins and Frohman 2005). The requirement for PA in this setting is reminiscent of the role of yeast PLD (Spo14) during meiosis, where it localizes to an electron-dense amorphous structure on the outer surface of spindle pole bodies, and, through generating PA there, recruits a PA-binding protein that is key for the subsequent developmental step (Nakanishi et al. 2006). Could MitoPLD/Zuc-generated PA play an analogous role? One possibility is that the PA might recruit a key protein required for piRNA production to the nuage. I have examined whether proteins known to be critical in the pathway, Miwi, Mili, MVH, Tdrd1, Tdrd6, Tdrkh (Tdrd2), and RanBP9, are recruited to the mitochondria in HeLa cells overexpressing MitoPLD, but did not observe PA-induced translocation (not shown). It is possible that formation of the proteins into a complex is required to expose a PA-binding domain, or that there

is a PA-responsive critical protein in the pathway that I have not yet examined. Another key protein, Gasz, localized to mitochondria independent of MitoPLD-generated PA (data not shown), and thus could potentially serve as an anchor for the pi-body protein complex, since it interacts with other components of the complex (Ma et al. 2009). However, this would not explain the requirement for PA. Alternately, the nuage structure has long been known to be strongly positively charged (Paniagua et al. 1985), due presumably to the high content of ribonucleoproteins. Since PA is a strongly negatively charged lipid, mitochondria with exofacial PA might simply be able to associate with and sandwich nuage via electrostatic interactions. A regulatory function for PA would still be required, but could involve conformational change or activation of some component of the piRNA-generating process through proximity with PA, rather than robust recruitment.

Finally, I report two functional roles for MitoPLD, one involving relatively low level expression that has effects on mitochondrial morphology in non-germ cells, and another involving high level expression that leads to mitochondrial aggregation. The mechanism underlying MitoPLD effects on mitochondrial morphology and fusion are unknown but may involve promoting transient outer leaflet trans-affinity to facilitate fusion and thus represent a weaker version of the role undertaken by MitoPLD during spermatogenesis. Which function evolved first represents another future question.

Fig. 3.1. *Drosophila* Zuc localizes to and aggregates mitochondria in an activity-dependent manner.

HeLa cells were transiently transfected with expression plasmids for tagged isoforms of human MitoPLD and *Drosophila* Zuc. One day later, the cells were fixed, permeabilized, immunostained for cytochrome (cyt) c to visualize mitochondria, and imaged using a Zeiss 510 confocal microscope. (A) WT human MitoPLD C-terminally tagged with EGFP; (B) Catalytically-inactive (H156N) human MitoPLD; (C) WT human MitoPLD N-terminally tagged with EGFP; (D) *Drosophila* Zuc C-terminally tagged with EGFP; (E) Catalytically-inactive (H169N) *Drosophila* Zuc. Asterisk, transfected cells demonstrating mitochondrial aggregation; arrow, non-transfected cell with tubular mitochondria; arrowhead, fragmented mitochondria; wavy arrow, co-localization of Zuc with mitochondrial tubules at low levels of expression. The cells shown are typical of cells observed in multiple fields for transfection experiments performed 3 or more times.

Fig. 3.1

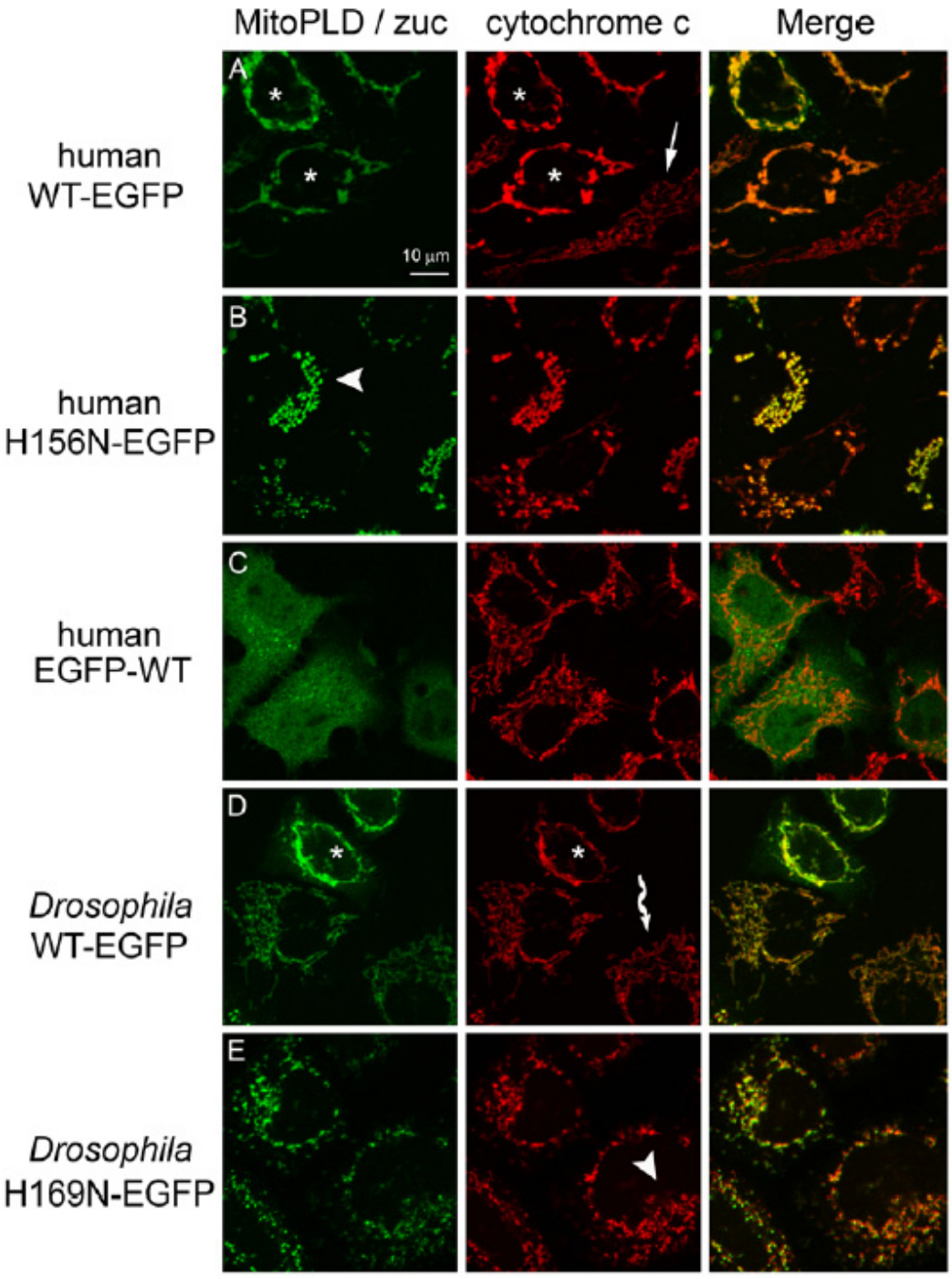
MitoPLD / zuc
cytochrome c
Merge
A
human
WT-EGFP
10 μm
B
human
H156N-EGFP
C
human
EGFP-WT
D
Drosophila
WT-EGFP
E
Drosophila
H169N-EGFP

Fig. 3.2. MitoPLD-generated PA can be detected by a cytosolic PA sensor.

(A-D) NIH3T3 control cells (A) or inducible cells expressing (B) WT MitoPLD, (C) catalytically-inactive H156N-MitoPLD, or (D) Mitofusin 1 were transfected with an expression plasmid encoding the PA binding domain of Raf1 fused with EGFP (Raf1-PABD). Arrow, localization of PA sensor to MitoPLD-aggregated mitochondria.

(E, F) A mutant form of the sensor that does not bind PA localizes to the cytoplasm both in NIH3T3 cells (left panel) and in NIH3T3 cells expressing high levels of MitoPLD that cause mitochondrial aggregation. Arrow, aggregated mitochondria.

Fig. 3.2

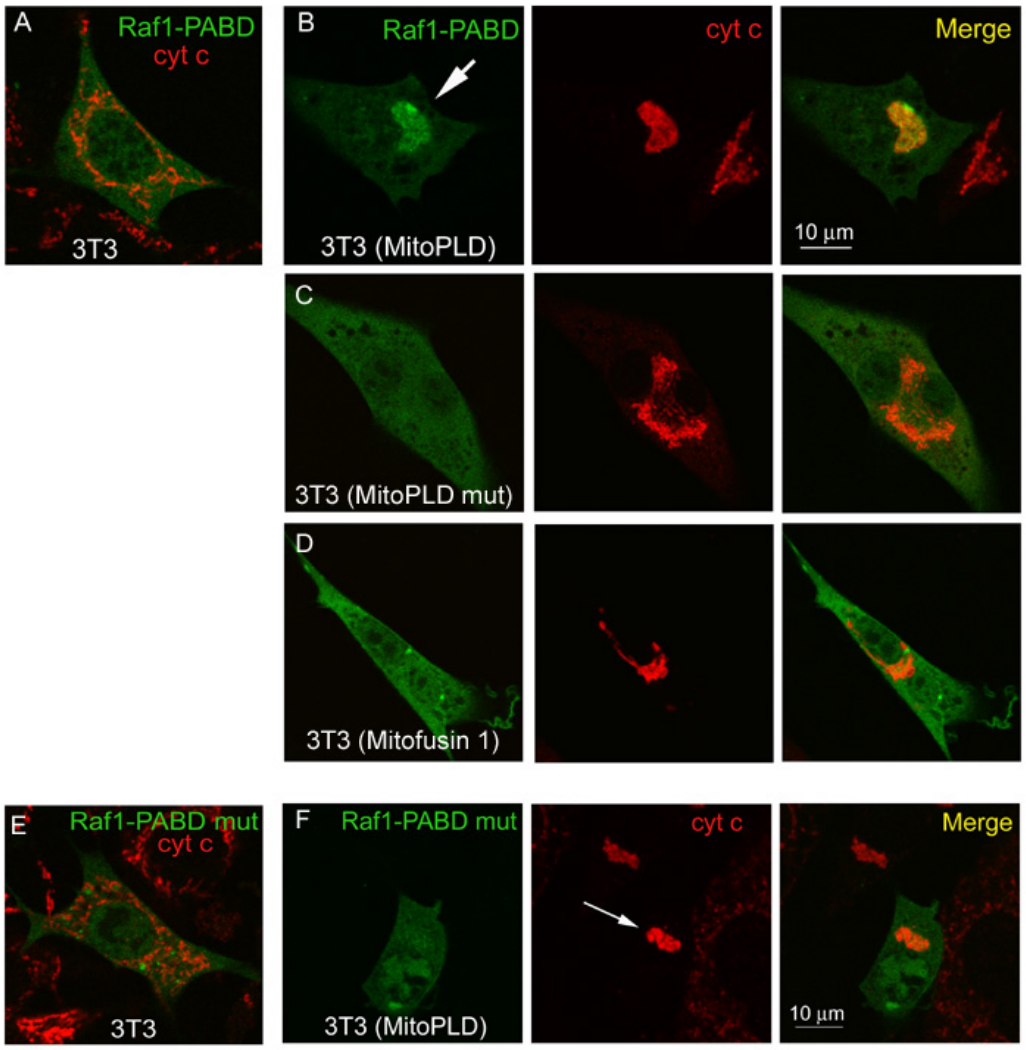
A
Raf1-PABD
cyt c
3T3
B
Raf1-PABD
3T3 (MitoPLD)
cyt c
Merge
10 µm
C
3T3 (MitoPLD mut)
D
3T3 (Mitofusin 1)
E
Raf1-PABD mut
cyt c
3T3
F
Raf1-PABD mut
3T3 (MitoPLD)
cyt c
Merge
10 µm

Fig. 3.3 Activity-dependent recruitment of Lipin 1b to mitochondria by MitoPLD.

NIH3T3 control cells (A) or inducible cells expressing (B) WT MitoPLD, (C) catalytically-inactive H156N-MitoPLD, or (D) Mitofusin 1 were co-transfected with MitoEGFP to visualize mitochondria and HA-tagged Lipin 1b. 1 day later, the cells were fixed, permeabilized, and immunostained with an anti-HA monoclonal antibody to detect Lipin 1b. Arrow, localization of Lipin 1b to MitoPLD-aggregated mitochondria.

Fig. 3.3

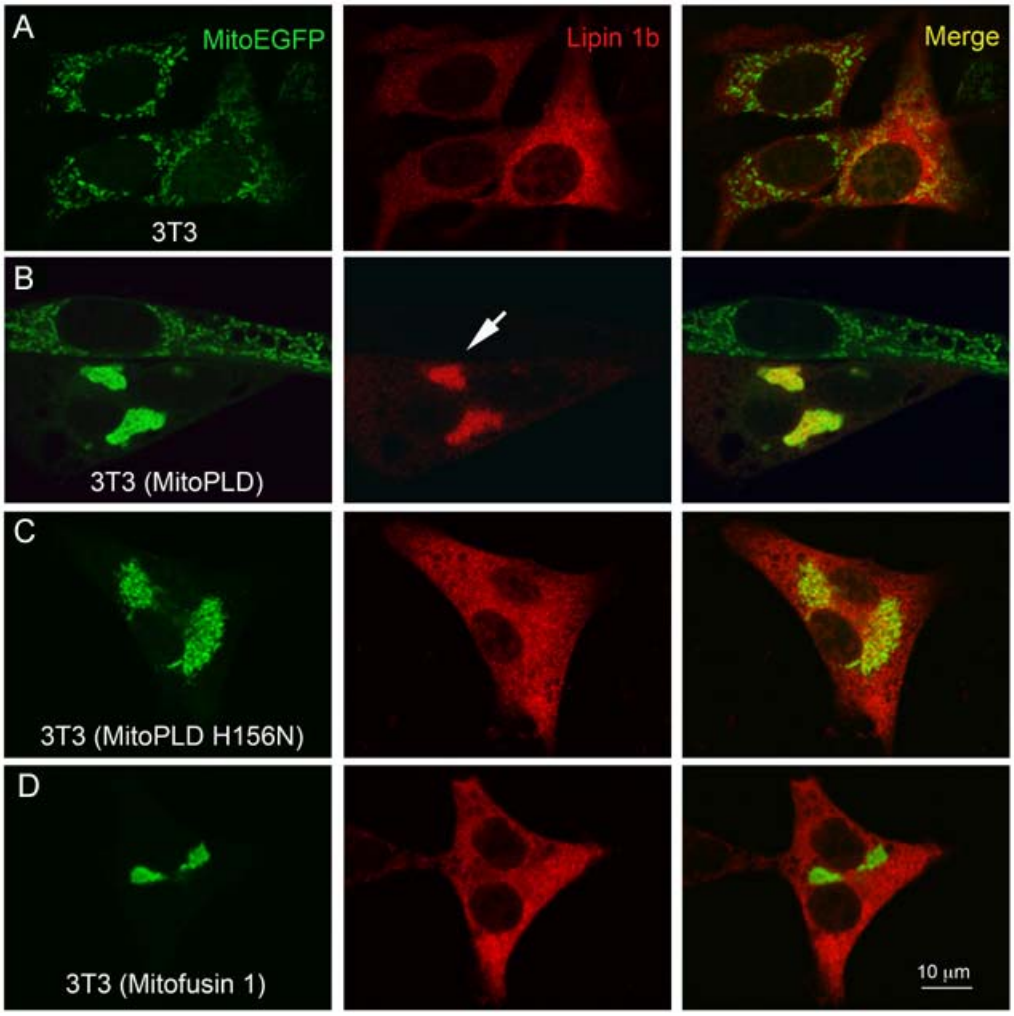
A
MitoEGFP
Lipin 1b
Merge
3T3
B
3T3 (MitoPLD)
C
3T3 (MitoPLD H156N)
D
3T3 (Mitofusin 1)
10 μm

Fig. 3.4 Lipin 1b can be recruited to the plasma membrane by elevating the level of PA production there.

Expression of flag-tagged Lipin 1b in CHO cells with (B) and without (A) induced expression of HA-tagged PLD2, a PLD family member that localizes to the plasma membrane and robustly generates PA there in the basal setting. Not shown, human Lipin 1 and mouse Lipin 1a also translocate to mitochondria and plasma membrane in a PA-dependent manner.

Fig. 3.4

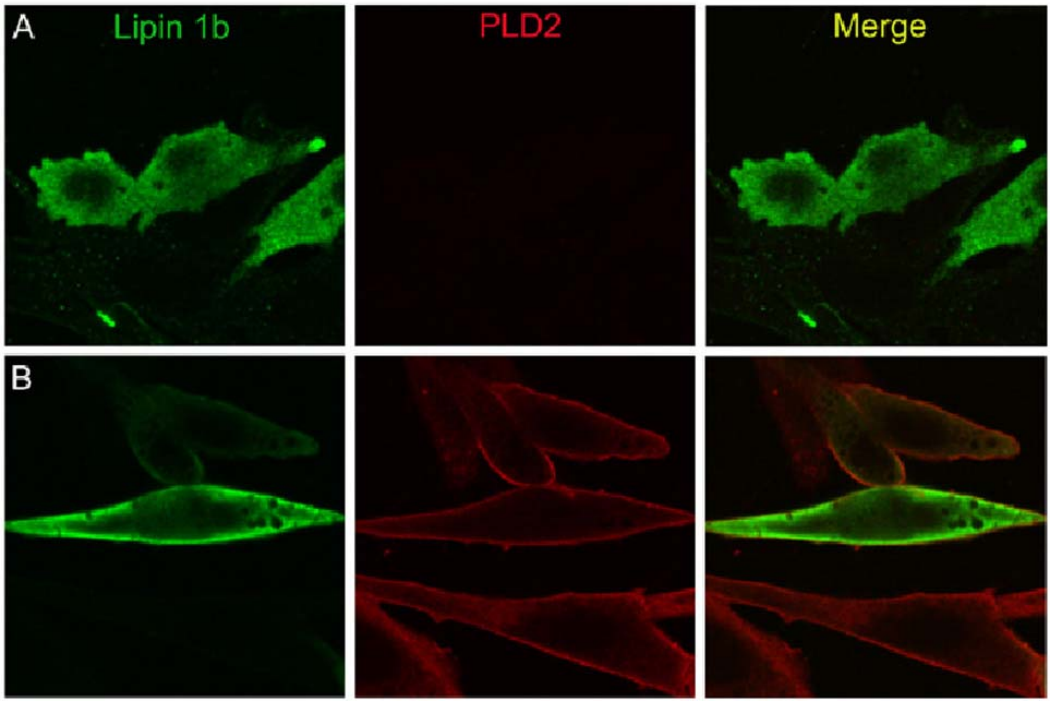

Fig. 3.5 Production of DAG on the mitochondrial surface following Lipin 1b translocation.

(A) Control NIH3T3 cells were transfected with an expression plasmid encoding the DAG-binding C1b domain of PKCδ fused with YFP (C1bδ-YFP) and immunostained to detect cytochrome c, or calreticulin as an endoplasmic reticulum (ER) marker and GM130 as a Golgi marker.

(B) C1bδ-YFP (green) was transiently transfected into NIH3T3 cells expressing MitoPLD-Flag, which was detected using an anti-Flag epitope monoclonal antibody.

(C) Co-transfection of HA-Lipin 1b and C1bδ-YFP into NIH3T3 cells expressing MitoPLD-Flag. g, Golgi; m, mitochondria. The cells shown are typical of >90% of the cells in multiple fields for transfection experiments performed 3 or more times.

(D, E) Lipin 1b generates DAG on the mitochondrial surface in an activity-dependent manner. (D) Co-expression of MitoPLD, Lipin 1b, and a DAG sensor causes mitochondrial aggregation, Lipin 1b recruitment, and DAG sensor translocation to the mitochondrial surface. (E) Co-expression of MitoPLD, catalytically-inactive Lipin 1b D712A, and the DAG sensor causes mitochondrial aggregation and Lipin 1b recruitment, but no translocation of the DAG sensor, indicating that DAG is not being produced on the mitochondrial surface. Note that the sensor localizes to the Golgi, but does not overlap in position with the aggregated mitochondria. fld, fatty liver dystrophy mice lacking Lipin 1. *fld/fld* cells were used since Lipin 1 multimerizes (unpublished observation) and thus the catalytically-inactive mutant allele might recruit wt Lipin 1 to the mitochondria in wt cells through complex formation.

Fig. 3.5

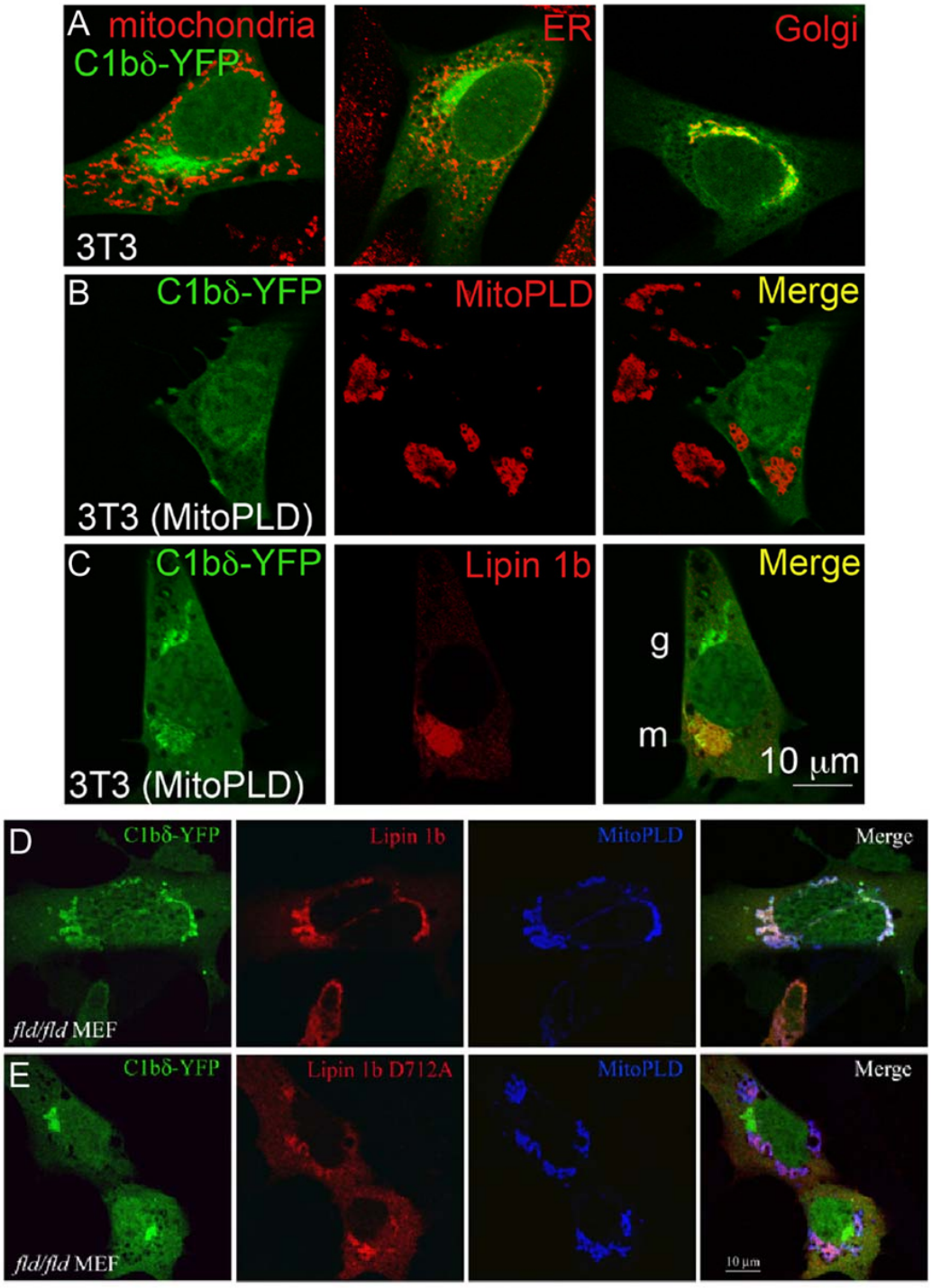
A mitochondria
C1bδ-YFP
3T3
ER
Golgi
B C1bδ-YFP
3T3 (MitoPLD)
MitoPLD
Merge
C C1bδ-YFP
3T3 (MitoPLD)
Lipin 1b
Merge
g
m
10 μm
D C1bδ-YFP
fld/fld MEF
Lipin 1b
MitoPLD
Merge
E C1bδ-YFP
fld/fld MEF
Lipin 1b D712A
MitoPLD
Merge
10 μm

Fig. 3.6. Lipin 1b is recruited to mitochondria via a central domain and promotes mitochondrial tubule shortening at physiological levels of PA in an activity-dependent manner.

(A) Lipin 1b overexpression shortens mitochondrial tubules. HeLa cells were transiently transfected with wt HA-Lipin 1b. 24 hours later, the cells were stained with anti-HA antibody (red) and cyt c (green). Asterisk, transfected cells with fragmented mitochondria; arrow, non-transfected cell with tubular mitochondria.

(B) Mitochondrial morphology was quantified to score the percentage of cells having predominantly tubular, intermediate and fragmented mitochondria (see Methods). The experiment was repeated three times with a total of 244 (control), 162 (Lipin 1b) and 144 (Lipin 1b D712A) cells counted. Bars indicate SEM.

(C) PA-dependent translocation depends on a central region of Lipin 1b. Deletion mutants of Lipin 1b as indicated were co-transfected with MitoEGFP into control and MitoPLD-expressing NIH3T3 cells and imaged as shown in Fig. 2C and D to identify the region that mediates PA-induced translocation to mitochondria. "+", translocation seen in >95% of co-transfected cells; "-", no translocation observed. n>100 cells for each construct, which were each transfected at least three separate experiments. Red lines, basic amino acid clusters; purple box, alternate exon included in Lipin 1b and excluded in Lipin 1a; yellow bar, catalytic motif.

Fig. 3.6

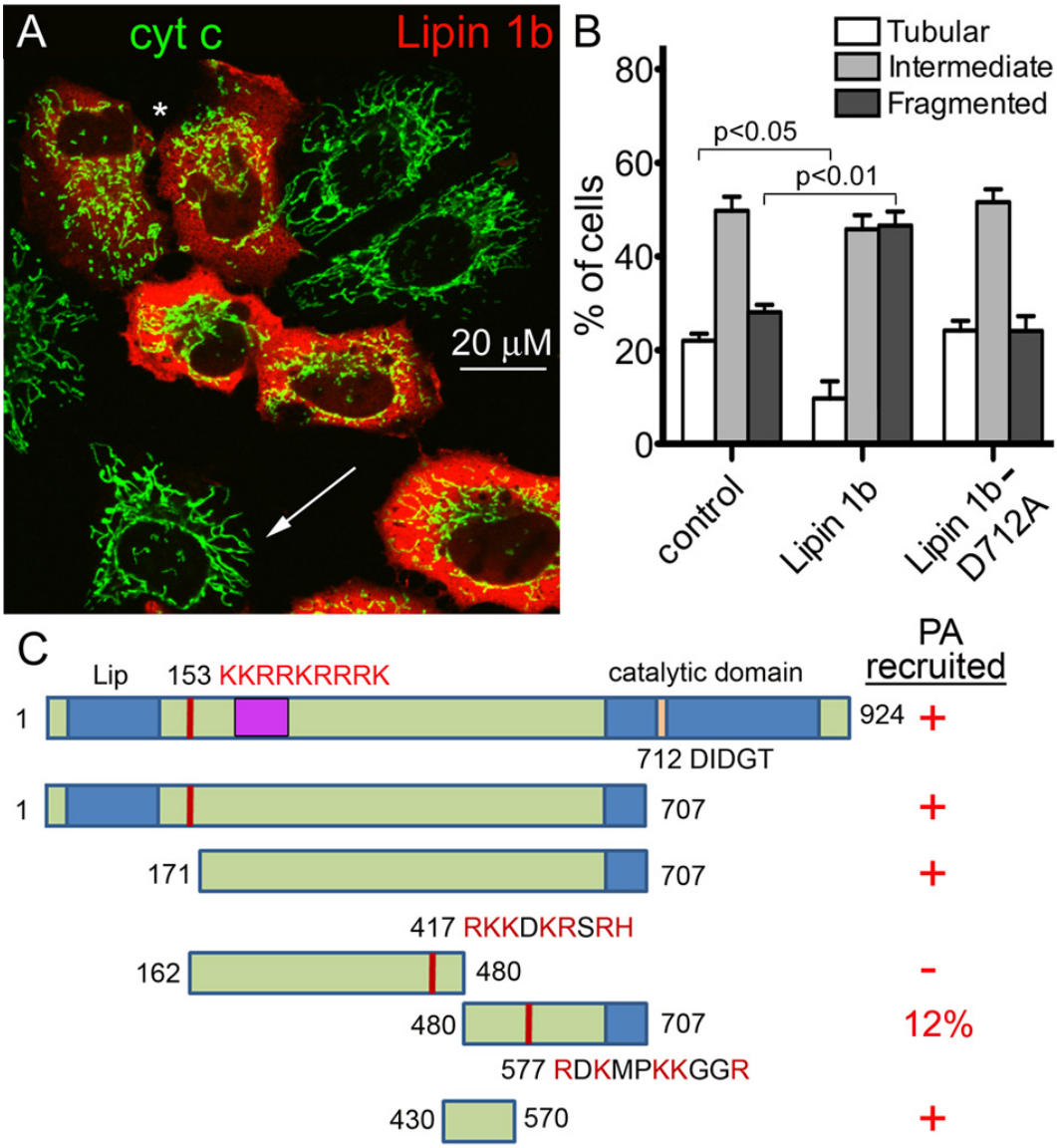
A
cyt c
Lipin 1b
*
20 µM
B
Tubular
Intermediate
Fragmented
% of cells
80
60
40
20
0
p<0.05
p<0.01
control
Lipin 1b
Lipin 1b-D712A
C
Lip
153 KKRRKRRRK
catalytic domain
PA recruited
1
924
+
712 DIDGT
1
707
+
171
707
+
417 RKKDKRSRH
162
480
-
480
707
12%
577 RDKMPKKGGR
430
570
+

Fig. 3.7 Lipin 1b 430-570 is recruited to the mitochondrial surface by MitoPLD-generated PA.

HA-Lipin 1b (430-570) and MitoEGFP were co-transfected into NIH3T3 control cells (A) or inducible cells expressing (B) WT MitoPLD, (C) catalytically-inactive H156N-MitoPLD, or (D) Mitofusin1. 1 day later, the cells were fixed, permeabilized, and immunostained with an anti-HA monoclonal antibody to detect Lipin 1b (430-570).

Fig. 3.7

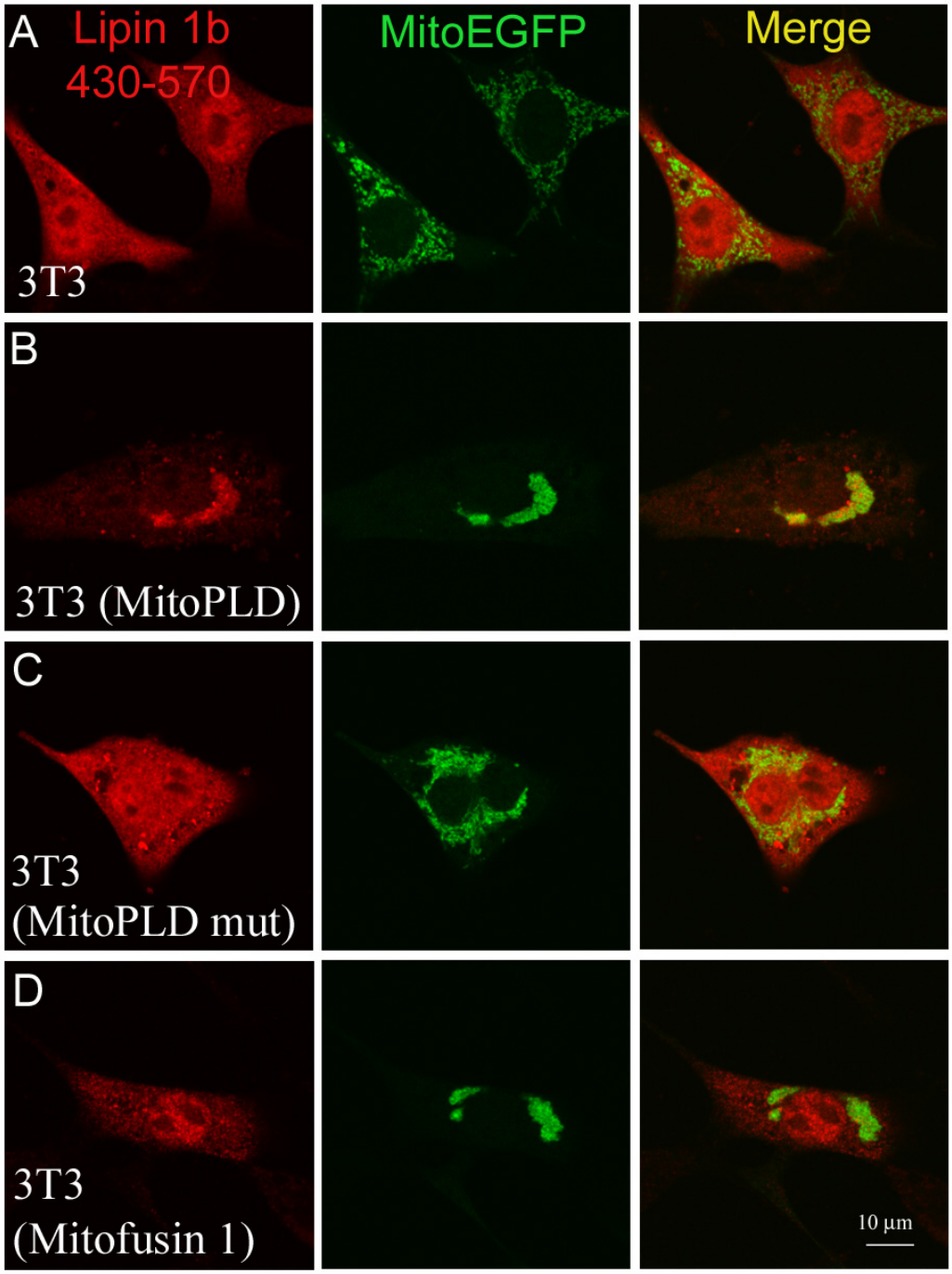
A
Lipin 1b
430-570
MitoEGFP
Merge
3T3
B
3T3 (MitoPLD)
C
3T3
(MitoPLD mut)
D
3T3
(Mitofusin 1)
10 µm

Fig. 3.8 Lipin 1b 430-570 can be recruited to the plasma membrane by elevating the level of PA production there.

Expression of Lipin 1b 430-570 in CHO cells with (B) and without (A) induced expression of PLD2, a PLD family member that localizes to the plasma membrane and robustly generates PA there in the basal setting.

Fig. 3.8

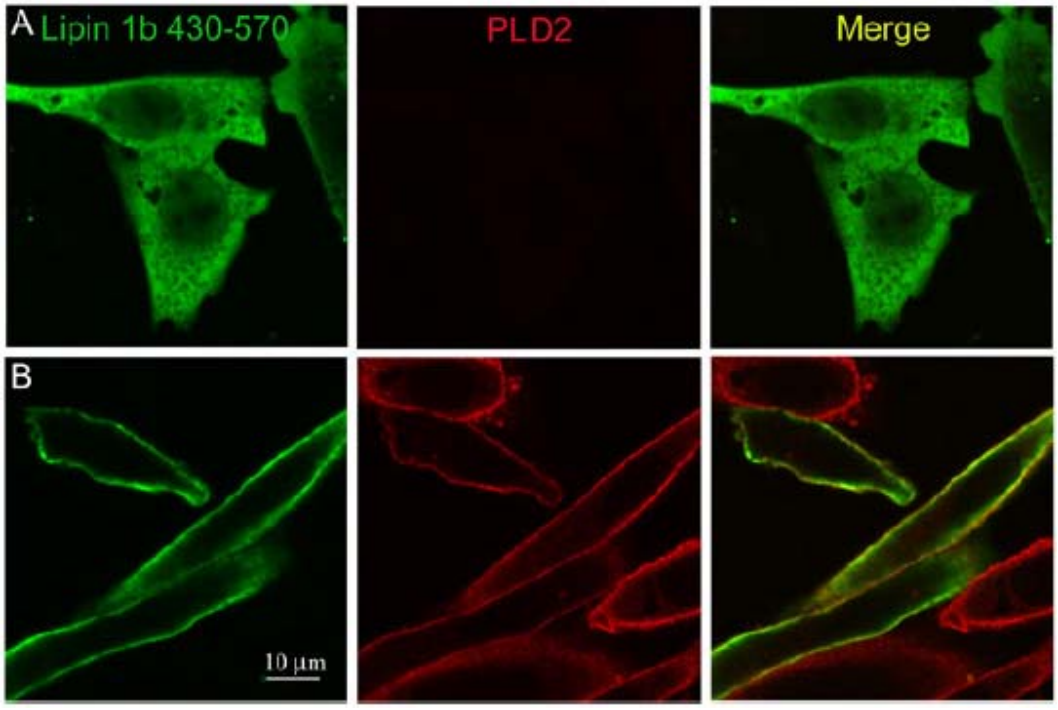

Fig. 3.9. The Lipin 1 catalytic domain translocates in a PA-independent manner to sites of presumptive mitochondrial fission and causes mitochondrial fragmentation.

(A-D) HeLa cells were transiently transfected with Lipin 1b 705-end and imaged as above. (A) Asterisk, non-transfected cell showing normal mitochondrial tubulation. Arrow, transfected cells with extensive fragmentation. (B) Magnification of fragmented tubules. Note the localization of HA-Lipin 1b to the tips of the fragments. (C) Example of a relatively infrequent transfected cell (<5%) that retained some tubulation. (D) Magnification of tubules decorated with HA-Lipin 1b.

(E-K) Co-localization of HA-Lipin 1b with endogenous Drp1 on tubules. (F, J) Lines and arrowheads indicate constrictions at which Drp1 and the Lipin 1 catalytic domain can be found, respectively. (I, K) Arrow, constriction at which only Drp1 is found.

Fig. 3.9

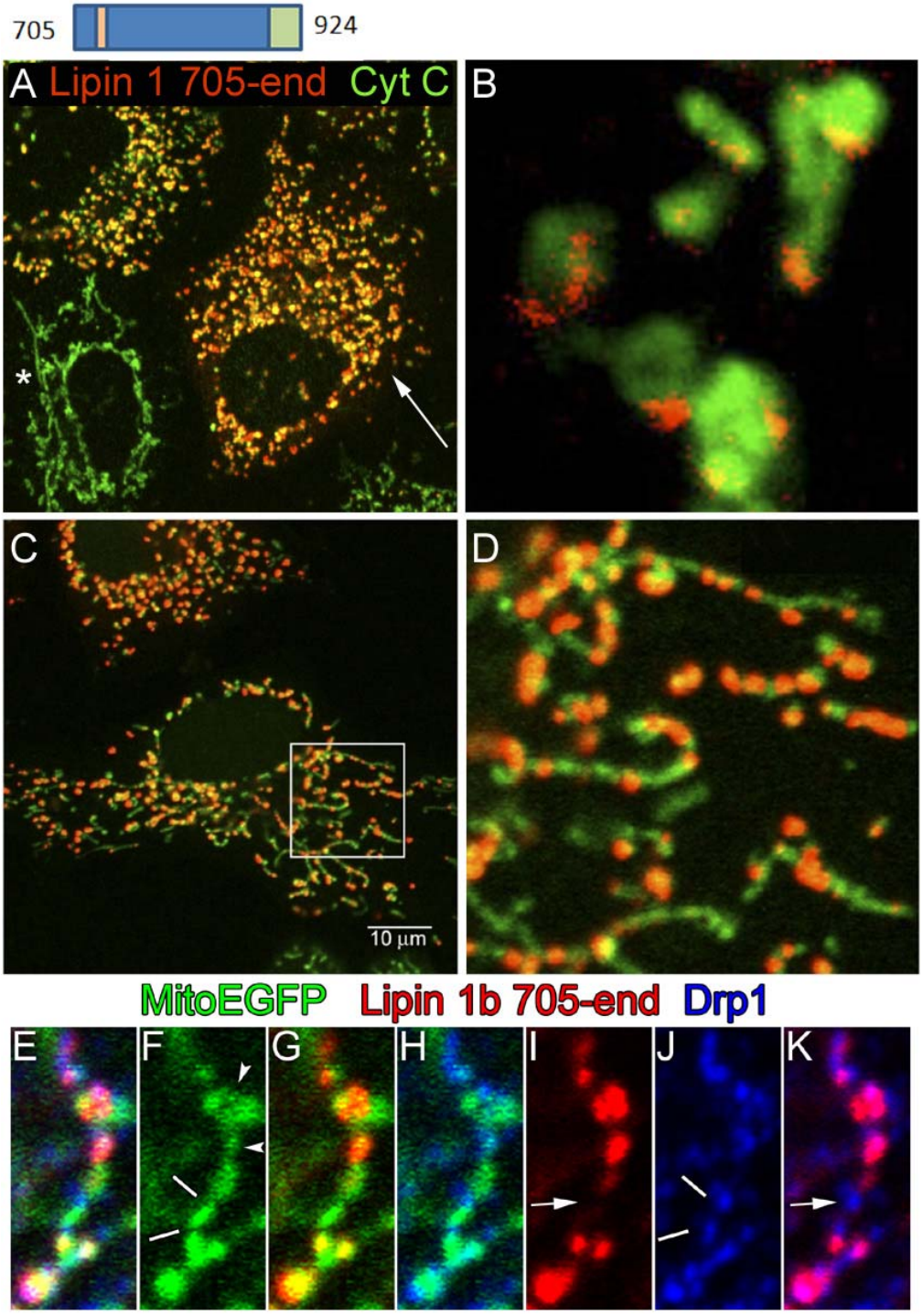
705
924
A Lipin 1 705-end Cyt C
B
C
D
10 µm
MitoEGFP Lipin 1b 705-end Drp1
E
F
G
H
I
J
K

Fig. 3.10. Lipin 1b 705-end localizes to mitochondria independently of PA and generates DAG there.

(A) Expressed Lipin 1b 705-end localizes to mitochondria in cells overexpressing MitoPLD (elevated PA) and generates DAG from the PA, causing recruitment of the DAG sensor.

(B) Lipin 1b 705-end also localizes to mitochondria in cells expressing a catalytically-inactive MitoPLD allele that functions as a dominant negative allele to prevent PA formation (which also leads to mitochondrial fragmentation).

Fig. 3.10

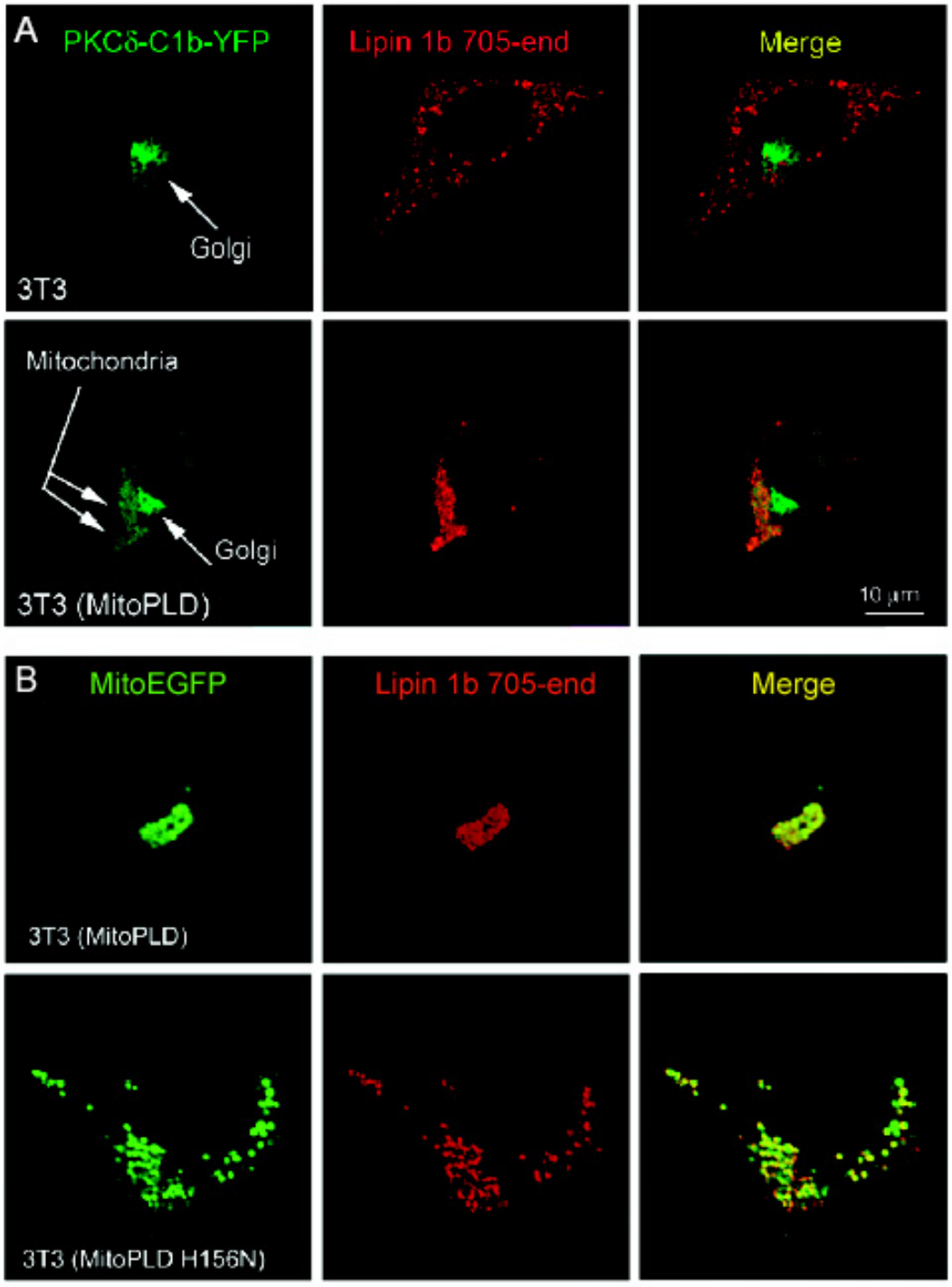
A
PKCδ-C1b-YFP
Lipin 1b 705-end
Merge
Golgi
3T3
Mitochondria
Golgi
3T3 (MitoPLD)
10 μm
B
MitoEGFP
Lipin 1b 705-end
Merge
3T3 (MitoPLD)
3T3 (MitoPLD H156N)

Fig. 3.11. Proposed model for regulated mitochondrial fusion and subsequent fission.

Production of PA by MitoPLD facilitates mitochondrial fusion followed by the recruitment of Lipin 1 to convert the PA into DAG, which promotes fission at nearby sites by interacting with the fission machinery. See text for details.

Fig. 3.11

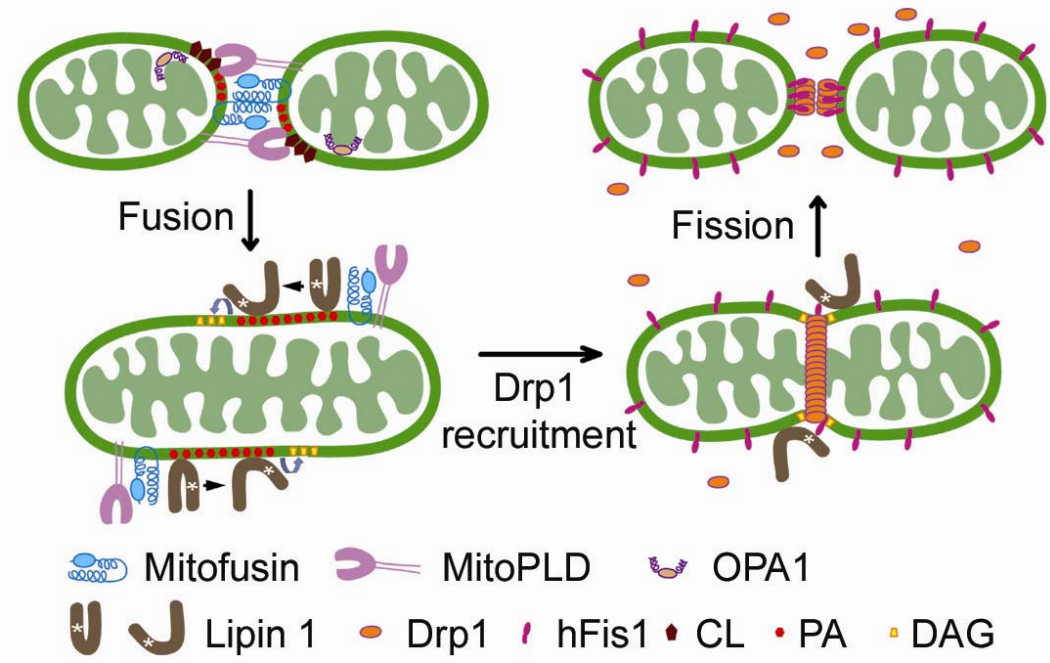
Fusion
Fission
Drp1
recruitment
Mitofusin
MitoPLD
OPA1
Lipin 1
Drp1
hFis1
CL
PA
DAG

Fig. 3.12 Targeted inactivation of MitoPLD.

Homologous recombination was used to flank Exon 2 with loxP sites which were then deleted in eggs using Cre-recombinase. All steps of generation and breeding of the mice were performed in the C57/B16 background. Genotyping primers and PCR are shown.

Fig. 3.12

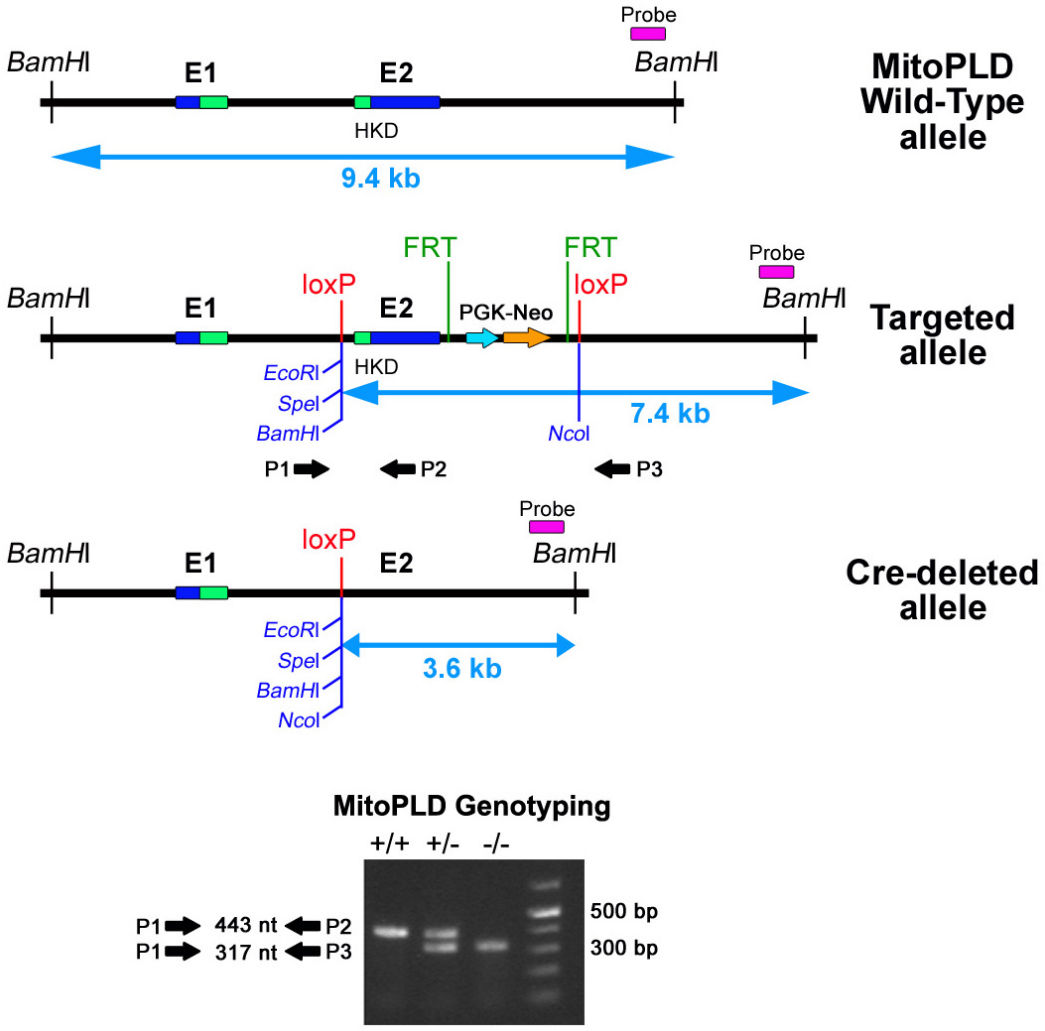
Probe
BamHI
E1
E2
BamHI
HKD
9.4 kb
MitoPLD Wild-Type allele
FRT
FRT
Probe
loxP
loxP
BamHI
E1
E2
PGK-Neo
BamHI
Targeted allele
EcoRI
SpeI
BamHI
HKD
7.4 kb
NcoI
P1
P2
P3
Probe
BamHI
loxP
E1
E2
BamHI
Cre-deleted allele
EcoRI
SpeI
BamHI
NcoI
3.6 kb
MitoPLD Genotyping
+/+ +/- -/-
P1 443 nt P2
P1 317 nt P3
500 bp
300 bp

Fig. 3.13. Loss of MitoPLD causes shortening of mitochondrial tubules in mouse embryo fibroblasts.

(A, B) MEFs prepared from WT and MitoPLD$^{-/-}$ day 13.5 embryos were fixed, immunostained for cyt c to visualize mitochondria, and scored for tubular morphology. (A) Typical fully-tubulated WT MEF. (B) Typical MitoPLD$^{-/-}$ MEF with shortened tubules and many mitochondrial fragments (arrow), particularly in periphery of cell. Thin circle, region containing mitochondrial fragments copied into thick circle with increased brightness.

(C) Quantitation of mitochondrial morphologies. MitoPLD$^{-/-}$ MEFs generally displayed at least a small amount of tubulation and thus were scored as intermediate rather than fragmented, despite obvious differences in appearance of the tubules. n= 5 experiments, 303 cells scored.

(D, E) Transient transfection of Lipin 1b 705-end in WT and MitoPLD$^{-/-}$ MEFs causes extensive fragmentation in both cell lines.

Fig. 3.13

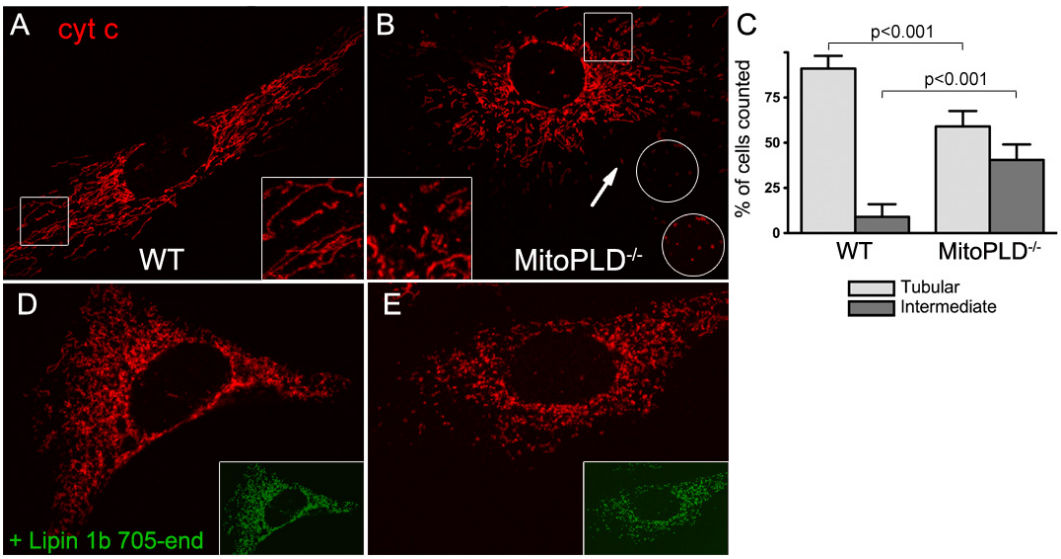
A
cyt c
WT
B
MitoPLD-/-
C
p<0.001
p<0.001
% of cells counted
75
50
25
0
WT
MitoPLD-/-
Tubular
Intermediate
D
+ Lipin 1b 705-end
E

Fig. 3.14. MitoPLD$^{-/-}$ mice exhibit meiotic arrest during spermatogenesis and loss of nuage.

(A) MitoPLD is expressed in testes. An affinity-purified anti-MitoPLD peptide rabbit antiserum that recognizes MitoPLD overexpressed in NIH3T3 cells (left panel) by Western blotting identifies a band of the correct size (35 kDa) in WT testes (right panel) that is absent in MitoPLD$^{-/-}$ testes. Tubulin, loading control.

(B,C) MitoPLD$^{-/-}$ testes were uniformly reduced in size compared to WT testes ($n>20$).

(D) Hematoxylin and eosin staining of sections from WT and MitoPLD$^{-/-}$ testes. White boxes, areas magnified in (E); asterisks, vacuole / cell drop-out sites; arrow, apoptotic cell with condensed, darkly staining nucleus; arrowhead, cell with disorganized chromosomal material (magnified in inset at lower right of panel).

(E) Insets from (D). a and e, prophase spermatocyte; b, meiotic spermatocyte; c, spermatid; d, spermatogonia; f, apoptotic cell (below) and cell with disorganized chromosomal material (above).

(F-K) Electron microscopy of WT (F-H) and MitoPLD$^{-/-}$ (I-K) testes. Arrowheads, nuage associated with aggregated mitochondria; arrow, nuage; asterisk, magnified region in (H, K, M). (L,M) NIH3T3 cells expressing elevated levels of MitoPLD.

Images presented in (D-K) are representative of > 400 images collected from 2-3 mice per genotype in different experiments. Mice were 2-4 months in age.

Fig. 3.14

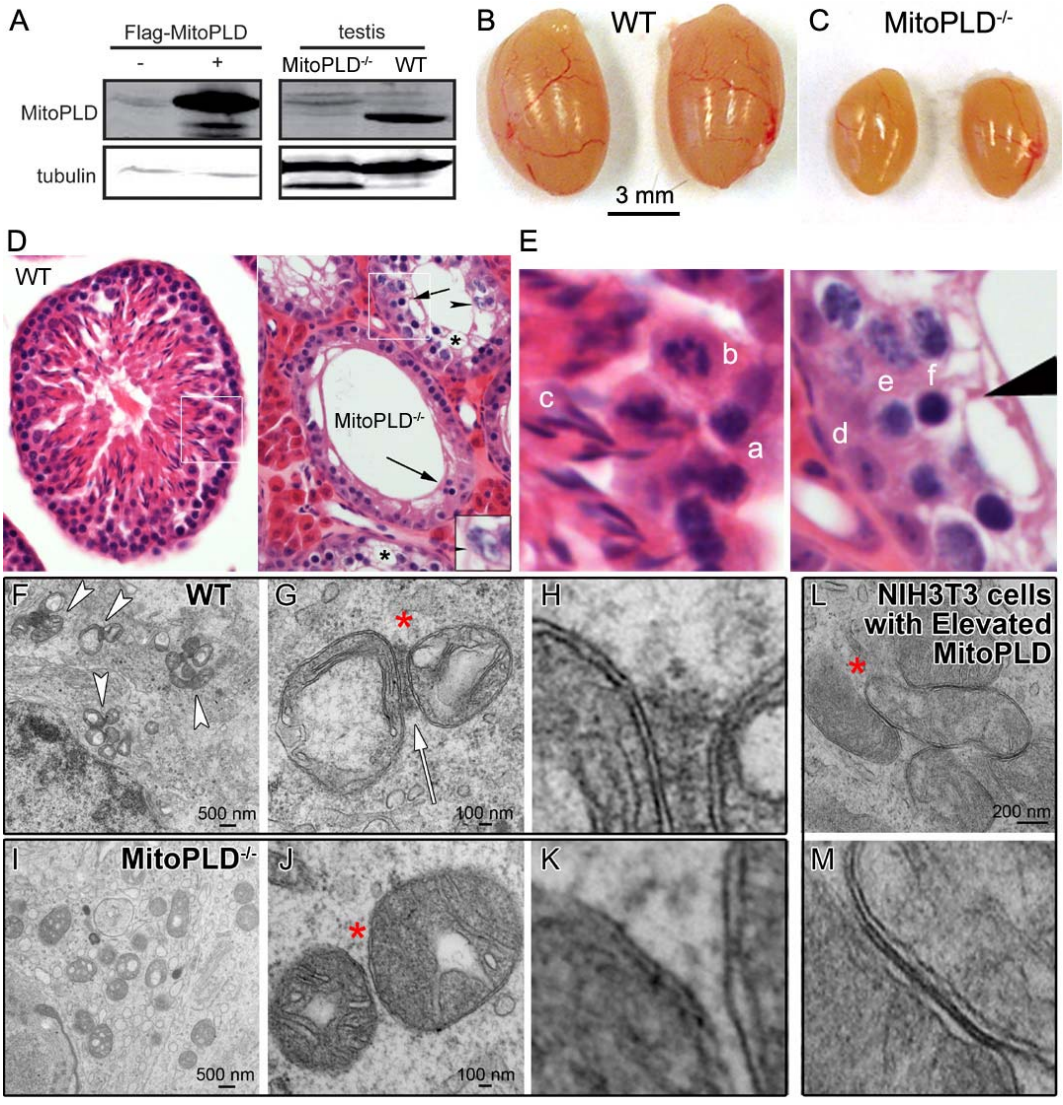
A
Flag-MitoPLD
-
+
testis
MitoPLD-/-
WT
MitoPLD
tubulin
B
WT
3 mm
C
MitoPLD-/-
D
WT
MitoPLD-/-
E
a
b
c
d
e
f
F
WT
500 nm
G
100 nm
H
L
NIH3T3 cells with Elevated MitoPLD
200 nm
I
MitoPLD-/-
500 nm
J
100 nm
K
M

Fig. 3.15. Loss of TDRD1 expression and increased double-strand breaks in MitoPLD$^{-/-}$ testes.

(A,B) Frozen sections of WT and MitoPLD$^{-/-}$ testes were fixed and stained with DAPI and immunostained with anti-TDRD1. Inset, magnification of area indicated by asterisk. Diffuse red haze in interstitial tissue in WT and MitoPLD$^{-/-}$ testes reflects non-specific staining.

(C-H) Frozen sections were stained with DAPI and immunostained with anti-γH2X. (C-E) γH2X images; (F-H) with DAPI to show all cells. Images representative of >40 sections examined from two separate immunostaining experiments.

All images were captured with the same intensity of laser and processed identically. Asterisk, center of tubule.

Fig. 3.15

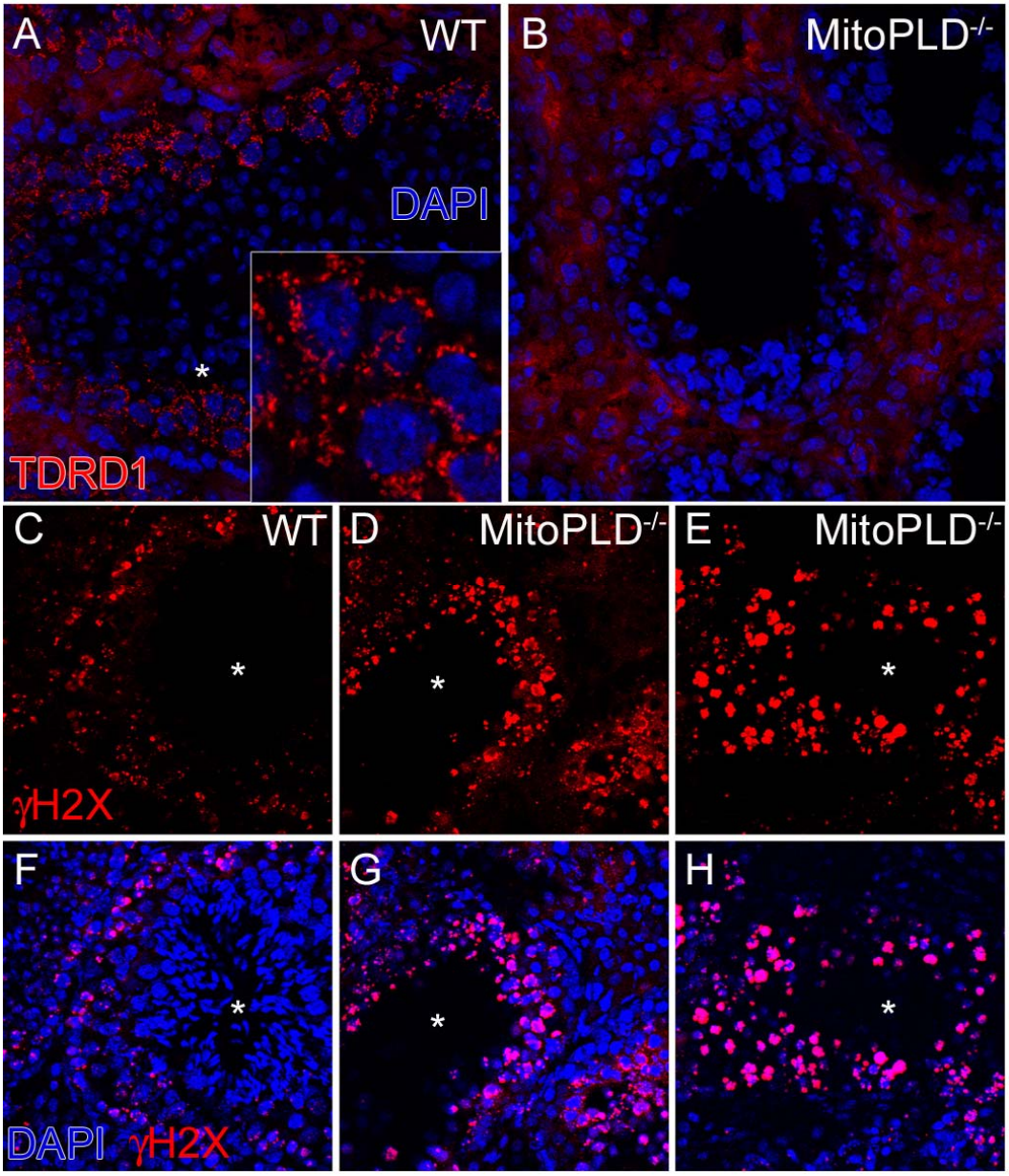
A
WT
DAPI
TDRD1
B
MitoPLD-/-
C
WT
γH2X
D
MitoPLD-/-
E
MitoPLD-/-
F
DAPI γH2X
G
H

Fig. 3.16. Increased nuage and altered TDRD1 localization in *fld/fld* testes.

(A-C) Electron microscopy images of *fld/fld* testes. Arrowheads, nuage; asterisk, white box, areas magnified in (B,C). Representative of >75 images from 3 adult (2-4 month old) mice.

(D) Normalized nuage density in WT and *fld/fld* testes. NIH ImageJ software was used to quantitate the density of nuage, which was then normalized to the density of adjacent mitochondrial matrix to control for contrast and darkness of image (compare panel C to Fig. 6H). n=21 measurements for each genotype, images used from multiple grids and experiments.

(E,F) Anti-TDRD1 and DAPI staining in frozen sections from *fld/fld* testes. n=2 experiments, 5 sections / experiment. Representative images.

Fig. 3.16

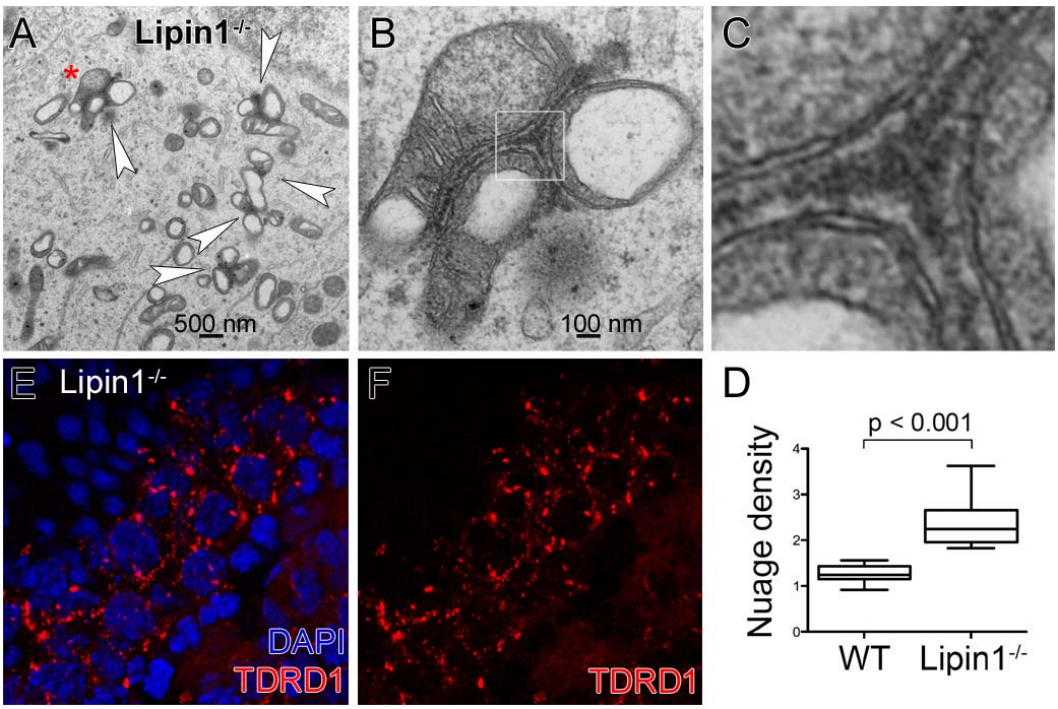
A
Lipin1-/-
500 nm
B
100 nm
C
E
Lipin1-/-
DAPI
TDRD1
F
TDRD1
D
p < 0.001
Nuage density
0
1
2
3
4
WT
Lipin1-/-

Fig. 3.17. A human MitoPLD SNP results in functional inactivation.

(A) SNP rs61738638 at position 565 of the mRNA identifies a C->G mutation that changes Asn173 to Lys. N173 is a highly conserved amino acid in the PLD superfamily and is invariant in the MitoPLD/Zuc/Nuc subfamily.

(B) Shown in figure is co-expression of MitoPLD N173K-EGFP and HA-Lipin 1b in HeLa cells.

Fig. 3.17

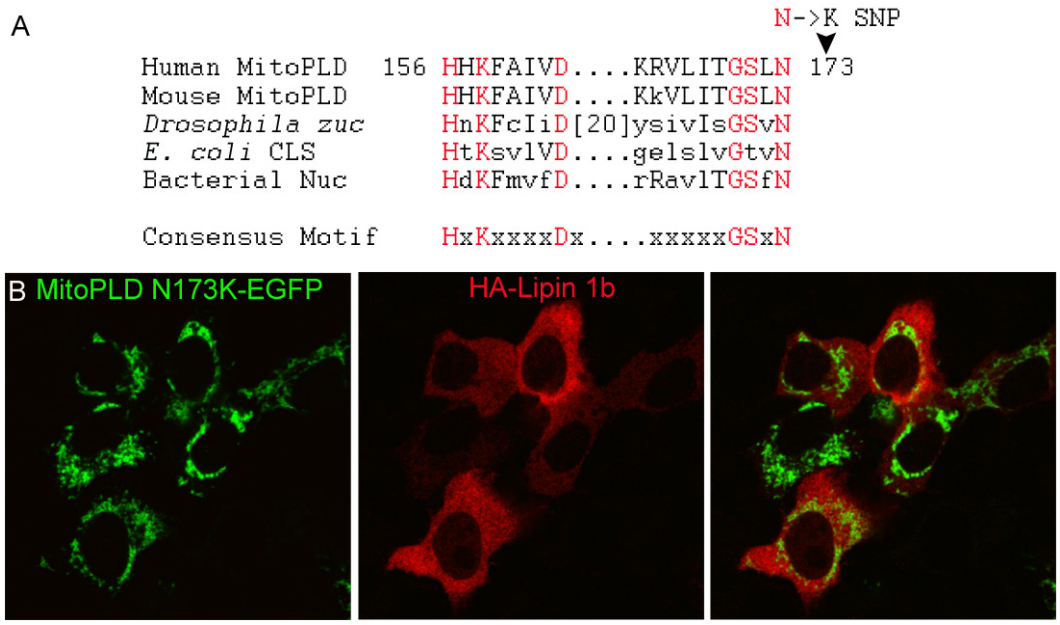
A
N->K SNP
Human MitoPLD 156 HHKFAIVD....KRVLITGSLN 173
Mouse MitoPLD HHKFAIVD....KkVLITGSLN
Drosophila zuc HnKFcIiD[20]ysivIsGSvN
E. coli CLS HtKsvlVD....gelslvGtvN
Bacterial Nuc HdKFmvfD....rRavlTGSfN
Consensus Motif HxKxxxxDx....xxxxxGSxN
B MitoPLD N173K-EGFP
HA-Lipin 1b

Chapter 4: Conclusions and future directions

4. 1 A quantitative assay for mitochondrial fusion

4.1.1 Overall conclusions regarding the quantitative assay

By targeting the N-terminal and C-terminal *Renilla* luciferase fragments into the mitochondria of two cell populations and then monitoring the luciferase activity generated from split-luciferase reconstitution after chemical-induced cell fusion followed by mitochondrial fusion, I have successfully developed an assay to quantitatively measure mitochondrial fusion activity. This is the first quantitative assay that records mitochondrial fusion on a population level, which is usable for high-throughput analysis.

I first followed the mitochondrial fusion rate in HeLa cells and found that the equilibrium of luciferase reconstitution and protein degradation leads to the peak of luciferase activity at 3 hours after cell fusion and thus reduced the assay time from 7-18 hours to 3 hours. As a control, cells with null mutations in both Mfn 1 and 2, proteins that are required for mitochondrial fusion, exhibited

minimal luciferase activity. Comparing the wt MEFs with Mfn1/2$^{-/-}$ MEFs, I determined that my assay background is only 6% of the signal, sensitive enough to adapt it to high-throughput analysis.

To further validate the fusion assay, a few mitochondrial inhibitors, which have been shown earlier to alter mitochondrial fusion behaviors, were applied to the cells during the assay period. Consistent with the previous findings using the classic fusion assay, I found mitochondrial fusion is dependent on intact membrane potential and glycolysis activity to different extents but independent on cytoplasmic ATP synthesis. I have also now quantitatively determined the extent of inhibition for each inhibitor.

Finally, I used my newly developed assay to study the significance of each cytoskeleton components for mitochondrial fusion. In agreement with the previous findings, mitochondrial fusion is independent of the actin or microtubule cytoskeleton. Interestingly however, I found that mitochondrial fusion depends on the integrity of the vimentin-based intermediate filaments, which might reflect an underestimated importance of this cytoskeleton component to mitochondrial fusion activity.

4.1.2 Further considerations regarding the quantitative assay

Are there other IFs involved in mitochondrial fusion?

I have uncovered the role of vimentin-based IF in mitochondrial fusion, possibly by altering the trafficking of the organelles. The IF family constitutes a variety of proteins, encoded by around 70 conserved genes, that populates different cell types (Hesse et al. 2001). Apart from proteins encoded by three lamin genes, all the other IF family members are cytoplasmic proteins, which theoretically could interact with mitochondria. It is possible that other types of IF also play a role in mitochondrial dynamics.

IFs are functioning in many important physiological processes, and the localization of them is closely related to the corresponding functions. There are at least seven kinds of IF networks in the cytoplasm of polarized cells, six of which are either restricted to a certain compartment of the cell or associated with granules or the Golgi apparatus (Iwatsuki and Suda 2010). The only one group that is theoretically possible to be involved in mitochondrial function is the one distributed to the entire cytoplasm, such as vimentin, nestin, glial fibrillary acidic protein (GFAP), keratin, desmin, and neurofilament. The association of mitochondria with nestin and GFAP has rarely been observed. However, the involvement of the rest IFs, namely keratin, desmin and neurofilament, in mitochondrial fusion has been suggested and requires further investigation.

Keratins are the most diverse proteins among IF, which are selectively expressed in epithelial cells with many cell type-specific isoforms. In hepatocytes, keratin 8 and keratin 18 are the only keratins expressed. It has been shown in

keratin 8 knockout mice that keratin 8-null mitochondria were significantly smaller, showed irregular distribution, and had more cytochrome c release after Ca^{2+} and oxidative stress, indicative of mitochondrial fragmentation (Tao et al. 2009). *In vitro* studies in liver cells also showed that mitochondria in mutant keratin 18-transfected cells were fragmented into small spheroids with less fluorescence recovery after photo-bleaching, suggesting of reduced mitochondrial fusion in these cells (Kumemura et al. 2008). These findings suggest that keratins in hepatocytes are directly or indirectly important for the maintenance of mitochondrial morphology and function.

Desmin is the muscle-specific IF protein, which expresses in the very early stage of myogenesis. In desmin-deficient skeletal and cardiac muscle, mitochondria abnormalities were detected earlier than other structure defects, including loss of proper distribution, number and respiratory function, which reflects alter in fusion-fission equilibrium leading to mitochondrial fragmentation (Milner et al. 2000). A transgenic mouse model with low level expression of L345P desmin mutation also showed ultrastructural changes in muscle with mitochondrial swelling and vacuolization (Kostareva et al. 2008). Patients with a desmin insertion mutation showed similar mitochondrial abnormalities due to the disruption of desmin network by aggregation (Schroder et al. 2003).

Neurofilament is the most abundant cytoskeleton component in axons. Abnormal accumulation of neurofilament has been associated with many

neurodegenerative disorders. Recently, several major neurodegenerative diseases such as Parkinson's disease, Alzheimer's disease and Huntington's disease have been shown to involve disruption in mitochondrial dynamics (Chen and Chan 2009). Interestingly, cultured primary dorsal root ganglion neurons derived from mice deficient from light neurofilament subunit have longer and more persistent movement of mitochondria, suggesting that neurofilament network hampers the mitochondria trafficking (Perrot and Julien 2009). Defects in both fusion and fission have been related to decreased mitochondrial movement. However, whether the mitochondrial movement defects can affect mitochondrial fusion and fission needs future study.

Taken together, various IFs proteins may regulate mitochondrial morphology in specific cells. However defects in trafficking can affect mitochondrial morphology without disrupting mitochondrial fusion and fission, which makes a sensitive mitochondrial fusion assay necessary to determine mitochondrial fusion perturbation in each case.

High-throughput screening of modulators of mitochondrial fusion

The advancement in modern technology has brought us highly versatile robotics to perform high-throughput screens for active compounds, antibodies, and genes that modulates a certain biological process or biomolecular pathway as long as a feasible and facile assay can be designed. However, all the available mitochondrial fusion assays require microscopic examination for readouts, which

hinders the high-throughput screening for modulators of mitochondrial fusion until I developed this assay using luminescence as readouts.

I believe that my quantitative assay is easily adaptable to a high-throughput analysis. Several companies have developed high-capacity microplate handlers that can integrate microplate washers, readers and liquid handling systems, a complete robotic system that meets all the requirements to operate an automated mitochondrial fusion assay. By treating the cells with an RNAi library or a small molecule library, we can easily discover new genes that are involved in mitochondrial fusion or mitochondrial fusion inhibitors.

Other applications and modifications of the quantitative fusion assay

Before my assay was published, closed-door presentation of it at mitochondria meetings led to many requests for collaborations, either for novel applications in new systems or to modify my *in vivo* fusion assay.

A group dedicated to studying the mechanisms of mitochondrial fusion is applying the assay to screen for Mitofusin 1/2 monoclonal antibodies that can function as fusion inhibitors. Currently, hybridoma supernatants containing antibody can be tested for binding ability in a high-throughput manner. However, antibodies that can bind the antigen do not necessarily neutralize it, thus requiring a further assay to assess neutralization. My quantitative mitochondrial fusion assay fits their exact needs for the screening process. Once good candidates are identified, it would be a useful tool to study the detailed mechanisms of

mitochondrial fusion and possibly rescue the phenotypes caused by perturbations in mitochondrial dynamics, just as the Drp1 inhibitor, mdivi-1, has led to a detailed analysis on the role of Drp1 in apoptosis and has successfully rescued the phenotype induced by human mutant PTEN-induced putative kinase 1 (Pink1), which can cause autosomal recessive Parkinson's disease (Cassidy-Stone et al. 2008; Cui et al. 2010).

Another collaborator is interested in the biochemical requirement for mitochondrial fusion and has adapted my assay to an *in vitro* mitochondrial fusion assay by introducing the split luciferase fragments into cells and purifying the two populations of mitochondria to perform an *in vitro* fusion assay. By doing so, they can control the constitution of the reaction environment and assay the significance of individual components in the mitochondrial fusion process. This assay system has allowed them to establish the energetic requirements and reveal a dependence on active protein phosphorylation for mitochondrial fusion (Schauss et al. 2010 *in press*). The same group is also generating transgenic mice to express each split luciferase fragment. The mice can then be crossed with several disease models and used to study the mitochondrial fusion behavior in different organs or tissues.

Above are only a few examples of new applications for the quantitative mitochondrial fusion assay. I believe with the ease to perform this assay, more and more new studies will find my assay useful to answer a variety of questions regarding mitochondrial fusion.

4.2 A mitochondrial surface lipid signaling pathway

4.2.1 Overall conclusions regarding the mitochondrial surface lipid signaling pathway

We reported previously that MitoPLD is a lipid enzyme and generates PA on the mitochondria. Here, I have further connected the production of this signaling lipid to the recruitment of a PA phosphatase, Lipin 1, and the conversion to an inter-related signaling lipid, DAG. I also explored one aspect of the physiological significance of this lipid signaling pathway to mitochondrial dynamics. Meanwhile, I also resolved contradictory reports regarding the *Drosophila* homolog of MitoPLD, denoted Zucchini, as a presumptive cytoplasmic nuclease in the piRNA pathway, which has led to many new exciting questions to be solved in the future.

Lipid signaling pathway on the mitochondrial surface

Our prior model for MitoPLD function suggested that after two mitochondria became juxtaposed together by Mfn 1 or 2, MitoPLD hydrolyzes

cardiolipin on the opposing mitochondria and presumably generated PA on the mitochondrial surface. I proved here by tracking the mobilization of a PA sensor that MitoPLD produces PA on the mitochondrial surface. Furthermore, I extended this lipid signaling pathway to the recruitment of Lipin 1b to the mitochondrial surface by this pool of PA and the following conversion of PA into DAG, indicated by the subsequent translocation of a DAG sensor to the mitochondria.

We previously uncovered the role for PA in promoting mitochondrial fusion. Here, overexpressing Lipin 1 in HeLa cells leads to shortened mitochondrial tubules, suggesting a role of Lipin 1 in mitochondrial fission at physiological levels of PA. More strikingly, the isolated Lipin 1 catalytic domain, amino acids 705-924, localizes to mitochondria in cells with physiological levels of PA and induces mitochondrial tubules to undergo almost complete fragmentation. These findings suggested a model in which MitoPLD-generated PA recruits Lipin 1 onto mitochondria and induces a conformational change in Lipin 1 to expose the encrypted binding region for fission sites and then promote mitochondrial fission.

We also characterized MEFs from MitoPLD$^{-/-}$ mice and observed shortened mitochondria compared with WT MEFs. Furthermore, Lipin 1 expression in MitoPLD$^{-/-}$ MEFs did not result in further shortening of mitochondrial tubules, confirming that Lipin 1 induced mitochondrial fission is dependent on MitoPLD-generated PA. However, the Lipin 1 catalytic domain

efficiently triggered fragmentation for both WT and MitoPLD$^{-/-}$ MEFs, indicating a PA-independent pathway in this process.

Meanwhile, in an effort to understand the mechanism of PA-directed recruitment, I dissected the Lipin 1 protein and mapped the PA-binding region to a central domain, amino acids 430-570, with dispersed basic amino acids that may mediate interaction with PA instead of the more compact positively-charged region characteristic of most other PA binding proteins.

Function of MitoPLD in mouse spermatogenesis is similar to the function of Zucchini in Drosophila oogenesis

In order to resolve the discrepancy of previous reports on human and *Drosophila* MitoPLD/Zuc, I expressed Zuc in HeLa cells and found that similar to MitoPLD, Zuc localizes to mitochondria and is able to trigger mitochondrial aggregation with high expression levels, which is also activity dependent since the catalytic mutant of Zuc, again in a similar way to the MitoPLD catalytic mutant, induces mitochondrial fragmentation. In *Drosophila*, Zucchini mediates piRNA generation, defects of which cause abnormal egg chamber and female infertility. Similarly, proteins involved in piRNA pathway in mice function in spermatogenesis and disturbance of most proteins lead to male infertility. Correspondingly, MitoPLD$^{-/-}$ mice exhibit meiotic arrest during spermatogenesis leading to reduced size of seminiferous tubules with a thin layer of

spermatogonia, sertoli cells and spermatocytes early in meiosis around the periphery, but no late or post meiotic spermatocytes nor spermatids.

Previous studies with piRNA components revealed that they localize in specified cytoplasmic loci called nuage. Interestingly, mitochondria-associated nuage, also known as intermitochondrial cement, was not observed in MitoPLD$^{-/-}$ samples. Therefore, consistent with studies of some other piRNA pathway components, loss of nuage results in loss of a critical component of piRNA pathway, TDRD1. As piRNA was proposed to be critical to suppress transposon activation, high level of γH2X expression was observed in MitoPLD$^{-/-}$ tubules as a consequence of transposon activation induced double strand breaks, which ultimately leads to meiotic arrest and apoptosis.

Interestingly, fatty liver dystrophy mice with Lipin 1 mutation are infertile with normal testis histology probably due to neurological dysfunction. Examination of adult fld mice testes revealed increased nuage with longer size and higher density. Considering that fld spermatocytes presumably have more PA on the mitochondria surface due to the mutation in Lipin 1, it is suggested that the assembly or recruitment of nuage to mitochondria is dependent on MitoPLD-generated PA.

Notably, a SNP of MitoPLD creates a non-conservative change (Asp173 to Lys) in the conserved HKD domain. Expression of the mutant allele in HeLa cells revealed that it caused mitochondrial fragmentation and failed to recruit

Lipin 1 to mitochondrial surface, which presents the possibility to underlie some instances of male infertility.

4.2.2 Future considerations regarding the mitochondrial surface lipid signaling pathway

What is the mechanism of Lipin 1 induced mitochondrial fission?

I concluded that Lipin 1 full-length protein-induced mitochondrial fission is PA dependent, while the catalytic C-terminus alone can trigger mitochondrial fission independently of PA. These two seemingly contradictory results might be the key to understand the mechanism of Lipin 1 function in mitochondrial fission.

The fact that the Lipin C-terminus alone is localized to mitochondria suggests that there is an encrypted binding domain within the C-terminus in the full length protein. When Lipin 1 is recruited by PA to the mitochondria, a conformational change of the protein exposes the binding domain to a specific but unknown mitochondrial outer membrane protein, possibly one involved in mitochondrial fission. With the C-terminus alone, the binding domain is constitutively exposed, which explains its mitochondrial localization. However, the detailed role of DAG in mitochondrial fission requires future studies.

From the morphological studies, we know that Lipin 1 shortens mitochondrial tubules in an activity dependent manner, suggesting the

requirement of DAG production for mitochondrial fission. However, the catalytic C-terminus functions independently of MitoPLD-generated PA, which could be interpreted as C-terminus functions completely independently of any PA or it can use the PA from other sources on the mitochondria, since the C-terminal fragment is still enzymatically functional indicated by the translocation of the DAG sensor to MitoPLD-overexpressed mitochondria in a similar way as the full length protein. The key question is whether DAG is required for mitochondrial fission after Lipin C-terminus binds to its partner or whether DAG functions before then just to facilitate the binding of Lipin to the mitochondrial protein. To answer this question, we could turn to the Lipin 1 catalytically inactive C-terminus. If the inactive mutant fails to fragment mitochondria tubules, DAG is required to induce mitochondrial fission, just as DAG is involved in COP1-coated Golgi vesicle budding (Fernandez-Ulibarri et al. 2007). On the other hand, if the inactive mutant can still fragment mitochondria, the binding domain alone is sufficient to induce mitochondrial fission.

However, without the knowledge of the binding partner for Lipin C terminus, we will never fully appreciate the mechanism of Lipin 1 function in mitochondrial fission. Unfortunately, we only have knowledge of a few proteins involved in the dynamically regulated complex machinery of mitochondrial fission. Interestingly, a protein identified in a genome-wide yeast two-hybrid screen to interact with Dnm1p (yeast homolog of Drp1), denoted Net2p (also

called Mdv1p or Gag3p in other reports (Fekkes et al. 2000; Tieu and Nunnari 2000)), has a very similar localization pattern with the Lipin C terminus. Aside from forming punctate structures on mitochondria, most Net2p colocalizes with Dnm1p with some of the dots containing only Dnm1p (Cerveny et al. 2001). However, there is no mammalian homolog identified for Net2p.

Regulation of the fission process is highly versatile. Drp1 is shown to be regulated by signaling-activated phosphorylation, dephosphorylation, ubiquitination, SUMOylation, and S-nitrosylation (Nakamura et al. 2006; Cereghetti et al. 2008; Han et al. 2008; Braschi et al. 2009; Cho et al. 2009). However, as a GTPase, the regulation of Drp1 activity is poorly understood with only one report finding enhanced SUMOylation of dominant negative Drp1 (K38A) (Figueroa-Romero et al. 2009). Conversely, guanine nucleotide exchange factors (GEFs) and GTPase activating proteins (GAPs) are classic factors that control small GTPase activity in general. However, as a large GTPase, Drp1 has not been reported to associate with any GEFs or GAPs. Interestingly, studies with dynamin revealed a GAP function of PLD2 for dynamin GTPase activity (Lee et al. 2006). Similarly, Lipin 1 could also regulate the GTPase activity for Drp1 either directly or indirectly through a yet-to-be-identified GAP or GEF for Drp1.

Besides testing known interacting candidates for Lipin 1, we could also do a Mass Spectrometry screening for the proteins co-immunoprecipitated with Lipin

C-terminus, possibly using only mitochondrial outer membrane preparations to decrease false positives.

Are the other two Lipins involved in mitochondrial fusion?

Lipin 2 and Lipin 3, although less intensely studied than Lipin 1, share 60% amino acid sequence similarity with Lipin 1. The sequence similarity is most apparent in the conserved NLIP and CLIP domains. However, we narrowed down the PA binding domain in Lipin to a central region, where the sequence similarity is less than 30%. Moreover, Lipin 2 and Lipin 3 are not recruited by MitoPLD-generated PA to the mitochondria, suggesting that they should not easily compensate for Lipin 1. However, considering that mitochondrial tubules in *fld/fld* MEF cells are not significantly longer than those in wt MEF cells, it is possible that the other two Lipin proteins may provide some compensation in the long-term knockout setting, in particular when the mitochondria are near the endoplasmic reticulum, a site at which all of the Lipins localize as well. But it might be a problem to test the triple knockout mice since the Lipin 1 knockout mice are already very sick and only rarely survive more than six months.

Is Lipin 1 involved in peroxisomal fission?

Peroxisomes are defined by a single organelle membrane and are indispensable in the metabolism of lipids and other essential biomolecules (Wanders and Waterham 2006). Mutations in genes for peroxisome assembly result in multiple defects of peroxisome function, and are the cause of the severe,

often fatal disorder of the Zellweger syndrome spectrum. Deficiency in a single peroxisomal function can cause X-linked adrenoleukodystrophy (Weller et al. 2003).

Recently, it has been found that peroxisomes and mitochondria are metabolically and physically interconnected. More surprisingly, they share some of the same fission machinery. Drp1 and Fis1 localize to both organelles and regulate fission of both in a similar manner (Koch et al. 2004; Koch et al. 2005; Schrader 2006). Another mitochondrial fission protein in mammals, denoted mitochondrial fission factor (Mff) is also involved in both mitochondrial and peroxisomal division (Gandre-Babbe and van der Bliek 2008). In yeast, the binding adaptor for Dnm1p and Fis1p, Mdv1p, and its close relative Caf4p are involved in the fission of both organelles (Motley et al. 2008; Nagotu et al. 2008). Since most of the mitochondrial fission proteins identified so far are also involved in peroxisomal fission, is it possible that Lipin 1 regulates peroxisomal fission as well?

While it is tempting to test the involvement of Lipin 1 in peroxisomal fission, it is noteworthy that fission of peroxisomes does not seem to be counterbalanced by fusion as is the case in mitochondria. Peroxisomal fission is mainly a way of proliferation in response to environmental cues (Thoms and Erdmann 2005). The mitochondrial fusion machinery cannot be similarly found in peroxisomes. Considering that the function of Lipin 1 is inter-connected with

MitoPLD-produced PA, a signal to promote mitochondrial fusion, the involvement of Lipin 1 in peroxisomal fission seems less likely. However, the Lipin C-terminus can fragment mitochondrial independently of MitoPLD-generated PA, suggesting a possible way for Lipin 1 to bypass PA to regulate membrane fission of other organelles.

Other possible phenotypes for MitoPLD$^{-/-}$ mice

Most of the components in the piRNA pathway are germline specific proteins. Phenotypes of the knockout mice are restricted to germ cell development, more specifically spermatogenesis. However, the multi-tissue expression array result showed that MitoPLD is widely expressed in virtually all tissues tested (Choi et al. 2006). As a PLD member that generates the potent lipid secondary messenger PA to regulate mitochondrial fusion, it is tempting to hypothesize that there will be other phenotypes for the MitoPLD knockout mice.

Defects in mitochondrial fusion have been closely associated with neurodegenerative diseases because mutations in the fusion genes Mfn2 and Opa1 can cause Charcot-Marie-Tooth type 2A, a peripheral neuropathy, and dominant optic atrophy, an optic neuropathy, respectively. Recently, additional neurodegenerative diseases have been found to have disrupted balance of mitochondrial fusion and fission, including Parkinson's, Alzheimer's and Huntington's disease (Chen and Chan 2009). Although each disease has its unique underlying mechanism, the susceptibility to neuronal cell death is caused

universally by defects in mitochondrial functions due to altered mitochondrial fusion, fission or movement, and artificially manipulating mitochondrial dynamics can partially rescue each phenotype. It is conceivable that mutations in new players, such as MitoPLD, in mitochondrial dynamics can equally cause neurodegenerative disorders. In fact, preliminary data already showed that mitochondria in MitoPLD$^{-/-}$ neurons are more fragmented than in wt neurons. It would be necessary to test the mitochondrial membrane potential, respiratory function, and susceptibility to apoptosis stimuli in MitoPLD$^{-/-}$ neurons.

Studies in yeast have shown that mutation in the fusion protein Fzo1p results in rapid and complete loss of mitochondrial DNA (mtDNA) (Hermann et al. 1998; Rapaport et al. 1998). However, deletion of Mfn or Opa1 in mammalian cells only results in loss of partial mtDNA, not enough to manifest any obvious respiratory dysfunction. Recently, using the Mfn1 and Mfn2 double conditional knockout mouse model, muscle atrophy, mtDNA depletion, and accumulation of mtDNA mutations have been shown to ensue from loss of mitochondrial fusion (Chen et al. 2010). Although this is an extreme example where mitochondrial fusion is completely blocked, as a highly metabolically active tissue, skeletal muscle fibers are often affected in diseases caused by mitochondrial dysfunction. It is possible that muscle cells with mild defects in mitochondrial fusion accumulate more mtDNA mutations and are more susceptible to physiological or environmental imperatives such as oxidative stress, especially in elder populations.

It would be interesting to test if there is any muscle dysfunction in the MitoPLD$^{-/-}$ mice.

References

Anesti, V. and Scorrano, L. 2006. The relationship between mitochondrial shape and function and the cytoskeleton. *Biochimica Et Biophysica Acta-Bioenergetics* **1757**(5-6): 692-699.

Aravin, A., Gaidatzis, D., Pfeffer, S., Lagos-Quintana, M., Landgraf, P., Iovino, N., Morris, P., Brownstein, M.J., Kuramochi-Miyagawa, S., Nakano, T. et al. 2006. A novel class of small RNAs bind to MILI protein in mouse testes. *Nature* **442**(7099): 203-207.

Aravin, A.A., Sachidanandam, R., Girard, A., Fejes-Toth, K., and Hannon, G.J. 2007. Developmentally regulated piRNA clusters implicate MILI in transposon control. *Science* **316**(5825): 744-747.

Aravin, A.A., van der Heijden, G.W., Castaneda, J., Vagin, V.V., Hannon, G.J., and Bortvin, A. 2009. Cytoplasmic Compartmentalization of the Fetal piRNA Pathway in Mice. *Plos Genetics* **5**(12).

Barila, D., Plateroti, M., Nobili, F., Muda, A.O., Xie, Y.H., Morimoto, T., and Perozzi, G. 1996. The Dri 42 gene, whose expression is up-regulated during epithelial differentiation, encodes a novel endoplasmic reticulum resident transmembrane protein. *Journal of Biological Chemistry* **271**(47): 29928-29936.

Barona, T., Byrne, R.D., Pettitt, T.R., Wakelam, M.J.O., Larijani, B., and Poccia, D.L. 2005. Diacylglycerol induces fusion of nuclear envelope membrane precursor vesicles. *Journal of Biological Chemistry* **280**(50): 41171-41177.

Boldogh, I.R. and Pon, L.A. 2007. Mitochondria on the move. *Trends in Cell Biology* **17**(10): 502-510.

Bossard, C., Bresson, D., Polishchuk, R.S., and Malhotra, V. 2007. Dimeric PKD regulates membrane fission to form transport carriers at the TGN. *J Cell Biol* **179**(6): 1123-1131.

Bowes, T. and Gupta, R.S. 2008. Novel mitochondrial extensions provide evidence for a link between microtubule-directed movement and mitochondrial fission. *Biochem Biophys Res Commun* **376**(1): 40-45.

Braschi, E., Zunino, R., and McBride, H.M. 2009. MAPL is a new mitochondrial SUMO E3 ligase that regulates mitochondrial fission. *Embo Reports* **10**(7): 748-754.

Brennecke, J., Aravin, A.A., Stark, A., Dus, M., Kellis, M., Sachidanandam, R., and Hannon, G.J. 2007. Discrete small RNA-generating loci as master regulators of transposon activity in *Drosophila*. *Cell* **128**(6): 1089-1103.

Brindley, D.N. 1984. Intracellular translocation of phosphatidate phosphohydrolase and its possible role in the control of glycerolipid synthesis. *Prog Lipid Res* **23**(3): 115-133.

Brindley, D.N., English, D., Pilquil, C., Buri, K., and Ling, Z.C. 2002. Lipid phosphate phosphatases regulate signal transduction through glycerolipids and sphingolipids. *Biochim Biophys Acta Mol Cell Biol Lipids* **1582**(1-3): 33-44.

Brindley, D.N., Pilquil, C., Sariahmetoglu, M., and Reue, K. 2009. Phosphatidate degradation: Phosphatidate phosphatases (lipins) and lipid phosphate phosphatases. *Biochim Biophys Acta Mol Cell Biol Lipids* **1791**(9): 956-961.

Campello, S., Lacalle, R.A., Bettella, M., Manes, S., Scorrano, L., and Viola, A. 2006. Orchestration of lymphocyte chemotaxis by mitochondrial dynamics. *J Exp Med* **203**(13): 2879-2886.

Capote, C. and Maccioni, R.B. 1998. The association of tau-like proteins with vimentin filaments in cultured cells. *Experimental Cell Research* **239**(2): 202-213.

Carman, G.M. and Han, G.S. 2006. Roles of phosphatidate phosphatase enzymes in lipid metabolism. *Trends BiochemSci* **31**(12): 694-699.

Carmell, M.A., Girard, A., van de Kant, H.J.G., Bourc'his, D., Bestor, T.H., de Rooij, D.G., and Hannon, G.J. 2007. MIWI2 is essential for spermatogenesis and repression of transposons in the mouse male germline. *Developmental Cell* **12**(4): 503-514.

Cassidy-Stone, A., Chipuk, J.E., Ingerman, E., Song, C., Yoo, C., Kuwana, T., Kurth, M.J., Shaw, J.T., Hinshaw, J.E., Green, D.R. et al. 2008. Chemical inhibition of the mitochondrial division dynamin reveals its role in Bax/Bak-dependent mitochondrial outer membrane permeabilization. *Developmental Cell* **14**(2): 193-204.

Cazzolli, R., Shemon, A.N., Fang, M.Q., and Hughes, W.E. 2006. Phospholipid signalling through phospholipase D and phosphatidic acid. *Iubmb Life* **58**(8): 457-461.

Cereghetti, G.M., Stangherlin, A., de Brito, O.M., Chang, C.R., Blackstone, C., Bernardi, P., and Scorrano, L. 2008. Dephosphorylation by calcineurin regulates translocation of Drp1 to mitochondria. *Proc Natl Acad Sci U S A* **105**(41): 15803-15808.

Cerveny, K.L., McCaffery, J.M., and Jensen, R.E. 2001. Division of mitochondria requires a novel DNM1-interacting protein, net2p. *Mol Biol Cell* **12**(2): 309-321.

Chada, S.R. and Hollenbeck, P.J. 2003. Mitochondrial movement and positioning in axons: the role of growth factor signaling. *J Exp Biol* **206**(12): 1985-1992.

Chada, S.R. and Hollenbeck, P.J. 2004. Nerve growth factor signaling regulates motility and docking of axonal mitochondria. *Curr Biol* **14**(14): 1272-1276.

Chan, D.C. 2006. Mitochondrial fusion and fission in mammals. *Annu Rev Cell Dev Biol* **22**: 79-99.

Chen, H. and Chan, D.C. 2009. Mitochondrial dynamics-fusion, fission, movement, and mitophagy-in neurodegenerative diseases. *Human Molecular Genetics* **18**: R169-R176.

Chen, H., Detmer, S.A., Ewald, A.J., Griffin, E.E., Fraser, S.E., and Chan, D.C. 2003. Mitofusins Mfn1 and Mfn2 coordinately regulate mitochondrial fusion and are essential for embryonic development. *J Cell Biol* **160**(2): 189-200.

Chen, H., McCaffery, J.M., and Chan, D.C. 2007. Mitochondrial fusion protects against neurodegeneration in the cerebellum. *Cell* **130**(3): 548-562.

Chen, H.C., Vermulst, M., Wang, Y.E., Chomyn, A., Prolla, T.A., McCaffery, J.M., and Chan, D.C. 2010. Mitochondrial Fusion Is Required for mtDNA Stability in Skeletal Muscle and Tolerance of mtDNA Mutations. *Cell* **141**(2): 280-289.

Chen, Y.G., Siddhanta, A., Austin, C.D., Hammond, S.M., Sung, T.C., Frohman, M.A., Morris, A.J., and Shields, D. 1997. Phospholipase D stimulates release of nascent secretory vesicles from the trans-Golgi network. *J Cell Biol* **138**(3): 495-504.

Cho, D.H., Nakamura, T., Fang, J.G., Cieplak, P., Godzik, A., Gu, Z., and Lipton, S.A. 2009. S-Nitrosylation of Drp1 Mediates beta-Amyloid-Related Mitochondrial Fission and Neuronal Injury. *Science* **324**(5923): 102-105.

Choi, S.Y., Huang, P., Jenkins, G.M., Chan, D.C., Schiller, J., and Frohman, M.A. 2006. A common lipid links Mfn-mediated mitochondrial fusion and SNARE-regulated exocytosis. *Nat Cell Biol* **8**(11): 1255-U1229.

Chuma, S., Hosokawa, M., Kitamura, K., Kasai, S., Fujioka, M., Hiyoshi, M., Takamune, K., Noce, T., and Nakatsuji, N. 2006. Tdrd1/Mtr-1, a tudor-related gene, is essential for male germ-cell differentiation and nuage/germinal granule formation in mice. *Proc Natl Acad Sci U S A* **103**(43): 15894-15899.

Clegg, N.J., Frost, D.M., Larkin, M.K., Subrahmanyan, L., Bryant, Z., and Ruohola-Baker, H. 1997. maelstrom is required for an early step in the establishment of *Drosophila* oocyte polarity: posterior localization of grk mRNA. *Development* **124**(22): 4661-4671.

Colley, W.C., Sung, T.C., Roll, R., Jenco, J., Hammond, S.M., Altshuller, Y., BarSagi, D., Morris, A.J., and Frohman, M.A. 1997. Phospholipase D2, a distinct phospholipase D isoform with novel regulatory properties that provokes cytoskeletal reorganization. *Curr Biol* **7**(3): 191-201.

Cook, H.A., Koppetsch, B.S., Wu, J., and Theurkauf, W.E. 2004. The *Drosophila* SDE3 homolog armitage is required for oskar mRNA silencing and embryonic axis specification. *Cell* **116**(6): 817-829.

Cox, D.N., Chao, A., Baker, J., Chang, L., Qiao, D., and Lin, H.F. 1998. A novel class of evolutionarily conserved genes defined by piwi are essential for stem cell self-renewal. *Genes Dev* **12**(23): 3715-3727.

Cox, D.N., Chao, A., and Lin, H.F. 2000. piwi encodes a nucleoplasmic factor whose activity modulates the number and division rate of germline stem cells. *Development* **127**(3): 503-514.

Cui, M., Tang, X.N., Christian, W.V., Yoon, Y., and Tieu, K. 2010. Perturbations in Mitochondrial Dynamics Induced by Human Mutant PINK1 Can Be Rescued by the Mitochondrial Division Inhibitor mdivi-1. *Journal of Biological Chemistry* **285**(15): 11740-11752.

De Vos, K.J., Sable, J., Miller, K.E., and Sheetz, M.P. 2003. Expression of phosphatidylinositol (4,5) bisphosphate-specific pleckstrin homology domains alters direction but not the level of axonal transport of mitochondria. *Mol Biol Cell* **14**(9): 3636-3649.

Deng, W. and Lin, H.F. 2002. miwi, a murine homolog of piwi, encodes a cytoplasmic protein essential for spermatogenesis. *Developmental Cell* **2**(6): 819-830.

Donkor, J., Sariahmetoglu, M., Dewald, J., Brindley, D.N., and Reue, K. 2007. Three mammalian lipins act as phosphatidate phosphatases with distinct tissue expression patterns. *Journal of Biological Chemistry* **282**(6): 3450-3457.

Donkor, J., Zhang, P.X., Wong, S., O'Loughlin, L., Dewald, J., Kok, B.P.C., Brindley, D.N., and Reue, K. 2009. A Conserved Serine Residue Is Required for the Phosphatidate Phosphatase Activity but Not the Transcriptional Coactivator Functions of Lipin-1 and Lipin-2. *Journal of Biological Chemistry* **284**(43): 29968-29978.

Drubin, D.G., Jones, H.D., and Wertman, K.F. 1993. Actin structure and function - roles in mitochondrial organization and morphogenesis in budding yeast and indetification of the phalloidin-binding site. *Mol Biol Cell* **4**(12): 1277-1294.

Du, G.W., Huang, P., Liang, B.T., and Frohman, M.A. 2004. Phospholipase D2 localizes to the plasma membrane and regulates angiotensin II receptor endocytosis. *Mol Biol Cell* **15**(3): 1024-1030.

English, D., Brindley, D.N., Spiegel, S., and Garcia, J.G.N. 2002. Lipid mediators of angiogenesis and the signalling pathways they initiate. *Biochim Biophys Acta Mol Cell Biol Lipids* **1582**(1-3): 228-239.

English, D., Garcia, J.G.N., and Brindley, D.N. 2001. Platelet-released phospholipids link haemostasis and angiogenesis. *Cardiovasc Res* **49**(3): 588-599.

Fekkes, P., Shepard, K.A., and Yaffe, M.P. 2000. Gag3p, an outer membrane protein required for fission of mitochondrial tubules. *J Cell Biol* **151**(2): 333-340.

Ferguson, P.J., Chen, S., Tayeh, M.K., Ochoa, L., Leal, S.M., Pelet, A., Munnich, A., Lyonnet, S., Majeed, H.A., and El-Shanti, H. 2005. Homozygous mutations in LPIN2 are responsible for the syndrome of chronic recurrent multifocal osteomyelitis and congenital dyserythropoietic anaemia (Majeed syndrome). *J Med Genet* **42**(7): 551-557.

Fernandez-Ulibarri, I., Vilella, M., Lazaro-Dieguez, F., Sarri, E., Martinez, S.E., Jimenez, N., Claro, E., Merida, I., Burger, K.N.J., and Egea, G. 2007. Diacylglycerol is required for the formation of COPI vesicles in the Golgi-to-ER transport pathway. *Mol Biol Cell* **18**(9): 3250-3263.

Figueroa-Romero, C., Iniguez-Lluhi, J.A., Stadler, J., Chang, C.R., Arnoult, D., Keller, P.J., Hong, Y., Blackstone, C., and Feldman, E.L. 2009. SUMOylation of the mitochondrial fission protein Drp1 occurs at multiple nonconsensus sites within the B domain and is linked to its activity cycle. *Faseb Journal* **23**(11): 3917-3927.

Finck, B.N., Gropler, M.C., Chen, Z.J., Leone, T.C., Croce, M.A., Harris, T.E., Lawrence, J.C., and Kelly, D.P. 2006. Lipin 1 is an inducible amplifier of the hepatic PGC-1 alpha/PPAR alpha regulatory pathway. *Cell Metab* **4**(3): 199-210.

Frank, S., Gaume, B., Bergmann-Leitner, E.S., Leitner, W.W., Robert, E.G., Catez, F., Smith, C.L., and Youle, R.J. 2001. The role of dynamin-related protein 1, a mediator of mitochondrial fission, in apoptosis. *Developmental Cell* **1**(4): 515-525.

Fransson, A., Ruusala, A., and Aspenstom, P. 2006. The atypical Rho GTPases Miro-1 and Miro-2 have essential roles in mitochondrial trafficking. *Biochem Biophys Res Commun* **344**(2): 500-510.

Gandre-Babbe, S. and van der Bliek, A.M. 2008. The novel tail-anchored membrane protein Mff controls mitochondrial and peroxisomal fission in mammalian cells. *Mol Biol Cell* **19**(6): 2402-2412.

Ghosh, I., Hamilton, A.D., and Regan, L. 2000. Antiparallel leucine zipper-directed protein reassembly: Application to the green fluorescent protein. *J Am Chem Soc* **122**(23): 5658-5659.

Giorgione, J.R., Lin, J.H., McCammon, J.A., and Newton, A.C. 2006. Increased membrane affinity of the C1 domain of protein kinase C delta compensates for the lack of involvement of its C2 domain in membrane recruitment. *Journal of Biological Chemistry* **281**(3): 1660-1669.

Girard, A., Sachidanandam, R., Hannon, G.J., and Carmell, M.A. 2006. A germline-specific class of small RNAs binds mammalian Piwi proteins. *Nature* **442**(7099): 199-202.

Goppelt-Struebe, M., Fickel, S., and Reiser, C.O.A. 2000. The platelet-derived-growth-factor receptor, not the epidermal-growth-factor receptor, is used by lysophosphatidic acid to activate p42/44 mitogen-activated protein kinase and to induce prostaglandin G/H synthase-2 in mesangial cells. *Biochem J* **345**: 217-224.

Grimsey, N., Han, G.S., O'Hara, L., Rochford, J.J., Carman, G.M., and Siniossoglou, S. 2008. Temporal and Spatial Regulation of the Phosphatidate Phosphatases Lipin 1 and 2. *Journal of Biological Chemistry* **283**(43): 29166-29174.

Grivna, S.T., Beyret, E., Wang, Z., and Lin, H.F. 2006a. A novel class of small RNAs in mouse spermatogenic cells. *Genes Dev* **20**(13): 1709-1714.

Grivna, S.T., Pyhtila, B., and Lin, H.F. 2006b. MIWI associates with translational machinery and PIWI-interacting RNAs (piRNAs) in regulating spermatogenesis. *Proc Natl Acad Sci U S A* **103**(36): 13415-13420.

Gunawardane, L.S., Saito, K., Nishida, K.M., Miyoshi, K., Kawamura, Y., Nagami, T., Siomi, H., and Siomi, M.C. 2007. A slicer-mediated mechanism for repeat-associated siRNA 5 ' end formation in *Drosophila*. *Science* **315**(5818): 1587-1590.

Guo, T., Gregg, C., Boukh-Viner, T., Kyryakov, P., Goldberg, A., Bourque, S., Banu, F., Haile, S., Milijevic, S., San, K.H.Y. et al. 2007. A signal from inside the peroxisome initiates its division by promoting the remodeling of the peroxisomal membrane. *J Cell Biol* **177**(2): 289-303.

Guo, X.F., Macleod, G.T., Wellington, A., Hu, F., Panchumarthi, S., Schoenfield, M., Marin, L., Charlton, M.P., Atwood, H.L., and Zinsmaier, K.E. 2005. The GTPase dMiro is required for axonal transport of mitochondria to *Drosophila* synapses. *Neuron* **47**(3): 379-393.

Hales, K.G. and Fuller, M.T. 1997. Developmentally regulated mitochondrial fusion mediated by a conserved, novel, predicted GTPase. *Cell* **90**(1): 121-129.

Han, G.S. and Carman, G.M. 2010. Characterization of the Human LPIN1-encoded Phosphatidate Phosphatase Isoforms. *Journal of Biological Chemistry* **285**(19): 14628-14638.

Han, G.S., Siniossoglou, S., and Carman, G.M. 2007. The cellular functions of the yeast lipin homolog pah1p are dependent on its phosphatidate phosphatase activity. *Journal of Biological Chemistry* **282**(51): 37026-37035.

Han, G.S., Wu, W.I., and Carman, G.M. 2006. The Saccharomyces cerevisiae lipin homolog is a Mg2+-dependent phosphatidate phosphatase enzyme. *Journal of Biological Chemistry* **281**(14): 9210-9218.

Han, X.J., Lu, Y.F., Li, S.A., Kaitsuka, T., Sato, Y., Tomizawa, K., Nairn, A.C., Takei, K., Matsui, H., and Matsushita, M. 2008. CaM kinase l alpha-induced phosphorylation of Drp1 regulates mitochondrial morphology. *J Cell Biol* **182**(3): 573-585.

Haucke, V. and Di Paolo, G. 2007. Lipids and lipid modifications in the regulation of membrane. *Curr Opin Cell Biol* **19**(4): 426-435.

Hay, B., Jan, L.Y., and Jan, Y.N. 1988. A protein-component of *Drosophila* polar granules is encoded by VASA and has extensive sequence similarity to ATP-dependent helicases. *Cell* **55**(4): 577-587.

He, Z.P., Kokkinaki, M., Pant, D., Gallicano, G.I., and Dym, M. 2009. Small RNA molecules in the regulation of spermatogenesis. *Reproduction* **137**(6): 901-911.

Hermann, G.J., Thatcher, J.W., Mills, J.P., Hales, K.G., Fuller, M.T., Nunnari, J., and Shaw, J.M. 1998. Mitochondrial fusion in yeast requires the transmembrane GTPase Fzo1p. *J Cell Biol* **143**(2): 359-373.

Herrlich, A., Daub, H., Knebel, A., Herrlich, P., Ullrich, A., Schultz, G., and Gudermann, T. 1998. Ligand-independent activation of platelet-derived growth factor receptor is a necessary intermediate in lysophosphatidic, acid-stimulated mitogenic activity in L cells. *Proc Natl Acad Sci U S A* **95**(15): 8985-8990.

Hesse, M., Magin, T.M., and Weber, K. 2001. Genes for intermediate filament proteins and the draft sequence of the human genome: novel keratin genes and a surprisingly high number of pseudogenes related to keratin genes 8 and 18. *J Cell Sci* **114**(14): 2569-2575.

Hollenbeck, P.J. and Saxton, W.M. 2005. The axonal transport of mitochondria. *J Cell Sci* **118**(23): 5411-5419.

Horwich, M.D., Li, C.J., Matranga, C., Vagin, V., Farley, G., Wang, P., and Zamore, P.D. 2007. The *Drosophila* RNA methyltransferase, DmHen1, modifies germline piRNAs and single-stranded siRNAs in RISC. *Curr Biol* **17**(14): 1265-1272.

Hosokawa, M., Shoji, M., Kitamura, K., Tanaka, T., Noce, T., Chuma, S., and Nakatsuji, N. 2007. Tudor-related proteins TDRD1/MTR-1, TDRD6 and TDRD7/TRAP: Domain composition, intracellular localization, and function in male germ cells in mice. *Developmental Biology* **301**(1): 38-52.

Houwing, S., Berezikov, E., and Ketting, R.F. 2008. Zili is required for germ cell differentiation and meiosis in zebrafish. *Embo J* **27**(20): 2702-2711.

Houwing, S., Kamminga, L.M., Berezikov, E., Cronembold, D., Girard, A., van den Elst, H., Filippov, D.V., Blaser, H., Raz, E., Moens, C.B. et al. 2007. A role for Piwi and piRNAs in germ cell maintenance and transposon silencing in zebrafish. *Cell* **129**(1): 69-82.

Hu, C.D., Chinenov, Y., and Kerppola, T.K. 2002. Visualization of interactions among bZip and Rel family proteins in living cells using bimolecular fluorescence complementation. *Mol Cell* **9**(4): 789-798.

Hu, C.D. and Kerppola, T.K. 2003. Simultaneous visualization of multiple protein interactions in living cells using multicolor fluorescence complementation analysis. *Nature Biotechnology* **21**(5): 539-545.

Huang, H.Y. and Frohman, M.A. 2009. Lipid signaling on the mitochondrial surface. *Biochim Biophys Acta Mol Cell Biol Lipids* **1791**(9): 839-844.

Huang, P., Altshuller, Y.M., Hou, J.C., Pessin, J.E., and Frohman, M.A. 2005. Insulin-stimulated plasma membrane fusion of Glut4 glucose transporter-containing vesicles is regulated by phospholipase D1. *Mol Biol Cell* **16**(6): 2614-2623.

Iwatsuki, H. and Suda, M. 2010. Seven Kinds of Intermediate Filament Networks in the Cytoplasm of Polarized Cells: Structure and Function. *Acta Histochemica Et Cytochemica* **43**(2): 19-31.

Jakobs, S. 2006. High resolution imaging of live mitochondria. *Biochim Biophys Acta-Mol Cell Res* **1763**(5-6): 561-575.

Jamal, Z., Martin, A., Gomezmunoz, A., and Brindley, D.N. 1991. Plasma-membrane fractions from rat-liver contain a phosphatidate phosphahydrolase distinct from that in the endoplasmic-reticulum and cytosol. *Journal of Biological Chemistry* **266**(5): 2988-2996.

Jasinska, R., Zhang, Q.X., Pilquil, C., Singh, I., Xu, J., Dewald, J., Dillon, D.A., Berthiaume, L.G., Carman, G.M., Waggoner, D.W. et al. 1999. Lipid phosphate phosphohydrolase-1 degrades exogenous glycerolipid and sphingolipid phosphate esters. *Biochem J* **340**: 677-686.

Jenkins, G.M. and Frohman, M.A. 2005. Phospholipase D: a lipid centric review. *Cell Mol Life Sci* **62**(19-20): 2305-2316.

Jensen, A.A., Hansen, J.L., Sheikh, S.P., and Brauner-Osborne, H. 2002. Probing intermolecular protein-protein interactions in the calcium-sensing receptor homodimer using bioluminescence resonance energy transfer (BRET). *European Journal of Biochemistry* **269**(20): 5076-5087.

Jun, Y., Fratti, R.A., and Wickner, W. 2004. Diacylglycerol and its formation by phospholipase C regulate Rab- and SNARE-dependent yeast vacuole fusion. *Journal of Biological Chemistry* **279**(51): 53186-53195.

Kai, M., Wada, I., Imai, S., Sakane, F., and Kanoh, H. 1996. Identification and cDNA cloning of 35-kDa phosphatidic acid phosphatase (Type 2) bound to plasma membranes - Polymerase chain reaction amplification of mouse H2O2-inducible hic53 clone yielded the cDNA encoding phosphatidic acid phosphatase. *Journal of Biological Chemistry* **271**(31): 18931-18938.

Kai, M., Wada, I., Imai, S., Sakane, F., and Kanoh, H. 1997. Cloning and characterization of two human isozymes of Mg2+-independent

phosphatidic acid phosphatase. *Journal of Biological Chemistry* **272**(39): 24572-24578.

Kaihara, A., Kawai, Y., Sato, M., Ozawa, T., and Umezawa, Y. 2003. Locating a protein-protein interaction in living cells via split Renilla luciferase complementation. *Analytical Chemistry* **75**(16): 4176-4181.

Karbowski, M., Arnoult, D., Chen, H.C., Chan, D.C., Smith, C.L., and Youle, R.J. 2004. Quantitation of mitochondrial dynamics by photolabeling of individual organelles shows that mitochondrial fusion is blocked during the Bax activation phase of apoptosis. *J Cell Biol* **164**(4): 493-499.

Kennerdell, J.R., Yamaguchi, S., and Carthew, R.W. 2002. RNAi is activated during *Drosophila* oocyte maturation in a manner dependent on aubergine and spindle-E. *Genes Dev* **16**(15): 1884-1889.

Koch, A., Schneider, G., Luers, G.H., and Schrader, M. 2004. Peroxisome elongation and constriction but not fission can occur independently of dynamin-like protein 1. *J Cell Sci* **117**(17): 3995-4006.

Koch, A., Yoon, Y., Bonekamp, N.A., McNiven, M.A., and Schrader, M. 2005. A role for Fis1 in both mitochondrial and peroxisomal fission in mammalian cells. *Mol Biol Cell* **16**(11): 5077-5086.

Koshiba, T., Detmer, S.A., Kaiser, J.T., Chen, H.C., McCaffery, J.M., and Chan, D.C. 2004. Structural basis of mitochondrial tethering by mitofusin complexes. *Science* **305**(5685): 858-862.

Kostareva, A., Sjoberg, G., Bruton, J., Zhang, S.J., Balogh, J., Gudkova, A., Hedberg, B., Edstrom, L., Westerblad, H., and Sejersen, T. 2008. Mice expressing L345P mutant desmin exhibit morphological and functional changes of skeletal and cardiac mitochondria. *Journal of Muscle Research and Cell Motility* **29**(1): 25-36.

Kumemura, H., Harada, M., Yanagimoto, C., Koga, H., Kawaguchi, T., Hanada, S., Taniguchi, E., Ueno, T., and Sata, M. 2008. Mutation in keratin 18 induces mitochondrial fragmentation in liver-derived epithelial cells. *Biochem Biophys Res Commun* **367**(1): 33-40.

Kuramochi-Miyagawa, S., Kimura, T., Ijiri, T.W., Isobe, T., Asada, N., Fujita, Y., Ikawa, M., Iwai, N., Okabe, M., Deng, W. et al. 2004. Mili, a mammalian member of piwi family gene, is essential for spermatogenesis. *Development* **131**(4): 839-849.

Kuramochi-Miyagawa, S., Kimura, T., Yomogida, K., Kuroiwa, A., Tadokoro, Y., Fujita, Y., Sato, M., Matsuda, Y., and Nakano, T. 2001. Two mouse piwi-related genes: miwi and mili. *Mechanisms of Development* **108**(1-2): 121-133.

Langner, C.A., Birkenmeier, E.H., Roth, K.A., Bronson, R.T., and Gordon, J.I. 1991. Characterization of the peripheral neuropathy in neonatal and adult

mice that are homozygous for the fatty liver dystrophy (fld) mutation. *Journal of Biological Chemistry* **266**(18): 11955-11964.

Lebiedzinska, M., Szabadkai, G., Jones, A.W.E., Duszynski, J., and Wieckowski, M.R. 2009. Interactions between the endoplasmic reticulum, mitochondria, plasma membrane and other subcellular organelles. *International Journal of Biochemistry & Cell Biology* **41**(10): 1805-1816.

Lee, C.S., Kim, I.S., Park, J.B., Lee, M.N., Lee, H.Y., Suh, P.G., and Ryu, S.H. 2006. The phox homology domain of phospholipase D activates dynamin GTPase activity and accelerates EGFR endocytosis. *Nat Cell Biol* **8**(5): 477-U101.

Legros, F., Lombes, A., Frachon, P., and Rojo, M. 2002. Mitochondrial fusion in human cells is efficient, requires the inner membrane potential, and is mediated by mitofusins. *Mol Biol Cell* **13**(12): 4343-4354.

Li, C.J., Vagin, V.V., Lee, S.H., Xu, J., Ma, S.M., Xi, H.L., Seitz, H., Horwich, M.D., Syrzycka, M., Honda, B.M. et al. 2009. Collapse of Germline piRNAs in the Absence of Argonaute3 Reveals Somatic piRNAs in Flies. *Cell* **137**(3): 509-521.

Lim, A.K. and Kai, T. 2007. Unique germ-line organelle, nuage, functions to repress selfish genetic elements in *Drosophila melanogaster*. *Proc Natl Acad Sci U S A* **104**(16): 6714-6719.

Liu, G.H. and Gerace, L. 2009. Sumoylation Regulates Nuclear Localization of Lipin-1 alpha in Neuronal Cells. *PLoS One* **4**(9).

Liu, X.G., Weaver, D., Shirihai, O., and Hajnoczky, G. 2009. Mitochondrial 'kiss-and-run': interplay between mitochondrial motility and fusion-fission dynamics. *Embo J* **28**(20): 3074-3089.

Ma, L., Buchold, G.M., Greenbaum, M.P., Roy, A., Burns, K.H., Zhu, H.F., Han, D.Y., Harris, R.A., Coarfa, C., Gunaratne, P.H. et al. 2009. GASZ Is Essential for Male Meiosis and Suppression of Retrotransposon Expression in the Male Germline. *Plos Genetics* **5**(9).

Magliery, T.J., Wilson, C.G.M., Pan, W.L., Mishler, D., Ghosh, I., Hamilton, A.D., and Regan, L. 2005. Detecting protein-protein interactions with a green fluorescent protein fragment reassembly trap: Scope and mechanism. *J Am Chem Soc* **127**(1): 146-157.

Mahowald, A.P. 2001. Assembly of the *Drosophila* germ plasm. in *International Review of Cytology - a Survey of Cell Biology, Vol 203*, pp. 187-213.

Malka, F., Guillery, O., Cifuentes-Diaz, C., Guillou, E., Belenguer, P., Lombes, A., and Rojo, M. 2005. Separate fusion of outer and inner mitochondrial membranes. *Embo Reports* **6**(9): 853-859.

Malone, C.D., Brennecke, J., Dus, M., Stark, A., McCombie, W.R., Sachidanandam, R., and Hannon, G.J. 2009. Specialized piRNA Pathways

Act in Germline and Somatic Tissues of the *Drosophila* Ovary. *Cell* **137**(3): 522-535.

Margineantu, D.H., Gregory Cox, W., Sundell, L., Sherwood, S.W., Beechem, J.M., and Capaldi, R.A. 2002. Cell cycle dependent morphology changes and associated mitochondrial DNA redistribution in mitochondria of human cell lines. *Mitochondrion* **1**(5): 425-435.

Mattenberger, Y., James, D.I., and Martinou, J.C. 2003. Fusion of mitochondria in mammalian cells is dependent on the mitochondrial inner membrane potential and independent of microtubules or actin. *FEBS Lett* **538**(1-3): 53-59.

McBride, H.M., Neuspiel, M., and Wasiak, S. 2006. Mitochondria: More than just a powerhouse. *Curr Biol* **16**(14): R551-R560.

Megosh, H.B., Cox, D.N., Campbell, C., and Lin, H.F. 2006. The role of PIWI and the miRNA machinery in *Drosophila* germline determination. *Curr Biol* **16**(19): 1884-1894.

Milner, D.J., Mavroidis, M., Weisleder, N., and Capetanaki, Y. 2000. Desmin cytoskeleton linked to muscle mitochondrial distribution and respiratory function. *J Cell Biol* **150**(6): 1283-1297.

Mor, A., Campi, G., Du, G.W., Zheng, Y., Foster, D.A., Dustin, M.L., and Philips, M.R. 2007. The lymphocyte function-associated antigen-1 receptor costimulates plasma membrane Ras via phospholipase D2. *Nat Cell Biol* **9**(6): 713-U182.

Motley, A.M., Ward, G.P., and Hettema, E.H. 2008. Dnm1p-dependent peroxisome fission requires Caf4p, Mdv1p and Fis1p. *J Cell Sci* **121**(10): 1633-1640.

Nadra, K., Charles, A.S.D., Medard, J.J., Hendriks, W.T., Han, G.S., Gres, S., Carman, G.M., Saulnier-Blache, J.S., Verheijen, M.H.G., and Chrast, R. 2008. Phosphatidic acid mediates demyelination in Lpin1 mutant mice. *Genes Dev* **22**(12): 1647-1661.

Nagotu, S., Krikken, A.M., Otzen, M., Kiel, J., Veenhuis, M., and van der Klei, I.J. 2008. Peroxisome fission in Hansenula polymorpha requires Mdv1 and Fis1, two proteins also involved in mitochondrial fission. *Traffic* **9**(9): 1471-1484.

Nakamura, N., Kimura, Y., Tokuda, M., Honda, S., and Hirose, S. 2006. MARCH-V is a novel mitofusin 2-and Drp1-binding protein able to change mitochondrial morphology. *Embo Reports* **7**(10): 1019-1022.

Nakanishi, H., Morishita, M., Schwartz, C.L., Coluccio, A., Engebrecht, J., and Neiman, A.M. 2006. Phospholipase D and the SNARE Sso1p are necessary for vesicle fusion during sporulation in yeast. *J Cell Sci* **119**(7): 1406-1415.

Nanjundan, M. and Possmayer, F. 2003. Pulmonary phosphatidic acid phosphatase and lipid phosphate phosphohydrolase. *Am J Physiol-Lung Cell Mol Physiol* **284**(1): L1-L23.

Nunnari, J., Marshall, W.F., Straight, A., Murray, A., Sedat, J.W., and Walter, P. 1997. Mitochondrial transmission during mating in Saccharomyces cerevisiae is determined by mitochondrial fusion and fission and the intramitochondrial segregation of mitochondrial DNA. *Mol Biol Cell* **8**(7): 1233-1242.

Olichon, A., Guillou, E., Delettre, C., Landes, T., Arnaune-Pelloquin, L., Emorine, L.J., Mils, V., Daloyau, M., Hamel, C., Amati-Bonneau, P. et al. 2006. Mitochondrial dynamics and disease, OPA1. *Biochim Biophys Acta-Mol Cell Res* **1763**(5-6): 500-509.

Pal-Bhadra, M., Leibovitch, B.A., Gandhi, S.G., Rao, M., Bhadra, U., Birchler, J.A., and Elgin, S.C.R. 2004. Heterochromatic silencing and HP1 localization in *Drosophila* are dependent on the RNAi machinery. *Science* **303**(5658): 669-672.

Pane, A., Wehr, K., and Schupbach, T. 2007. zucchini and squash encode two putative nucleases required for rasiRNA production in the *Drosophila* germline. *Developmental Cell* **12**(6): 851-862.

Paniagua, R., Nistal, M., Amat, P., and Rodriguez, M.C. 1985. Presence of ribonucleoproteins and basic-proteins in the nuage and intermitochondrial bars of human spermatogonia. *Journal of Anatomy* **143**: 201-206.

Patterson, G.H. and Lippincott-Schwartz, J. 2002. A photoactivatable GFP for selective photolabeling of proteins and cells. *Science* **297**(5588): 1873-1877.

Paulmurugan, R. and Gambhir, S.S. 2007. Combinatorial library screening for developing an improved split-firefly luciferase fragment-assisted complementation system for studying protein-protein interactions. *Analytical Chemistry* **79**(6): 2346-2353.

Pawlikowska, P., Gajkowska, B., and Orzechowski, A. 2007. Mitofusin 2 (Mfn2): a key player in insulin-dependent myogenesis in vitro. *Cell Tissue Res* **327**(3): 571-581.

Perrot, R. and Julien, J.P. 2009. Real-time imaging reveals defects of fast axonal transport induced by disorganization of intermediate filaments. *Faseb Journal* **23**(9): 3213-3225.

Peterfy, M., Phan, J., Xu, P., and Reue, K. 2001. Lipodystrophy in the fld mouse results from mutation of a new gene encoding a nuclear protein, lipin. *Nature Genet* **27**(1): 121-124.

Pyne, S., Kong, K.C., and Darroch, P.I. 2004. Lysophosphatidic acid and sphingosine 1-phosphate biology: the role of lipid phosphate phosphatases. *Semin Cell Dev Biol* **15**(5): 491-501.

Pyne, S., Lee, S.C., Long, J., and Llyne, N.J. 2009. Role of sphingosine kinases and lipid phosphate phosphatases in regulating spatial sphingosine 1-phosphate signalling in health and disease. *Cell Signal* **21**(1): 14-21.

Rapaport, D., Brunner, M., Neupert, W., and Westermann, B. 1998. Fzo1p is a mitochondrial outer membrane protein essential for the biogenesis of functional mitochondria in Saccharomyces cerevisiae. *Journal of Biological Chemistry* **273**(32): 20150-20155.

Remy, I. and Michnick, S.W. 2006. A highly sensitive protein-protein interaction assay based on Gaussia luciferase. *Nature Methods* **3**(12): 977-979.

Ren, H., Federico, L., Huang, H.Y., Sunkara, M., Drennan, T., Frohman, M.A., Smyth, S.S., and Morris, A.J. 2010. A phosphatidic acid binding/nuclear localization motif determines Lipin1 function in lipid metabolism and adipogenesis. *Mol Biol Cell (in press)*.

Riebeling, C., Morris, A.J., and Shields, D. 2009. Phospholipase D in the Golgi apparatus. *Biochim Biophys Acta Mol Cell Biol Lipids* **1791**(9): 876-880.

Rizzo, M.A., Shome, K., Watkins, S.C., and Romero, G. 2000. The recruitment of Raf-1 to membranes is mediated by direct interaction with phosphatidic acid and is independent of association with Ras. *Journal of Biological Chemistry* **275**(31): 23911-23918.

Rizzo, M.A., Springer, G., Segawa, K., Zipfel, W.R., and Piston, D.W. 2006. Optimization of pairings and detection conditions for measurement of FRET between cyan and yellow fluorescent proteins. *Microscopy and Microanalysis* **12**(3): 238-254.

Russell, L. and Frank, B. 1978. Ultrastructural characterization of nuage in spermatocytes of rat testis. *Anatomical Record* **190**(1): 79-97.

Saffman, E.E. and Lasko, P. 1999. Germline development in vertebrates and invertebrates. *Cell Mol Life Sci* **55**(8-9): 1141-1163.

Sager, P.R. 1989. Cytoskeletal effects of acrylamide and 2,5-hexanedione - selective aggregation of vimentin filaments. *Toxicology and Applied Pharmacology* **97**(1): 141-155.

Saito, K., Inagaki, S., Mituyama, T., Kawamura, Y., Ono, Y., Sakota, E., Kotani, H., Asai, K., Siomi, H., and Siomi, M.C. 2009. A regulatory circuit for piwi by the large Maf gene traffic jam in *Drosophila*. *Nature* **461**(7268): 1296-U1135.

Saito, K., Nishida, K.M., Mori, T., Kawamura, Y., Miyoshi, K., Nagami, T., Siomi, H., and Siomi, M.C. 2006. Specific association of Piwi with rasiRNAs derived from retrotransposon and heterochromatic regions in the *Drosophila* genome. *Genes Dev* **20**(16): 2214-2222.

Saito, K., Sakaguchi, Y., Suzuki, T., Siomi, H., and Siomi, M.C. 2007. Pimet, the *Drosophila* homolog of HEN1, mediates 2 '-O-methylation of PIWI-interacting RNAs at their 3 ' ends. *Genes Dev* **21**(13): 1603-1608.

Schauss, A.C., Huang, H.Y., Choi, S.Y., Xu, L., Soubeyrand, S., Bilodeau, P., Zunino, R., Rippstein, P., Frohman, M.A., and McBride, H.M. 2010. A novel cell-free mitochondrial fusion assay amenable for high-throughput screening of fusion modulators. *BMC Biology (in press)*.

Schrader, M. 2006. Shared components of mitochondrial and peroxisomal division. *Biochim Biophys Acta-Mol Cell Res* **1763**(5-6): 531-541.

Schroder, R., Goudeau, B., Simon, M.C., Fischer, D., Eggermann, T., Clemen, C.S., Li, Z.L., Reimann, J., Xue, Z.G., Rudnik-Schoneborn, S. et al. 2003. On noxious desmin: functional effects of a novel heterozygous desmin insertion mutation on the extrasarcomeric desmin cytoskeleton and mitochondria. *Human Molecular Genetics* **12**(6): 657-669.

Schug, Z.T. and Gottlieb, E. 2009. Cardiolipin acts as a mitochondrial signalling platform to launch apoptosis. *Biochimica Et Biophysica Acta-Biomembranes* **1788**(10): 2022-2031.

Schupbach, T. and Wieschaus, E. 1991. Female sterile mutations on the 2nd chromosome of *Drosophila melanogaster*. II. Mutations blocking oogenesis or altering egg morphology. *Genetics* **129**(4): 1119-1136.

Sciorra, V.A. and Morris, A.J. 1999. Sequential actions of phospholipase D and phosphatidic acid phosphohydrolase 2b generate diglyceride in mammalian cells. *Mol Biol Cell* **10**(11): 3863-3876.

Sesaki, H. and Jensen, R.E. 2001. UGO1 encodes an outer membrane protein required for mitochondrial fusion. *J Cell Biol* **152**(6): 1123-1134.

Shoji, M., Tanaka, T., Hosokawa, M., Reuter, M., Stark, A., Kato, Y., Kondoh, G., Okawa, K., Chujo, T., Suzuki, T. et al. 2009. The TDRD9-MIWI2 Complex Is Essential for piRNA-Mediated Retrotransposon Silencing in the Mouse Male Germline. *Developmental Cell* **17**(6): 775-787.

Siomi, M.C., Mannen, T., and Siomi, H. 2010. How does the Royal Family of Tudor rule the PIWI-interacting RNA pathway? *Genes Dev* **24**(7): 636-646.

Smirnova, E., Shurland, D.L., Ryazantsev, S.N., and van der Bliek, A.M. 1998. A human dynamin-related protein controls the distribution of mitochondria. *J Cell Biol* **143**(2): 351-358.

Smith, S.W., Weiss, S.B., and Kennedy, E.P. 1957. The enzymatic dephosphorylation of phosphatidic acids. *Journal of Biological Chemistry* **228**(2): 915-922.

Soper, S.F.C., van der Heijden, G.W., Hardiman, T.C., Goodheart, M., Martin, S.L., de Boer, P., and Bortvin, A. 2008. Mouse maelstrom, a component of nuage, is essential for spermatogenesis and transposon repression in meiosis. *Developmental Cell* **15**(2): 285-297.

Stukey, J. and Carman, G.M. 1997. Identification of a novel phosphatase sequence motif. *Protein Sci* **6**(2): 469-472.

Suen, D.F., Norris, K.L., and Youle, R.J. 2008. Mitochondrial dynamics and apoptosis. *Genes Dev* **22**(12): 1577-1590.

Summerhayes, I.C., Wong, D., and Chen, L.B. 1983. Effect of microtubules and intermediate filaments on mitochondrial distribution. *J Cell Sci* **61**(MAY): 87-105.

Taguchi, N., Ishihara, N., Jofuku, A., Oka, T., and Mihara, K. 2007. Mitotic phosphorylation of dynamin-related GTPase Drp1 participates in mitochondrial fission. *Journal of Biological Chemistry* **282**(15): 11521-11529.

Tanaka, A. and Youle, R.J. 2008. A chemical inhibitor of DRP1 uncouples mitochondrial fission and apoptosis. *Mol Cell* **29**(4): 409-410.

Tanaka, S.S., Toyooka, Y., Akasu, R., Katoh-Fukui, Y., Nakahara, Y., Suzuki, R., Yokoyama, M., and Noce, T. 2000. The mouse homolog of *Drosophila* Vasa is required for the development of male germ cells. *Genes Dev* **14**(7): 841-853.

Tang, H.L., Lung, H.L., Wu, K.C., Le, A.H.P., Tang, H.M., and Fung, M.C. 2008. Vimentin supports mitochondrial morphology and organization. *Biochem J* **410**: 141-146.

Tao, G.Z., Looi, K.S., Toivola, D.M., Strnad, P., Zhou, Q., Liao, J., Wei, Y.Q., Habtezion, A., and Omary, M.B. 2009. Keratins modulate the shape and function of hepatocyte mitochondria: a mechanism for protection from apoptosis. *J Cell Sci* **122**(21): 3851-3855.

Thoms, S. and Erdmann, R. 2005. Dynamin-related proteins and Pex11 proteins in peroxisome division and proliferation. *Febs Journal* **272**(20): 5169-5181.

Thomson, T. and Lin, H.F. 2009. The Biogenesis and Function of PIWI Proteins and piRNAs: Progress and Prospect. *Annu Rev Cell Dev Biol* **25**: 355-376.

Tieu, Q. and Nunnari, J. 2000. Mdv1p is a WD repeat protein that interacts with the dynamin-related GTPase, Dnm1p, to trigger mitochondrial division. *J Cell Biol* **151**(2): 353-365.

Tinel, H., Cancela, J.M., Mogami, H., Gerasimenko, J.V., Gerasimenko, O.V., Tepikin, A.V., and Petersen, O.H. 1999. Active mitochondria surrounding the pancreatic acinar granule region prevent spreading of inositol trisphosphate-evoked local cytosolic Ca2+ signals. *Embo J* **18**(18): 4999-5008.

Twig, G., Elorza, A., Molina, A.J.A., Mohamed, H., Wikstrom, J.D., Walzer, G., Stiles, L., Haigh, S.E., Katz, S., Las, G. et al. 2008. Fission and selective fusion govern mitochondrial segregation and elimination by autophagy. *Embo J* **27**(2): 433-446.

Twig, G., Graf, S.A., Wikstrom, J.D., Mohamed, H., Haigh, S.E., Elorza, A., Deutsch, M., Zurgil, N., Reynolds, N., and Shirihai, O.S. 2006. Tagging

and tracking individual networks within a complex mitochondrial web with photoactivatable GFP. *Am J Physiol-Cell Physiol* **291**(1): C176-C184.

Unhavaithaya, Y., Hao, Y., Beyret, E., Yin, H., Kuramochi-Miyagawa, S., Nakano, T., and Lin, H.F. 2009. MILI, a PIWI-interacting RNA-binding Protein, Is Required for Germ Line Stem Cell Self-renewal and Appears to Positively Regulate Translation. *Journal of Biological Chemistry* **284**(10): 6507-6519.

Vagin, V.V., Sigova, A., Li, C.J., Seitz, H., Gvozdev, V., and Zamore, P.D. 2006. A distinct small RNA pathway silences selfish genetic elements in the germline. *Science* **313**(5785): 320-324.

Vasileva, A., Tiedau, D., Firooznia, A., Muller-Reichert, T., and Jessberger, R. 2009. Tdrd6 Is Required for Spermiogenesis, Chromatoid Body Architecture, and Regulation of miRNA Expression. *Curr Biol* **19**(8): 630-639.

Vitale, N., Caumont, A.S., Chasserot-Golaz, S., Du, G., Wu, S., Sciorra, V.A., Morris, A.J., Frohman, M.A., and Bader, M.F. 2001. Phospholipase D1: a key factor for the exocytotic machinery in neuroendocrine cells. *Embo J* **20**(10): 2424-2434.

Wanders, R.J.A. and Waterham, H.R. 2006. Biochemistry of mammalian peroxisomes revisited. *Annual Review of Biochemistry* **75**: 295-332.

Watanabe, T., Takeda, A., Tsukiyama, T., Mise, K., Okuno, T., Sasaki, H., Minami, N., and Imai, H. 2006. Identification and characterization of two novel classes of small RNAs in the mouse germline: retrotransposon-derived siRNAs in oocytes and germline small RNAs in testes. *Genes Dev* **20**(13): 1732-1743.

Waterham, H.R., Koster, J., van Roermund, C.W.T., Mooyer, P.A.W., Wanders, R.J.A., and Leonard, J.V. 2007. A lethal defect of mitochondrial and peroxisomal fission. *N Engl J Med* **356**(17): 1736-1741.

Weller, S., Gould, S.J., and Valle, D. 2003. Peroxisome biogenesis disorders. *Annual Review of Genomics and Human Genetics* **4**: 165-211.

Wilson-Fritch, L., Nicoloro, S., Chouinard, M., Lazar, M.A., Chui, P.C., Leszyk, J., Straubhaar, J., Czech, M.P., and Corvera, S. 2004. Mitochondrial remodeling in adipose tissue associated with obesity and treatment with rosiglitazone. *J Clin Invest* **114**(9): 1281-1289.

Wong, E.D., Wagner, J.A., Scott, S.V., Okreglak, V., Holewinske, T.J., Cassidy-Stone, A., and Nunnari, J. 2003. The intramitochondrial dynamin-related GTPase, Mgm1p, is a component of a protein complex that mediates mitochondrial fusion. *J Cell Biol* **160**(3): 303-311.

Yang, J.S., Gad, H., Lee, S.Y., Mironov, A., Zhang, L.L., Beznoussenko, G.V., Valente, C., Turacchio, G., Bonsra, A.N., Du, G.W. et al. 2008. A role for

phosphatidic acid in COPI vesicle fission yields insights into Golgi maintenance. *Nat Cell Biol* **10**(10): 1146-1153.

Yin, H. and Lin, H.F. 2007. An epigenetic activation role of Piwi and a Piwi-associated piRNA in *Drosophila melanogaster*. *Nature* **450**(7167): 304-U316.

Zeharia, A., Shaag, A., Houtkooper, R.H., Hindi, T., de Lonlay, P., Erez, G., Hubert, L., Saada, A., de Keyzer, Y., Eshel, G. et al. 2008. Mutations in LPIN1 Cause Recurrent Acute Myoglobinuria in Childhood. *Am J Hum Genet* **83**(4): 489-494.

Zhang, Q.X., Pilquil, C.S., Dewald, J., Berthiaume, L.G., and Brindley, D.N. 2000. Identification of structurally important domains of lipid phosphate phosphatase-1: implications for its sites of action. *Biochem J* **345**: 181-184.

Zuchner, S., Mersiyanova, I.V., Muglia, M., Bissar-Tadmouri, N., Rochelle, J., Dadali, E.L., Zappia, M., Nelis, E., Patitucci, A., Senderek, J. et al. 2004. Mutations in the mitochondrial GTPase mitofusin 2 cause Charcot-Marie-Tooth neuropathy type 2A. *Nature Genet* **36**(5): 449-451.